Investigating the atypical role of beta-arrestins in the regulation of Hedgehog signalling

Hattie Ollerton

Submitted in accordance with the requirements for the degree of Doctor of Philosophy

The University of Leeds
Faculty of Biological Sciences
School of Molecular and Cellular Biology
November 2024

Intellectual property rights

The candidate confirms that the work submitted is her own and that appropriate credit has been given where reference has been made to the work of others.

Acknowledgements

Firstly, I would like to thank my supervisor, Dr Natalia Riobo-Del Galdo. Since we first met during my BSc you have welcomed, encouraged, and supported me in more ways than were expected or necessary. Despite everything I have been through in the last few years, you never doubted me and that has been so valuable in this journey. I admire both your professional and personal lives greatly, and I hope you can continue to raise Hedgehogs in your lab for a long time to come!

I would also like to extend my thanks to my co-supervisors Dr Vas Ponnambalam and Professor Darren Tomlinson. In particular, the added support from the Tomlinson group has been greatly appreciated and allowed me to extend the scope of my project and include techniques I would have been unable to use otherwise.

Thanks also go to members of the Hedgehog Lab, past and present. Dr Danai Gkotsi, your extensive knowledge and willingness to share it were incredible and so helpful, but even more than that, your friendship. We miss you terribly! Dr Felix, Esther, and our adopted Hedgehog Ellen, you all made my PhD life so fun, I'm grateful for you all and I hope we stay in touch. In addition the office of Miall 7.19, you are all great people and I've missed seeing you every day since I've been in writing hibernation! And Jack, you have become one of my closest friends this past year and supported me in so many ways. Thank you for all the laughs and really helping me through this last leg of my PhD.

To all of my friends and family, your support has meant so much to me as well as your understanding throughout my countless stresses and periods of radio silence. I can't wait to have my social life back and celebrate with you all! It means so much to me to have a great network of people around me, I appreciate every one of you.

Mum and Dad. Words will never be enough. Your unwavering love and support in every aspect of my life are absolutely invaluable. I certainly would not have been able to do this without you. I am so grateful to you both, and proud to be your daughter. I love you. I now expect you to tell every living soul you raised a genius.

Abstract

The developmental Hedgehog (HH) signalling network plays a pivotal role in cellular processes, and dysregulation has been implicated in various cancers. This project unveils a complex interplay between PTCH1, a key receptor in the HH pathway, and β-arrestins (βarrs), multifunctional regulators and scaffold proteins.

Preliminary studies showed a novel interaction between the PTCH1 CTD and βarrs, primarily βarr1. Ubiquitination is not necessary for this interaction, although likely coordinates with βarr1 binding to promote SHH-mediated PTCH1 turnover.

Guided by a phosphorylation code, *p*x(x)*pxxp*/E/D, bioinformatic study of the PTCH1 primary sequence identified a phosphorylation-dependent binding motif, and this motif was validated through site-directed mutagenesis, co-immunoprecipitation assays, fluorescence confocal microscopy, and mass spectrometry. The motif, pSEYpSSQpT spans PTCH1 residues S1223-T1229, and disruption of the phosphorylation sites blocks PTCH1-βarr1 binding. Inhibition of GRK2/3 reduces this interaction, as does SHH stimulation. Therefore βarr1 recruitment to PTCH1 is mediated both by SHH and GRK2/3.

Functional assays using βarr siRNA and a βarr-null PTCH1 mutant (S1223A and T1229A, SATA) provided insights into the physiological consequences of this interaction. The PTCH1-βarr interaction has no effect on Gli-luciferase reporter activity, βarrs only act through SMO to modulate canonical signalling. The PTCH1-βarr1 interaction does enhance SHH-mediated PTCH1 degradation, as well as cell viability and clonogenicity, while decreasing apoptotic signalling through PTCH1. This highlights the influence of this interaction on non-canonical, downstream signalling events.

Structural predictions using the AI-based tool, AlphaFold 3, confirmed experimental results, showing that phospho-motif pSEYpSSQpT is necessary and sufficient for βarr1 binding to the PTCH1 CTD.

These results unveil a phosphorylation-dependent regulatory axis, enhancing our molecular understanding of PTCH1 modulation within HH signalling. By regulating PTCH1 stability and downstream signalling in HH-driven malignancies, the identified PTCH1-βarr1 interaction provides a promising avenue for targeted interventions of HH-associated cancers.

Table of Contents

List of Figures

List of Tables

List of Abbreviations

AF3	Alphafold 3
AI	Artificial intelligence
AMP	Adenosine monophosphate
APBS	Adaptive Poisson-Boltzmann solver
ARRDC	Arrestin-domain-containing protein
ATG101	Autophagy-related protein 101
BCC	Basal cell carcinoma
BCS	Bovine calf serum
BMP	Bone morphogenetic protein
BOC	Brother of CDO
Boi	Brother of Ihog
BSA	Bovine serum albumin
cAMP	Cyclic adenosine monophosphate
CDK1	Cyclin-dependent kinase 1
CDO	Cell adhesion molecule-related, down-regulated by oncogenes
CHX	Cycloheximide
CK1	Casein kinase 1
CRD	Cysteine-rich domain
cryo-EM	Cryo-electron microscopy
CST	Cell Signaling Technology
CTD	C-terminal domain
DHH	Desert hedgehog
DISP1	Dispatched-1
DMEM	Dulbecco's Modified Eagle Medium
DMSO	Dimethyl sulfoxide
DNA	Deoxyribonucleic acid
dpp	Decapentaplegic
ECD	Extracellular domain
ECL	Extracellular loop
EDTA	Ethylenediaminetetraacetic acid
ER	Endoplasmic reticulum
ERK	Extracellular signal-regulated kinase
ETD	Electron transfer dissociation
FBS	Fetal bovine serum
Gas1	Growth arrest–specific gene 1
GFP	Green fluorescent protein

GliA	Activator form of GLI
GliR	Repressor form of GLI
GPCR	G-protein coupled receptor
Grb2	Growth factor receptor-bound protein 2
GRK	G-protein coupled receptor kinase
GSK3β	Glycogen synthase kinase-3 beta
HCD	Higher-energy collisional dissociation
HEK	Human embryonic kidney
HH	Hedgehog
HHAT	Hedgehog acyltransferase
Hip	Hedgehog interacting protein
HRP	Horseradish peroxidase
ICL	Intracellular loop
IDR	Intrinsically disordered region
IFT	Intraflagellar transport
IHH	Indian hedgehog
Ihog	Interference hedgehog
IP	Immunoprecipitation
ipTM	Interface predicted template modelling
ITCH	E3 ubiquitin-protein ligase Itchy homolog
KCOT	Keratocystic odontogenic tumour
kDa	Kilodaltons
LB	Luria-Bertani
MAPK	Mitogen-activated protein kinase
MEF	Mouse embryonic fibroblast
mL	Millilitres
mM	Millimolar
MPF	M-phase promoting factor
MS	Mass spectrometry
NBCCS	Nevoid basal cell carcinoma syndrome
nL	Nanolitres
nM	Nanomolar
NPC1	Niemann-Pick C1 protein
NTD	N-terminal domain
PBS	Phosphate-buffered saline
PcG	Polycomb group
PDB	Protein Data Bank
PEI	Polyethylenimine

PKA	Protein kinase A
pLDDT	Predicted local distance difference test
PMSF	Phenylmethylsulfonyl fluoride
PRD	Proline-rich domain
PTCH	Patched
PTM	Post-translational modification
pTM	Predicted template modelling
PVDF	Poly(vinylidene fluoride)
RNA	Ribonucleic acid
RND	Resistance-nodulation-division
rpm	Revolutions per minute
RT	Room temperature
SATA	S1223A, T1229A
SDS	Sodium dodecyl-sulfate
SEM	Standard error of the mean
SHH	Sonic hedgehog
ShhC	C-terminal SHH product
ShhN	N-terminal SHH product
siRNA	Small interfering RNA
SMO	Smoothened
SSD	Sterol-sensing domain
SuFu	Suppressor of Fused
T5	Transporter 5® transfection reagent
TBS	Tris-buffered saline
TCGA	The Cancer Genome Atlas
TM	Transmembrane
TM	Template modelling
TMD	Transmembrane domain
ULK	Unc51-like autophagy activating kinase
WB	Western blot
wg	Wingless
β2-AR	B2-adrenergic receptor
βarr	Beta-arrestin
µL	Microlitres
µM	Micromolar

Chapter 1

Introduction

Chapter 1

Introduction

1.1 Hedgehog signalling

1.1.1 Brief introduction to Hedgehog signalling

Many cellular signalling pathways choreograph the processes necessary for life. Hedgehog signalling plays essential roles in embryonic development, tissue homeostasis, and disease progression in eukaryotes . Since the discovery of the Hedgehog (Hh) gene in 1980 (Nüsslein-Volhard and Wieschaus, 1980), decades of research have unveiled a vast network of interactions conserved across species. Hedgehog signalling is complex and many elements are still yet to be defined, however due to its implication in many human diseases it has become the primary interest of many research groups and thus the field is expanding continuously.

Initially, *Hh* was identified as a crucial gene in the context of embryonic patterning in *Drosophila melanogaster*. The expressed morphogenic HH protein directs proper segment definition and alignment of the fruit fly (Martinez-Arias and Lawrence, 1985). The name is coined from the *Hh* mutant larvae of early experiments which, without proper segment polarity from HH, possess a phenotype of denticles across their surface resembling that of a hedgehog.

In *Drosophila*, HH has been studied intensely and roles throughout embryogenesis have been characterised. For example, segmental patterning is controlled primarily by HH secretion in posterior cells, which causes variable expression of proteins decapentaplegic (dpp) and wingless (wg) in anterior cells and in turn, growth and patterning of distinct cell populations (Basler and Struhl, 1994).

1.1.2 Canonical Hedgehog signalling in mammals

Unlike *Drosophila*, vertebrates have a family of three HH members: Sonic hedgehog (Shh), Indian hedgehog (Ihh), and Desert hedgehog (Dhh), each with their own distinct expression domains and biological roles. The three genes are located in the human genome at positions 7q36, 12q12-q13.1, and 2q35 respectively (Odent et al., 1999, Tate et al., 2000, Yuksel-Apak et al., 2012). DHH is the most closely related homolog to *Drosophila* HH, and has key roles in germ and Schwann cells (Pathi et al., 2001). IHH and SHH are more closely related to each other than to DHH or *Drosophila* HH, however are no less important in vertebrate HH signalling. For

example, IHH has been shown to regulate chondrocyte differentiation in cartilage elements, preceding ossification to form the skeleton (Vortkamp et al., 1996). SHH is the most studied vertebrate HH protein and has early roles in embryonic patterning processes of the central nervous system and limbs in mammals. Neural tube patterning demonstrates the molecular developmental role of SHH and the morphogenic ability of the HH pathway to trigger signalling events at distant sites. In combination with Wnt and bone morphogenetic protein (BMP) families, SHH creates gradients along the anterior-posterior and dorsal-ventral axes of the neural tube which directs the differentiation of neurons and eventually forms the brain and spinal cord (Dessaud et al., 2008).

The molecular components of Hedgehog signalling are highly conserved throughout evolution (Ingham et al., 2011) and the mechanisms through which they signal have similarities across species, even between invertebrates and vertebrates (Ingham and McMahon, 2001). Figure 1.1 depicts simplified SHH-dependent signalling in mammalian cells. After synthesis in a HH secreting cell, the ~45kDa precursor SHH protein is translocated through the endoplasmic reticulum (ER) and Golgi apparatus where it undergoes autoproteolytic cleavage to form the cholesterol-modified N-terminal fragment $ShhN_{Ch}$, the remaining amino-terminal part of the protein. SHH is also modified with palmitate at the N-terminus to form the mature active ligand ($_{p}SHHN_{Ch}$) (hereafter referred to simply as SHH). Through the dual action of membrane transporter Dispatched-1 (DISP1) and glycoprotein Scube2, SHH is secreted to signal in autocrine (the same cell), paracrine (neighbouring cell), and endocrine (distant cell) manners.

Canonical HH signalling remains in the inactive state when SHH protein is absent (Figure 1.1, left). In this state, PTCH1 is localised to the primary cilium and holds inhibition over Smoothened (SMO), a 7 transmembrane receptor that mediates canonical HH signalling. Primary cilia are non-motile organelles which protrude from the surface of nearly all cell types, particularly epithelial cells, and are the 'reaction centre' for canonical HH protein-protein interactions. It is thought that this repression occurs through PTCH1 controlling the local cholesterol availability in the cilium, since PTCH1 can act as a cholesterol transporter and SMO is activated by accessible cholesterol, although this phenomenon is not fully understood (Huang et al., 2016, Bidet et al., 2011). Inhibited SMO remains in intracellular vesicles, while active SMO accumulates in membrane of the primary cilium. In the primary cilia, the transporter protein Kif7 along with Suppressor of Fused (SuFu) regulates localisation and processing of GLI proteins via microtubule transport. The GLI family of proteins has three members: GLI1, GLI2, and GLI3. GLI1 is a transcriptional

activator, whereas GLI2 and GLI3 can undergo differential processing to form activators or repressors. GLI2 and GLI3 are constitutively expressed and to respond to the SHH signal, inducing the expression of GLI1 which amplifies this response.

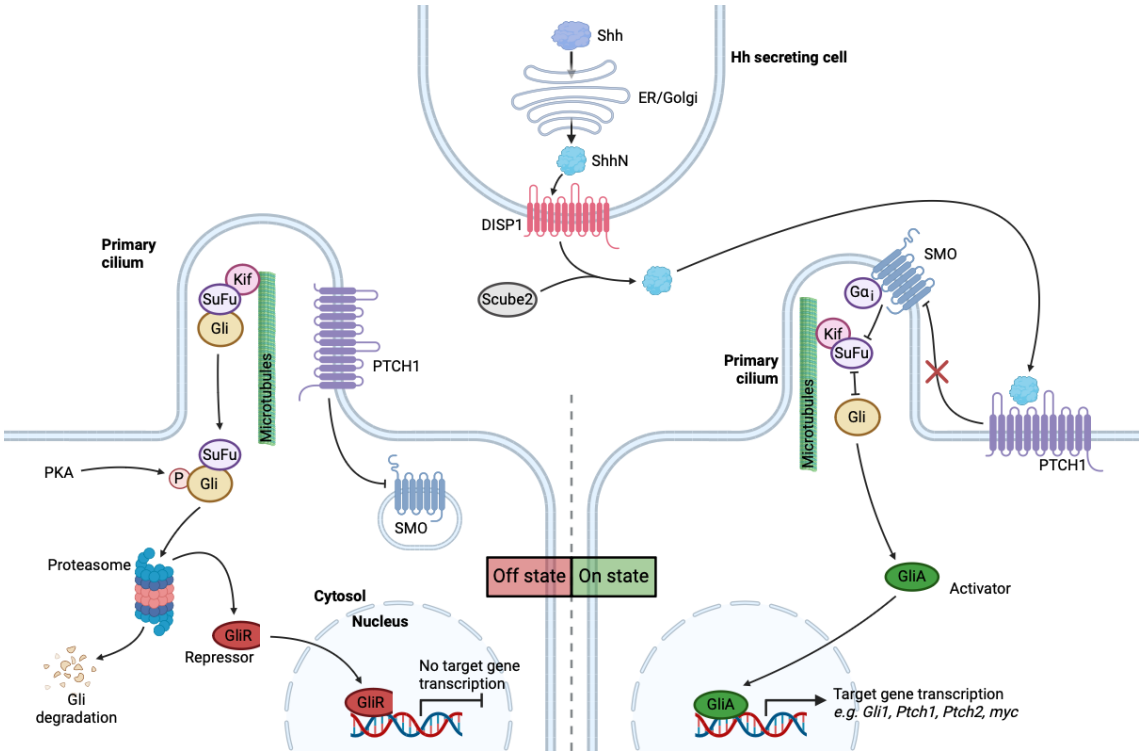

Figure 1.1 Canonical hedgehog signalling
Created with BioRender.com. Designed using elements from an article by Cell Signaling Technology (Technology, 2014) and existing knowledge. In the off state, in the absence of SHH, PTCH1 in the cilium represses SMO which is kept in an intracellular vesicle. GLI is held at the base of the cilia via SuFu and Kif, leading to negative phosphorylation by PKA. GLI is either fully or partially degraded by the proteasome, the partially degraded becoming the repressor form GliR, which inhibits transcription of target genes. Conversely, SHH is synthesised, processed, and secreted from a HH secreting cell, and upon binding to PTCH1, activates the HH pathway. PTCH1 is inactivated, exits the cilium and no longer holds repression over SMO. Active SMO causes dissociation of GLI from SuFu and Kif, and GLI is alternatively phosphorylated to the active form, GliA. GliA translocates to the nucleus and promotes transcription of target genes.

Briefly, in the inactive state, GLI2/3 remain bound to Kif7/SuFu. This allows GLI2/3 phosphorylation by cytosolic enzymes such as casein kinase 1 (CK1), protein kinase A (PKA), and glycogen synthase kinase-3 beta (GSK3β). This phosphorylation occurs at a cluster of residues known as P1-6 (Niewiadomski et al., 2014), and leads to proteasomal degradation of GLI2/3, either to completion or partially via proteasomal stalling to form the repressor fragments GLI2R or GLI3R. GLI2/3R nuclear translocation and DNA binding inhibits transcription of HH target genes, and thus the pathway is inactive in this condition.

When SHH binds to PTCH1 at the ciliary membrane (Figure 1.1, right), the inhibitory function of PTCH1 on SMO is lifted, PTCH1 is internalised and degraded, and SMO is trafficked to the membrane of primary cilia. Accumulation of SMO in the cilia triggers its activation via phosphorylation-mediated oligomerisation. This accumulation of active SMO causes the release of GLI2/3 proteins from Kif7/SuFu, and their activation by dephosphorylation of the negative phospho-cluster, and phosphorylation at an activating cluster. These GLI2/3A proteins translocate to the nucleus and, conversely to their repressive counterparts, induce transcription of HH target genes including *PTCH1* and *GLI1*.

1.1.3 Hedgehog receptors

There are 2 isoforms of PTCH in mammals, PTCH1 and PTCH2. They have very similar topology, both comprising 12 transmembrane helices, N- and C-terminal tails, a large middle intracellular loop, and 2 large extracellular loops (ECLs). The biggest difference between the two isoforms is the length of the C-terminal domains (CTDs), the CTD of PTCH1 spanning 272 residues, compared to the 89 residues of PTCH2. The ECLs of PTCH1 and PTCH2 form the binding domain for Hedgehog ligands, and the specifics of this interaction will be discussed later in this chapter.

PTCH2 does have some overlapping function with PTCH1, repressing SMO and responding to SHH (Alfaro et al., 2014), however is much weaker compared to PTCH1. Deficiency of PTCH2 results in a subtle and survivable phenotype, only becoming apparent when combined with PTCH1 defects (Lee et al., 2006).

Co-receptors of HH are more recently understood to be important in HH signalling. Interference Hedgehog (Ihog) and its homolog brother of Ihog (Boi), are positive regulators of Hedgehog signalling in *drosophila* (Yao et al., 2006). The vertebrate orthologues of Ihog, cell adhesion molecule down-regulated by oncogenes (Cdo) and brother of Cdo (Boc), maintain similar function to the *drosophila* Ihogs (Tenzen et al., 2006). An additional co-receptor, growth arrest–specific gene 1 (Gas1), has little sequence homology to Ihogs, but has a similar and equally crucial function. The importance of these 3 co-receptors is demonstrated by the lack of functionality of a SHH mutant which can bind PTCH1 but is unable to bind Cdo, Boc, or Gas1 (Izzi et al., 2011). It has been demonstrated that the function of these co-receptors is to facilitate the transfer of the fully processed SHH ligand from SCUBE proteins, which are soluble chaperones, to PTCH1, since SCUBE blocks the SHH-PTCH1 interaction (Wierbowski et al., 2020).

1.1.4 Sonic Hedgehog

Of the 3 Hedgehog isoforms found in mammals, SHH has been studied the most due to its leading role in neural and limb development. IHH and DHH are still crucial, however are studied less in the context of developmental disorders and cancers. Depending on the context, SHH can act as a morphogen, mitogen, survival factor, or guidance molecule (Ingham and McMahon, 2001).

The role of a morphogen is to act as a positional cue. Concentration gradients direct specific cell fates, for example long-range control of cell differentiation via SHH diffusion in the neural tube (Briscoe et al., 2001). Additionally, the mitogenic role of SHH is demonstrated by the increased proliferation of retinal precursor cells upon SHH treatment, directly increasing cell division (Jensen and Wallace, 1997). As a survival factor, SHH can increase signalling that enhances cell survival, or decrease cell death-associated signalling. This is observed in mouse limb muscles, where inactivating SHH mutations significantly hinder their formation (Krüger et al., 2001). Studies into spinal cord development have shown that SHH can guide axon growth in a position-dependent manner, for example the switch of SHH-directed commissural axon growth from SHH attraction to repulsion after crossing the floor plate (Yam et al., 2012). Together, these studies show the many context-dependent roles of SHH in development and maintenance of vertebrates, and why its proper expression and regulation is so important.

The *SHH* gene is translated into a 45 kDa precursor protein which is sequentially processed to form a 19 kDa lipid-modified signalling ligand. As outlined in Figure 1.2, newly synthesised SHH is made of 2 domains: an N-terminal signalling domain, and a C-terminal autoprocessing domain. Following its translation in the ER, the C-terminal domain performs an autoproteolytic cleavage, separating the signalling and autoprocessing domains, a process during which a cholesterol moiety is added to the newly formed C-terminus of the signalling domain (Porter et al., 1996). Following this, the autoprocessing domain is degraded by the proteasome. The signalling domain is then finally palmitoylated by Hedgehog acetyltransferase (HHAT), a palmitoylacyltransferase with specificity for SHH (Buglino and Resh, 2008). This end product is the active SHH ligand, generally referred to in this thesis simply as ‘SHH’. It is released from the producing cell through the joint action of DISP1 and SCUBE2, as discussed in Section 1.1.2. The transporter function of DISP1 for SHH cell exit is thought to be mediated by its sterol sensing domain (SSD), which uses the SHH cholesterol moiety to transfer it to the cell surface where SCUBE2 assists with release and transport (Burke et al., 1999, Tukachinsky et al., 2012).

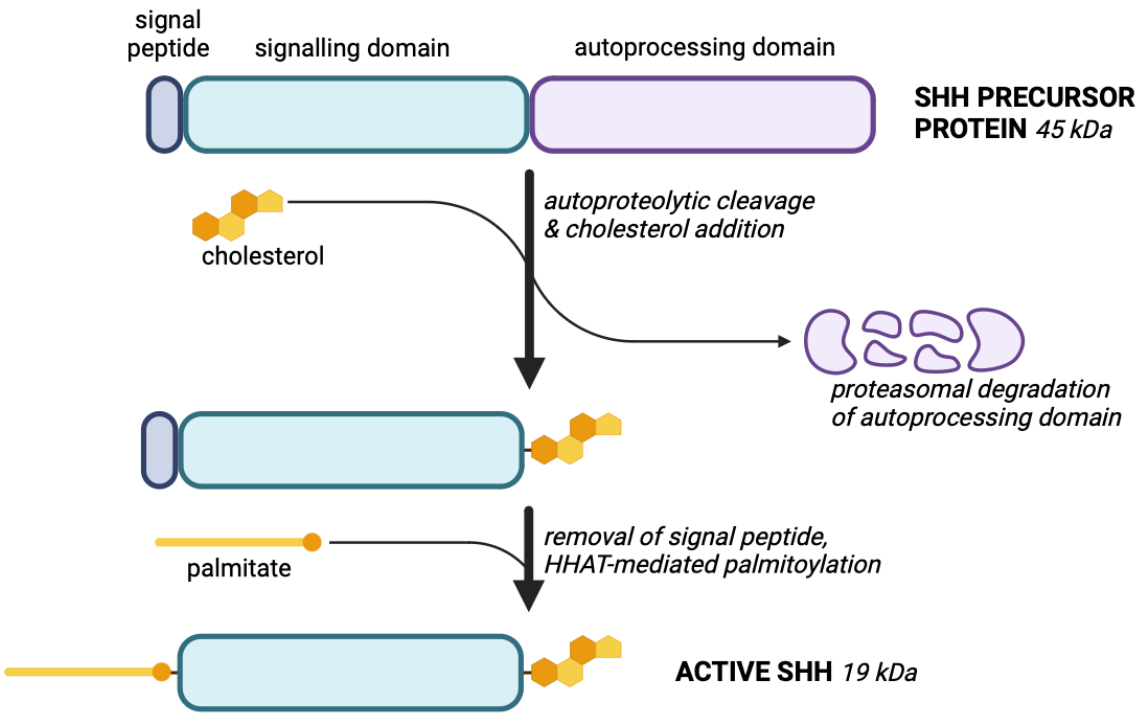

Figure 1.2 SHH protein synthesis and processing
SHH precursor protein undergoes autoproteolytic cleavage by its C-terminal autoprocessing domain which also adds a cholesterol moiety to the C-terminus of the signalling domain. HHAT adds a palmitate to the N terminal region to form the active SHH ligand. Created with Biorender.com.

1.1.5 Smoothened

SMO is a member of the G protein-coupled receptor (GPCR) superfamily, comprising an extracellular cysteine-rich domain (CRD), a short linker, a bundle of 7 membrane-spanning helices, and a long C-terminal tail. SMO is coupled specifically to the G_i family of heterotrimeric G proteins, as has been shown experimentally through cell-based assays and in structural studies (Riobo et al., 2006, Qi et al., 2019).

SMO activity is not regulated by direct interaction with the Hedgehog ligands, rather, the indirect action of HH ligand binding to PTCH1, which blocks PTCH1 activity. Active PTCH1 is able to suppress SMO activity. The process by which it does this has been unknown in the field for some time, although recent evidence is building a convincing story that PTCH1 acts as a cholesterol transporter, regulating the levels of accessible cholesterol which is required for SMO activation. There are two cholesterol binding sites within SMO, one in the transmembrane domain (TMD), and another in the CRD (Siebold and Rohatgi, 2023). SMO is fully inactive when no cholesterol is bound. It becomes primed, exerting a low level of basal activity, when cholesterol is bound to the TMD site, however becomes fully active upon secondary binding of cholesterol to the CRD. It seems the TMD cholesterol is not regulated by

PTCH1 but instead comes from the cholesterol that is embedded within the phospholipid bilayer of the cell membrane. The CRD cholesterol however is regulated by the cholesterol transporter function of PTCH1, which controls accessible cholesterol, that is, cholesterol at the surface of the bilayer which can be bound by the SMO CRD.

Following HH ligand binding to PTCH1, SMO undergoes a 2-step activation process: translocation from intracellular vesicles to the ciliary membrane, and phosphorylation by GPCR kinases (GRKs). Cell surface translocation alone is not sufficient for SMO activation, since the SMO inhibitor cyclopamine can induce translocation but in an inactive conformation, thus still preventing activity (Wang et al., 2009). Phosphorylation is also required for full SMO activation. In both *drosophila* and mammals, the N-terminal regions of SMO associate to create multimers, while clusters of basic residues maintain distance between the C-terminal domains. Phosphorylation of several Ser/Thr residues among these basic clusters neutralises the positive charge, allowing the C-tails to move closer together, a process necessary for the accumulation of ciliary SMO, since deletion of the basic residues induces this accumulation (Zhao et al., 2007). In addition, this C-tail phosphorylation reduces ubiquitination of this domain and the resulting endocytosis and degradation of SMO (Li et al., 2012, Xia et al., 2012)

Mammalian SMO is known to be phosphorylated by GRK2 as well as CK1α in the presence of HH proteins (Chen et al., 2011). GRK2-mediated phosphorylation induces recruitment of beta-arrestins (βarrs) in most GPCRs. The role of βarrs in Hedgehog signalling is the focus of this thesis. Their regulation of canonical signalling will be discussed later in this chapter, and their novel role in non-canonical signalling will be discussed throughout the rest of this thesis, since this has not been reported before.

1.1.6 Primary cilia

The primary cilium is an organelle that protrudes from the surface of most cell types, where cells form a single primary cilium through the process of ciliogenesis during interphase. The cilium is disassembled before mitosis, since the microtubule organising centre (basal body) is a specialised version of the centriole, which is duplicated during cell division to form the mitotic spindle. After mitosis, each daughter cell inherits a single centriole which will become the cilium basal body (Plotnikova et al., 2009).

The structure of the primary cilium differs slightly from that of motile cilia. Microtubules make up the length of the cilia and this is known as the axoneme. The axoneme of motile cilia has 9 sets of microtubule doublets surrounding 2 central microtubules which they connect to with proteins important for coordinating their movement such as dynein. This is known as a 9 + 2 arrangement. However, primary cilia lack the central microtubules, so their axoneme is known to have a 9 + 0 arrangement (Ainsworth, 2007). At the base, a structure called the basal body controls the assembly of the axoneme, and anchors it in place (Brown and Zhang, 2020).

The primary cilium contains a transport network known as the intraflagellar transport (IFT) system, which controls movement of proteins along the axoneme. The two protein complexes, IFT-A and IFT-B are required for proper transport within the primary cilia (Wang et al., 2021), and thus regulation of signalling that relies on ciliary protein migration such as HH signalling.

Proper function of the HH pathway relies on ciliary transport. In the off state, PTCH1 resides at the base of the cilia, which blocks accumulation of SMO in the ciliary membrane (Ho and Stearns, 2021). In this state, GLI2 and GLI3 are also sequestered at the ciliary basal body via SuFu, and processed into repressors via cytosolic phosphorylation as previously discussed (He et al., 2014). In the presence of HH ligand, PTCH1 is internalised and eventually degraded (Petrov et al., 2021). SMO is then translocated to the ciliary membrane, a process which represses PKA activity through its GPCR activity with G_i and removal of Gpr161 (Hwang et al., 2021). In addition, SMO has recently been shown to also repress PKA activity by binding to and sequestering the PKA catalytic subunit via its C-tail (Arveseth et al., 2021). This reduces the levels of repressor-forming GLI2/3 phosphorylation, as well as promoting formation of GLI2/3 activators through their transport to the ciliary tip where they are positively phosphorylated by kinases such as ULK3 and STK36, and dissociate from SuFu for nuclear translocation and transcriptional activation (Han et al., 2019, Cai et al., 2022).

1.1.7 Non-canonical Hedgehog signalling

Canonical HH signalling, that is, the HH-regulated transcriptional activity of GLI proteins, is so called since it has dominated the focus of the field for many years. However more recently there has been an increasing number of studies showing GLI-independent mechanisms through which HH signals. These ‘non-canonical’

pathways are proving to be of comparable importance in the development and maintenance of organisms.

Non-canonical signalling is subdivided into two distinct components: type I signalling independently of SMO, and type II signalling through SMO but not requiring GLI transcription factors (Figure 1.3). Type I non-canonical signalling through PTCH1 is known to inhibit proliferation and autophagy and enhance apoptosis (Takizawa and Morgan, 2000, Thibert et al., 2003, Caballero-Ruiz et al., 2023). Type II signalling relies on the GPCR activity of SMO, which downstream plays a part in cytoskeleton regulation via RHOA and RAC1 (Polizio et al., 2011), as well as inducing fluctuations in Ca^{2+} ions particularly in neural cell types to stimulate processes such as migration (Komuro and Rakic, 1996).

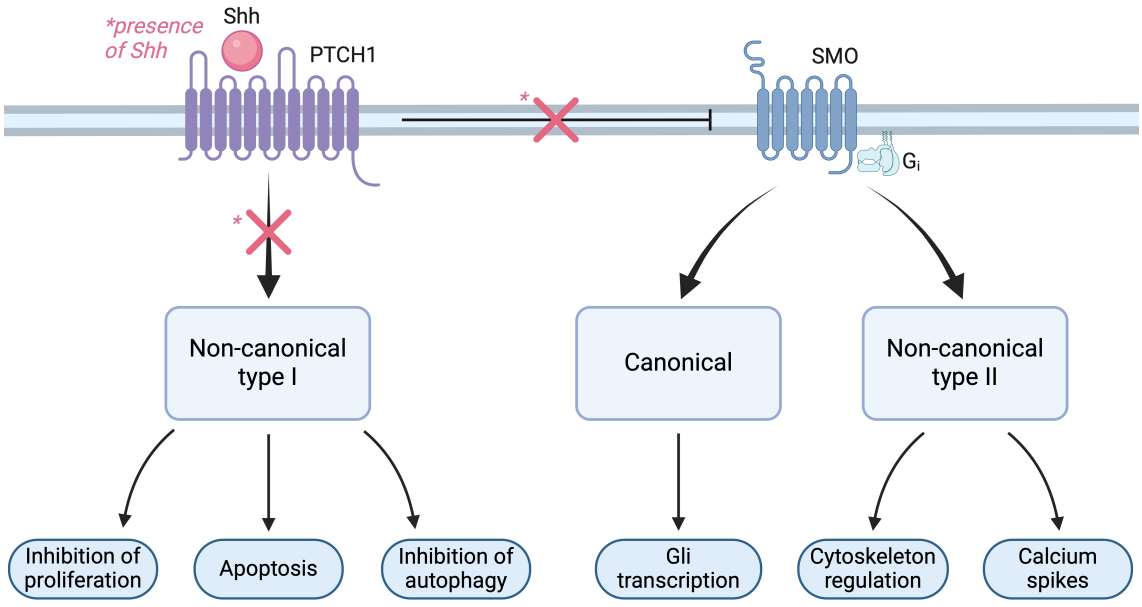

Figure 1.3 Canonical and non-canonical Hedgehog signalling
Simplified schematic showing active PTCH1 inhibiting SMO and non-canonical signalling type I. SHH binding (shown in pink) inhibits PTCH1, blocking non-canonical type I and releasing the inhibition of SMO, allowing canonical and non-canonical type II to proceed. Created with Biorender.com.

This thesis focuses mostly on non-canonical signalling type I, which proceeds directly through PTCH1. PTCH1 has many functions separate from SMO through direct interactions with effector proteins. For example, as well as regulating proliferation and apoptosis, it has also been shown to regulate autophagic flux. These interactions and functions will be discussed in section 1.2.3, and novel interactions and roles are the focus of this project so will be discussed throughout the rest of this thesis.

1.2 Patched1, the principal Hedgehog receptor

1.2.1 PTCH1 topology

PTCH1 is a 12-transmembrane (TM) receptor of HH proteins SHH, DHH, and IHH in mammalian cells (Marigo et al., 1996). The human *PTCH1* gene contains 23 exons, which through alternative splicing can generate 3 common isoforms of the PTCH1 protein; PTCH1-L, PTCH1-M and PTCH1-S (Nagao et al., 2005). PTCH1-M has a truncated N-terminal domain (NTD) and PTCH1-S lacks the entire NTD and first TM helix, the sequence beginning with a slightly truncated ECLI. The PTCH1-S isoform is less stable than M or L, which also results in a lower level of GLI activity suppression.

The most common and well-studied isoform is the L isoform, which is 1447 residues long and has a mass of 160 kDa. This isoform is the canonical isoform in the field and is the focus of this thesis. From this point onwards, 'PTCH1' refers to PTCH1-L. Along with the 12 TM helices that span the plasma membrane, PTCH1 also has several key cytosolic and extracellular domains that are involved in its function (Figure 1.4). There are two large extracellular loops (ECLs), ECLI and ECLII, which form a domain containing the main binding interfaces with the HH ligands. PTCH1 mutants lacking ECLII are dominant negative, having lost the ability to bind HH ligands so cannot be inactivated, and therefore increased repression of SMO is observed (Briscoe et al., 2001).

The bundle of TM helices 2-6 is known as the sterol-sensing domain (SSD) of PTCH1 based on similarity in sequence and structure to other cholesterol-interacting proteins such as Niemann-Pick C1 protein (NPC1) which is involved in cholesterol transport and trafficking (Blanchette-Mackie, 2000). PTCH1 also shares sequence homology with the resistance-nodulation-division (RND) family of transporters which are found in bacteria and are responsible for pumping lipophilic toxins and heavy metals out of the cell via a proton gradient (Hasanovic and Mus-Veteau, 2018, Routh et al., 2011). PTCH1 contains a conserved motif (GXXXD) that has been shown to be required for the transporter function of RND pumps. This motif in PTCH1 is mutated in several occurrences of Gorlin's syndrome (Lindström et al., 2006), suggesting a conserved function. Together, this evidence points to PTCH1's role as a cholesterol transporter to regulate the accessible cholesterol for SMO activation and by this mechanism regulates canonical HH activity.

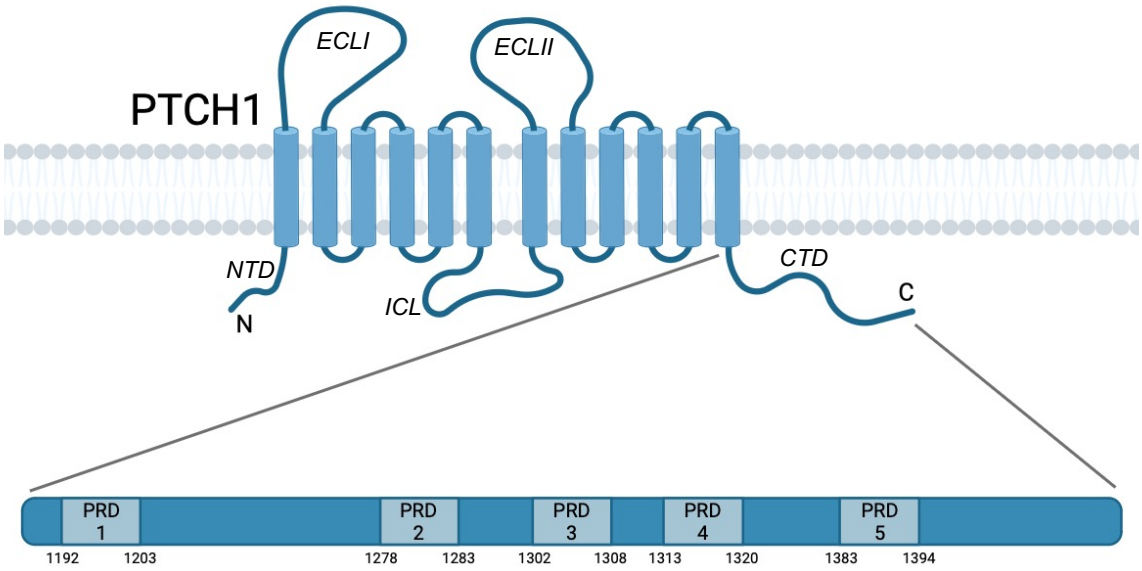

Figure 1.4 PTCH1 topology
Simplified schematic showing PTCH1 topology. 12 transmembrane (TM) helices span the cell membrane, with disordered N-terminal domain (NTD) and C-terminal domain (CTD) intracellularly at either end. TM helices joined by small loops except large intracellular loop (ICL) between TM helices 6 and 7, and large extracellular loops (ECLs) between TM helices 1 and 2, and 7 and 8. Zoom shows location of proline-rich domains (PRDs) along CTD. Created with Biorender.com.

The NTD is a region of PTCH1 that has not been heavily studied. There are no known interactions and the specific function of this region of PTCH1 is not well understood. It is likely that it plays some role in the stability and proper folding of PTCH1, with the residues adjacent to the membrane anchoring the protein and ensuring proper placement of TM helix 1 and allowing proper functional folding of ECLI. Some germline mutations truncating the NTD have been found, around residues 86-97 (Lindström et al., 2006). The germline nature of these mutations suggest that they do not have significant functional effect on the PTCH1 protein, since organisms have survived to adulthood to be able to pass these mutations on to offspring.

A function of the ICL is its co-participation in the oligomerisation of PTCH1. Previously it has been shown that the *Drosophila* homolog of PTCH1 forms trimers (Lu et al., 2006), and studies of human PTCH1 have shown an interaction of the two large cytoplasmic domains of PTCH1, the ICL and CTD, to allow PTCH1 oligomerisation which modulates PTCH1 activity, although does not seem to be necessary for HH signalling regulation (Fleet et al., 2016).

Spanning residues 1176-1447, the CTD extends into the cytosol, allowing it to interact with many intracellular proteins. For example, E3 ubiquitin-protein ligase Itchy homolog (Itch) interacts with a PPXY motif in the PTCH1 CTD and ubiquitinates

K1413 (Chen et al., 2014). This interaction regulates PTCH1 stability via modulating its internalisation and degradation, as well as increasing GLI transcriptional activity.

The CTD of PTCH1 is of interest for novel interactions because it contains 5 proline-rich domains (PRDs) (Figure 1.4) which appear ubiquitously in the eukaryotic proteome. PRDs are hotspots for protein-protein interactions, acting as docking sites for many proteins, particularly in intrinsically disordered regions such as the PTCH1 CTD (Morgan and Rubenstein, 2013, Theillet et al., 2013). Prolines have a context-dependent ability to act either as disorder-promoting residues, or cause compaction of a protein (Mateos et al., 2020), which would support an 'induced fit' mechanism of binding between the CTD and cytosolic interactors.

1.2.2 Structural basis of SHH binding to PTCH1

As previously mentioned, the ECLs of PTCH1 form a domain for HH ligand binding. Studies focussing on SHH have identified two distinct binding interfaces. Figure 1.5 shows the structure (PDB ID: 6E1H) of SHH bound to an asymmetrical dimer of PTCH1 determined by cryo-EM (Qi et al., 2018). The PTCH1 monomer coloured in cyan is denoted as PTCH1 G, since it binds with the globular part of SHH, and the dark blue monomer is PTCH1 P, since it creates an interface with the palmitate of SHH.

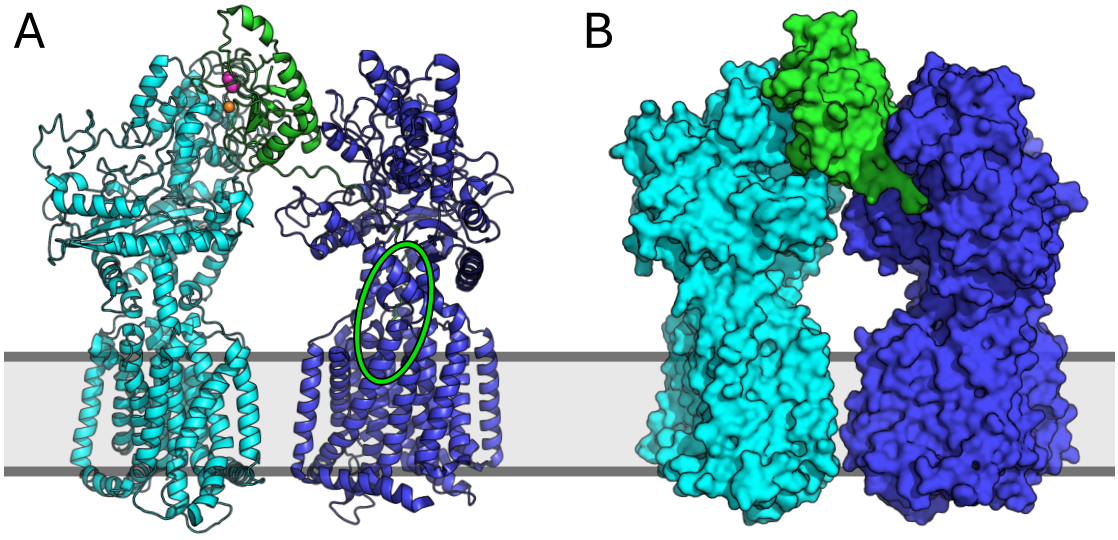

Figure 1.5 SHH ligand in complex with asymmetric PTCH1 dimer
PDB ID: 6E1H. PTCH1 G in cyan, PTCH1 P in blue, SHH in green, calcium ions in pink, Zinc ions in orange. (A) Cartoon representation. Palmitate in SSD circled in green since it is buried in the helical bundle so hard to visualise. (B) Surface representation of A.

Studies before this presented contradictory structures, one reporting an interface between SHH and PTCH1 via SHH helices 1 and 2 coordinating Ca^{2+} ions with ECLI of PTCH1, and another presented an interaction where the palmitate on the N-terminal end of SHH is fed through ECLII and buried in the SSD of PTCH1 (Gong et al., 2018, Qi et al., 2018). In fact, this study demonstrated that both of these interfaces are formed, and each is necessary for maximal canonical signalling in cells.

Structures have shown sterol-like densities within a tunnel of PTCH1 that would equate to a cholesterol-transport tunnel (Zhang et al., 2018). It is suggested that the cholesterol moiety of SHH binds to an extracellular steroid binding site (ESBS) formed between ECLI and ECLII, which would block the cholesterol transporting tunnel of PTCH1 and provide a basis for the SHH-mediated inactivation of PTCH1 and derepression of SMO activity (Qian et al., 2019).

1.2.3 PTCH1 cytosolic interactions

The large, intrinsically disordered ICL and CTD of PTCH1 in the cytosol can form many interactions, in part due to their disorder and thus flexibility, and additionally the large number of PRDs as discussed previously.

The large ICL of PTCH1 is a loop of 150 residues between TM helices 6 and 7. This section of the protein has been identified as a regulator of cell growth and proliferation through its interaction with the cell cycle regulator cyclin B1 (Barnes et al., 2001). Cyclin B1 is important for G2/M phase transition during the cell cycle through its association with cyclin-dependent kinase 1 (CDK1, sometimes referred to as cdc2). The two proteins associate to form M-phase promoting factor (MPF) which translocates to the nucleus during late G2 and promotes mitotic progression by phosphorylation of nuclear substrates (Peter et al., 1990). However, PTCH1 is able to recruit phosphorylated cyclin B1 and prevent its nuclear accumulation. Therefore it is proposed that PTCH1 regulates MPF localisation through its ICL and thus participates in cell cycle control.

The PTCH1 CTD is known to have an ‘interactome’ with many interactions identified and studied, and more being discovered continuously. It has been shown to interact with an autophagy-specific protein ATG101 (Chen et al., 2018, Caballero-Ruiz et al., 2023) which, as part of the unc51-like autophagy activating kinase (ULK) complex, induces autophagy (Mizushima and Levine, 2010). Autophagy is a necessary cellular process which involves degradation of damaged or misfolded proteins and

cellular components, and is induced by stress signals. These targets are engulfed by the autophagosome, a membrane-bound vesicle, which then fuses with lysosomes where degradation of the damaged cargo takes place (Tanida, 2011). In the absence of SHH, the PTCH1-ATG101 interaction attenuates this process.

Another CTD interaction is with a multi-protein complex that includes pro-caspase-9, triggering caspase-9 activation and apoptosis (Mille et al., 2009). A PTCH1 mutant with increased stability has been shown to increase cell death through over-activation of caspase-9 (Chen et al., 2014). Crucially, SHH has been shown to prevent this process by disrupting the interaction of PTCH1 with the protein complex, and therefore increasing cell survival (Chinchilla et al., 2010).

An interaction between the PTCH1 CTD and growth factor receptor-bound protein 2 (Grb2) suggests a potential role of the CTD in modulating ERK activity, since Grb2 scaffolds interactions in the MAPK/ERK pathway. Active PTCH1 decreases ERK activation, which is potentially driven by this CTD-Grb2 interaction (Chang et al., 2010).

1.2.4 PTCH1 post-translational modifications and regulation

Post-translational modifications (PTMs) of PTCH1's CTD add multifunctionality, modulating outputs beyond its canonical role in HH signalling. Some additional CTD interactors not discussed in the previous section include enzymes responsible for adding these modifications. For instance, ubiquitination promotes internalisation and degradation of PTCH1, while negatively regulating the pro-apoptotic activity of PTCH1 (Zhang and Jiang, 2021, Chen et al., 2014).

There are two PPXY motifs in PTCH1, one in the large ICL and one in the CTD (Yue et al., 2014). PPXY (Pro-Pro-X-Tyr, where X is any amino acid) motifs are recognised by WW domains which the Nedd4 family of E3 ubiquitin ligases all contain. The PTCH1 CTD interacts with several of these ubiquitin ligases: Itch, Nedd4, Nedd4-2, Smurf1, Smurf2, and WWP2. However Itch is the preferential E3 ubiquitin ligase for PTCH1, both interacting strongly and inducing the most significant level of ubiquitination out of these enzymes tested (Chen et al., 2014). In the absence of HH, it ubiquitinates K1426 of human PTCH1 (K1413 of mouse Ptch1), and consequently reduces levels of PTCH1 at the plasma membrane, enhances PTCH1 degradation, and therefore activates GLI transcription via canonical signalling.

Ubiquitination of PTCH1 causes internalisation into intracellular vesicles, while a portion of expressed PTCH1 remains at the cell membrane. Stimulation with SHH causes increased ubiquitination, entry into the endocytic pathway, and degradation of PTCH1 (Chen et al., 2014). The precise method of PTCH1 internalisation is not well understood and reports are contradictory. There is evidence to support caveolin-mediated endocytosis, since PTCH1 has been found in lipid rafts associated with caveolin-1 (Karpen et al., 2001), although PTCH1 has also been observed within clathrin-coated pits (Yue et al., 2014). Caveolin-dependent endocytosis is more likely at the ciliary pocket, while clathrin-dependent endocytosis could regulate PTCH1 in the extraciliary plasma membrane. In addition, the mechanism of PTCH1 degradation is not clear. Again there is evidence for different processes, one group indicating a role of autophagy (Yang et al., 2021), and another demonstrating a requirement of the proteasome (Yu et al., 2017).

Phosphorylation of PTCH1 has not been extensively studied to date. Phosphates at T1195 and S1197 were identified by a proteomic study (Shiromizu et al., 2013), and further confirmed in a study within the Hedgehog Lab (Cross, 2023), which identified a role of Erk1 in catalysing this phosphorylation. However, despite the identification of a T1195S mutation in Gorlin syndrome patients (Boutet et al., 2003), the significance of this phosphorylation in PTCH function, regulation, or interactions is has not been identified.

Interestingly, an interaction between PTCH1 and GRK2 has been reported (Jiang et al., 2009). GRK2 is a unique member of the GRK family since lethality has been observed in mice with GRK2 ablated, unlike other members (Jaber et al., 1996). While investigating the relationship between PTCH1 and cyclin B1, they found that following SHH stimulation, GRK2 binds PTCH1 which mediates dissociation of cyclin B1 and therefore promotes nuclear accumulation of cyclin B1. Crucially, the association of PTCH1 with GRK2, a kinase canonically liked to GPCRs, suggests further novel interactions for PTCH1 that may depend on phosphorylation.

1.2.5 PTCH1 as a tumour suppressor

PTCH1 is known to be a tumour-suppressor protein, with its canonical and non-canonical outputs leading to decreases in cancer-forming and -maintaining phenotypes. It commonly carries mutations that lead to loss of function and subsequent cancer formation, predominantly in basal cell carcinoma (BCC) and medulloblastoma (Tang et al., 2010). Additionally, *PTCH1* mutations are common in Gorlin syndrome, also known as nevoid basal cell carcinoma syndrome (NBCCS),

a disorder which causes patients to present with skin lesions, jaw cysts, cerebellar calcification, and developmental issues, and additionally carry a very high risk of developing BCC or medulloblastoma (Lo Muzio, 2008).

The focus of a lot of research in the last few decades has been the association of HH signalling in BCC and medulloblastoma. PTCH1 dysfunction-causing mutations are found in approximately 90% of BCCs and 20% of medulloblastomas (Epstein, 2008, Raffel et al., 1997). Loss-of-function mutations in PTCH1 result in constitutive activation of the HH pathway, which is a common presentation in these diseases (Guo et al., 2013, Yu et al., 2014).

There are several studies that have identified *PTCH1* mutations in a subset of other cancer types. A study of 19 samples of keratocystic odontogenic tumours (KCOTs), which are lesions that affect the jaw, identified 19 *PTCH1* mutations, one of which caused a frameshift within the CTD. Additionally, 30 samples of basaloid squamous cell carcinoma (BSCC) identified a total of 16 *PTCH1* mutations, 13 of which were in the CTD. Furthermore, a study of the relationship between HH signalling and breast cancer recurrence studied tissue samples of 22 patients who suffered from recurrence within 24 months of surgery, and 22 patients who did not. *PTCH1* mutations were significant in both of these samples, however were twice as frequent in the recurrence group (68%) than the control group (34%). A significant proportion of *PTCH1* mutations occur in the CTD. Of 1373 cancer mutations reported in cohorts TCGA-UCEC, TCGA-COAD, and TCGA-STAD in The Cancer Genome Atlas (TCGA) database, 126 are PTCH1 mutations, and of these, 52 occur within the CTD. That means that 41% of PTCH1 mutations are within the CTD, a 2.19-fold increase compared to what would be the expected number if the occurrence of mutations in this domain was relative to its size, which is 19% of the whole PTCH1 protein (Caballero-Ruiz et al., 2023).

Around half of these CTD mutations are frameshift mutations that cause premature truncation of PTCH1 at S1203, R1308, and Y1316. Given the frequency of protein-protein interactions that occur in the PTCH1 CTD, it is unsurprising that these truncations would be pathogenic. For this reason, it is crucial that research into the CTD interactome continues, and identification of as yet unidentified non-canonical signalling streams are characterised and targeted for therapy, since their loss is crucial in human health.

At present, small molecule HH pathway inhibitors targeting SMO exist (vismodegib, sonidegib, and glasdegib) and are used in the treatment of BCC, medulloblastoma

and acute myeloid leukaemia (Von Hoff et al., 2009, Rudin et al., 2009). Unfortunately, results of clinical trials show that the effects of this kind of drug are limited to these cancers, as other solid tumours did not respond to treatment (LoRusso et al., 2011). This gap in current therapeutic options warrants research leading to a much better understanding of the intricacies of HH signalling interactions and regulation. It is likely that targeting PTCH1 either separately or in combination with these current therapies could bridge this gap, since non-canonical signalling is proving to be just as important in cellular maintenance.

1.3 Arrestins

1.3.1 The arrestin family of proteins

Arrestins are a family of proteins involved in many regulatory systems for signalling, first discovered and largely characterised in relation to their regulation of GPCRs. Four proteins form a subfamily: arrestins 1, 2, 3, and 4. They have similar structures yet are distinct and specific in their roles, and are known as the visual and beta arrestins. The other subfamily – alpha-arrestins, or arrestin-domain-containing proteins (ARRDCs) as they are known in mammals – have more recently been discovered and assigned to the arrestin family (Puca and Brou, 2014).

While arrestin 1 (visual arrestin) and arrestin 4 (cone arrestin) are found only in rods and cones of the retina, arrestin 2 (β-arrestin1, βarr1) and arrestin 3 (β-arrestin2, βarr2) are ubiquitously expressed in most mammalian cell types (Lefkowitz et al., 2006). β-arrestins 1 and 2 were first discovered through their binding and desensitising of β2-adrenergic receptors (β2-ARs) (Benovic et al., 1987). Interestingly, β-arrestins 1 and 2 have demonstrated an ability to functionally substitute for one another to some extent. In mice, single βarr1 or βarr2 knockouts demonstrate little phenotypic effect, whereas double knockouts are embryonic lethal (DeWire et al., 2007).

1.3.2 Beta-arrestins

Initially perceived as mere terminators of GPCR signalling, βarrs 1 and 2 (47 and 46 kDa respectively) are now recognised as versatile scaffolds capable of mediating GPCR internalization, trafficking, and an array of G protein-independent signalling pathways. Their structure conveys a degree of conformational flexibility which is what makes these proteins so effective and adaptable for binding to and scaffolding various protein substrates.

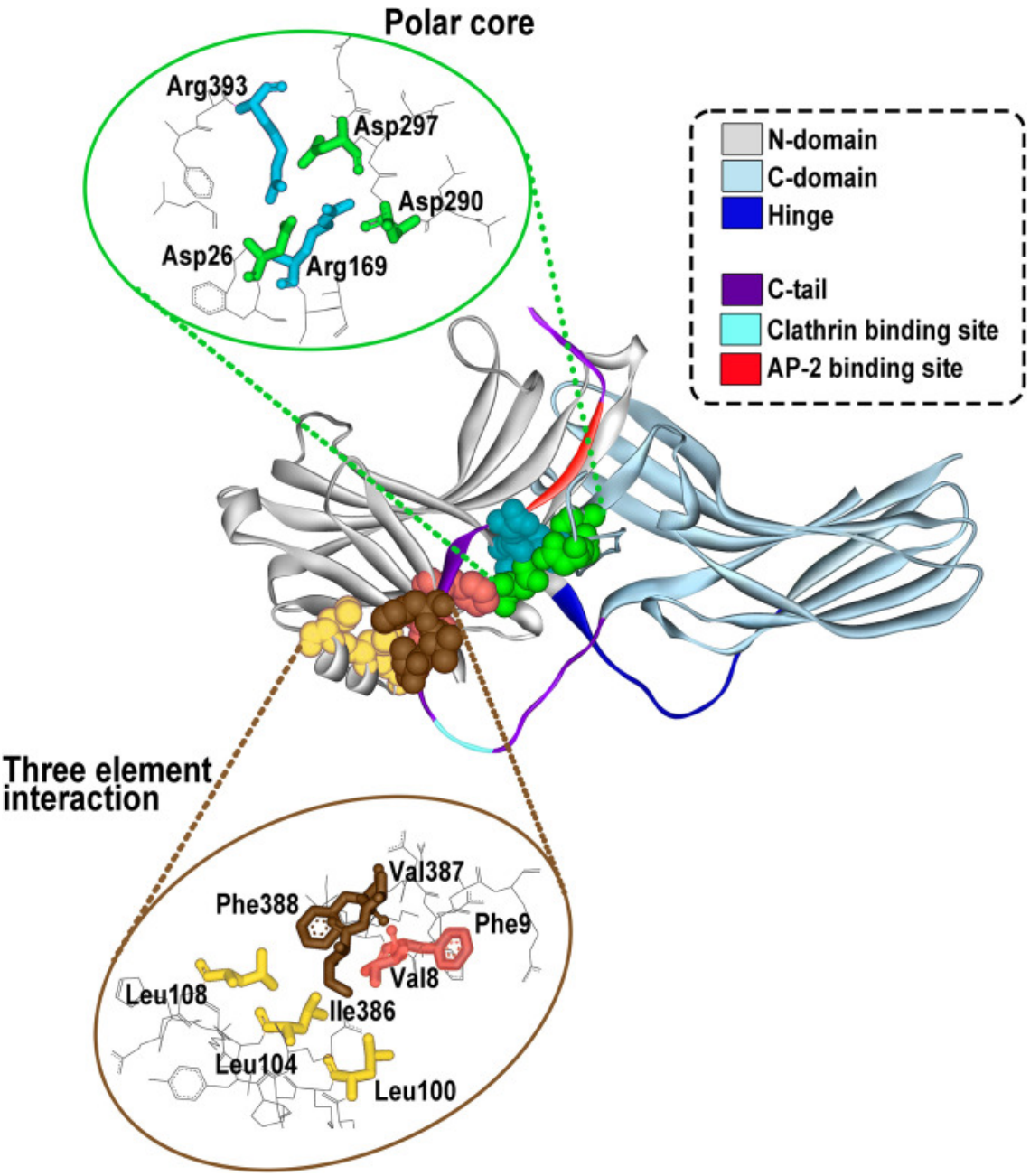

Figure 1.6 General β-arrestin structure
Taken from (Wess et al., 2023). Elements are coloured by the legend in the image and are described in the main body of text.

Figure 1.6 illustrates the key elements of βarr structure (Wess et al., 2023). The two main domains are the N-domain (grey) and the C-domain (blue-grey) and are joined by a hinge region of 12 residues (dark blue). There is a flexible C-tail (magenta) that is anchored to the N-domain via a 'three-element interaction' involving Phe, Leu, and Val residues, in addition to the polar core of Asp and Arg residues. The three-element interaction and polar core stabilise this basal conformation through their interaction with the C-tail, and this is disrupted upon GPCR binding which causes rotation of the N- and C-domain by 20°. Additionally, there are binding sites within

the C-terminus for both clathrin and its adaptor AP2 (light blue and red, respectively).

Traditionally, βarrs are known for GPCR desensitisation which via steric blockade causes G protein uncoupling, preventing GDP/GTP exchange and downstream signalling cascades. This can also lead to the trafficking, recycling, or degradation of GPCRs. Additionally, βarrs act as scaffolds and adaptors to facilitate interactions between other proteins, including non-GPCRs.

1.3.3 GPCR regulation by beta-arrestins

Beta-arrestins are most widely studied regarding their role in regulation of GPCR signalling. GPCRs receive extracellular signals and stimulate activity of adjacent heterotrimeric G proteins via a ligand-induced conformational change of the G protein subunits Gα, Gβ, and Gγ. This conformational change leads to GDP/GTP exchange on the Gα subunit, allowing the Gβ/Gγ dimer to dissociate and the two separate complexes to induce their own signalling cascades. Desensitisation of GPCRs is a 2-step process, firstly the active receptor is phosphorylated by a GRK, and subsequently βarrs bind to the phosphorylated receptor which interferes with GPCR-G protein coupling (Kang et al., 2015).

There are two main interfaces between GPCRs and βarrs. The N-domain binds to the phosphorylated receptor C-tail (Shukla et al., 2013, Zhuo et al., 2014), and the finger loop is able to insert into a cavity within the part of the transmembrane core that protrudes into the cytosol (Kang et al., 2015, Böttke et al., 2020), supported by additional membrane contacts made by the shorter loops of the C-domain (Lally et al., 2017, Staus et al., 2020). It is only the dual interaction with the GPCR C-tail and transmembrane core that blocks G protein coupling, as GPCRs bound to βarrs at the C-tail alone are still able to signal through their G protein partners (Thomsen et al., 2016).

1.3.4 Beta-arrestins and post-translational modifications

Emerging research suggests the complex and varied roles of βarrs are coordinated by post-translational modification of both themselves and their targets. For example, the ubiquitination of βarrs can increase their affinity for membranes and membrane receptors (Shenoy et al., 2007), as well as mediating endocytosis (Lin et al., 2008). The two βarrs additionally can modulate endocytosis of their targets via both ubiquitination and deubiquitination (Shenoy et al., 2001, Jean-Charles et al.,

2016). For example, NOTCH1 ubiquitination and resulting degradation is promoted by βarr1 (Shu et al., 2020).

One study proposed a specific phosphorylation motif common to GPCRs which is required for βarr recruitment (Zhou et al., 2017). They studied 825 GPCRs and found a common "phosphorylation code" that facilitates βarr binding. Of these, 517 receptors are known to recruit βarrs to their C-tails, and 84% of these contained their motif. Additionally, the remaining GPCRs that were not shown to contain a C-tail instance of this code instead had one in ICL3 (intracellular loop 3) which is consistent with the ICL3-dependent binding of many of their family members. They summarised their results as follows: 'a phosphorylation code required for high-affinity arrestin binding is predicted to be *p*x*p*xx*p*/E/D (denoted as short code) or *p*xx*p*xx*p*/E/D (denoted as long code), in which *p* represents a phospho-serine or phospho-threonine and x any amino acid residue, except proline in the second xx occurrence'. These two motifs are combined by the code '*p*x(x)*p*xx*p*/E/D', which forms the basis of much of the research in this thesis.

The GRK isoform GRK2 phosphorylates SMO, inducing recruitment of βarr2 (Chen et al., 2004). This process affects both canonical signalling through GLI and type 2 non-canonical signalling. So far there has been little research characterising any modulation βarrs may have on type 1 non-canonical signalling. Since SMO, GRK2, PTCH1, and βarrs are all able to localise to the cilia and contribute to HH signalling, and a physical interaction between PTCH1 and GRK2 has been demonstrated (Jiang et al., 2009), we hypothesised that βarrs may be recruited to PTCH1 in a manner similar to that following GRK2 phosphorylation of SMO.

1.3.5 Arrestins can associate with non-GPCRs

More recently, β-arrestins have been implicated in signalling processes independent of G protein-mediated signalling. They commonly act as adaptors and scaffolds to bring proteins into close proximity with each other in order to carry out their functions, for example the βarr-mediated localisation of the E3 ligase Mdm2 to ubiquitinate β2-AR (Shenoy et al., 2001).

Research has also suggested that βarrs play a role in regulating the extracellular signal-regulated kinase (ERK) and mitogen-activated protein kinase (MAPK) pathway by scaffolding ERK-GPCR interactions, increasing phosphorylation of cytosolic ERK, and altering the ratio of cytosolic and nuclear ERK to reduce ERK-regulated transcription (Tohgo et al., 2002). This nuclear trafficking ability of βarrs

has been seen in other investigations, including cellular localisation studies of ubiquitin ligase Mdm2 and kinase JNK3 demonstrating their transport by free arrestin (Song et al., 2006).

In fact, both βarrs have been shown to interact with hundreds of other non-GPCR proteins and soluble proteins (Xiao et al., 2007). These include growth factor receptors (Lin et al., 1998), kinases and ligases such as JNK3, c-Raf1 and Mdm2 (Song et al., 2006, Coffa et al., 2011), and messenger proteins like calmodulin (Wu et al., 2006). This thesis will describe a further non-GPCR interaction, PTCH1-βarr1, which has not been reported previously.

Chapter 2

Materials and Methods

Chapter 2

Materials and Methods

2.1 Cell Lines and Culture Procedures

The cell lines used in this project are listed in Table 2.1. HEK293, Ptc1$^{-/-}$ mouse embryonic fibroblast (MEF), and MCF7 cells were cultured in Dulbecco's Modified Eagle Medium (DMEM) with 10 % fetal bovine serum (FBS) (Merck, F7524), 100 U/ml penicillin and 100 µg/ml streptomycin. NIH 3T3 were cultured in the same way with bovine calf serum (BCS) (Merck, 12138C) instead of FBS. All cells were maintained in a humidified incubator at 37 °C with 5 % CO_2.

Cell line	Organism	Cell type	Tissue	Properties/ disease	Maximum passage
HEK293	Human	Epithelial	Embryonic kidney	Adherent	30
MCF7	Human	Epithelial	Breast	Adherent/ adenocarcinoma	20
MEF Ptc1$^{-/-}$	Mouse	Fibroblast	Embryo	Adherent	20
NIH3T3	Mouse	Fibroblast	Embryo	Adherent	20

Table 2.1 Cell lines used in experimental procedures
Table details origin, properties, and maximum passage used for each cell line. All cells were sourced from ATCC, except Ptc1$^{-/-}$ MEFs were gifted from Dr Andrew Scott.

2.2 Freezing and Thawing Cells

Cells were grown to ~80-90 % confluence in a T175 flask, trypsinised, and centrifuged at 200 G for 5 min. Cell pellet was resuspended in 5 mL freezing media (FBS + 10 % DMSO), 1 mL aliquots added to cryovials, frozen stepwise for 1 h at -20 °C and overnight at -80 °C, followed by storage at -80 °C for up to 6 months or in liquid nitrogen for long-term storage.

2.3 Cell Counting

Where necessary, cells were prepared for counting using a small aliquot of trypsinised and resuspended cells before centrifugation, and diluted 1:1 with 0.4% Trypan Blue. Ten µL were added to each side of a Countess™ Cell Counting Chamber Slide (Invitrogen, C10228) and counted using a Countess™ II Automated Cell Counter (Invitrogen, AMQAX1000). Live cell concentration was recorded and

doubled to correct for Trypan Blue dilution. Cells were then resuspended in appropriate media at a concentration relevant to the experiment.

2.4 Transient cell transfection using Transporter 5 (T5)

HEK293 cells were transfected using Transporter 5® Transfection Reagent (T5) (Generon, 26008-50), a polyethylenimine (PEI)-based commercial reagent. Cells were seeded at $3x10^5$ cells/mL to reach approximately 80 % confluence after 24 h. Before transfection, media was changed to DMEM + 2 % FBS without antibiotics, and incubated for around 1 h before addition of transfection mixes. Transfection mixes were prepared by adding the relevant volume of NaCl to each tube (Table 2.2), followed by the DNA dilution (generally all plasmid stock solutions were diluted to 250 ng/µL for equal volume additions). Tubes were briefly vortexed, followed by addition of T5, vortexed for 5 seconds, centrifuged briefly to collect all reagent at the bottom, and incubated at room temperature (RT) for 20 min to allow formation of PEI-DNA complexes. After incubation, the transfection mix was added dropwise to each well, and the plates gently rocked to distribute the complexes before placing back in the incubator. Unless the experiment requires different conditions, after 4-6 h the media was changed back to DMEM + 10 % FBS without antibiotics to improve cellular protein production. Cells were incubated for 24 h before addition of treatments or harvesting.

Culture vessel	Culture volume (mL)	NaCl (µL)	Plasmid DNA (µg)	T5 (µL)
6-well plate	2	200	2	8
10cm dish	10	1000	10	40

Table 2.2 Transfection volumes for T5
Table contains volumes of reagents used for T5 transfection in one well of a 6-well plate or a 10 cm dish.

2.5 Transient reverse transfection using TransIT-X2

$Ptc1^{-/-}$ MEFs used in Gli-Luciferase assays were reverse transfected into 96-well plates using TransIT-X2® Dynamic Delivery System (Mirus Bio, MIR 6000). The following describes preparation for one well, and volumes we scaled up accordingly. Cells were trypsinised, centrifuged and resuspended in DMEM + 10 % FBS without antibiotics at a concentration of $3.5x10^5$ cells/mL. Transfection complexes were prepared in parallel by adding sequentially adding 0.1 ug DNA and 0.3 uL TransIT-X2 to 9 uL OptiMEM in an eppendorf tube, and, pipette mixing in between, and incubating for 15-30min. One hundred uL of the cell suspension was

added to the tube containing the complexes, pipette mixed and transferred to each well.

2.6 Transient transfection of MCF7 cells using Lipofectamine 3000

MCF7 cells were seeded in DMEM + 10 % FBS at a concentration of $5x10^5$ cells/mL in 12- or 6-well plates. . After 24 h, cells were transfected using Lipofectamine 3000. Briefly, 2 tubes were prepared for each condition as indicated in Table 2.3. Then, Tube 1 and Tube 2 were mixed together and incubated at room temperature for 15min, followed by addition of the final mixture dropwise to each well. Cells were generally incubated for 24 h before treating or harvesting.

Culture plate type	Culture volume (µL)	Tube 1		Tube 2		
		OptiMEM (µL)	L3000 (µL)	OptiMEM (µL)	DNA (ng)	P3000 (µL)
96 well	100	5	0.3	5	100	0.2
24 well	500	25	1.5	25	500	1
12 well	1000	50	3	50	1000	2
6 well	2000	100	6	100	2000	4

Table 2.3 Transfection volumes for forward transfection of MCF7 cells using Lipofectamine 3000
Table details volumes used for transfecting each size of well used for experiments in this thesis.

2.7 Transient reverse transfection using Lipofectamine 3000

Lipofectamine 3000 was used to transfect $Ptc1^{-/-}$ MEFs for Erk/Akt activity western blots and co-localisation studies, and to transfect MCF7 cells where specified. Both cell lines were reverse transfected, but with different seeding densities and transfection reagent volumes, following optimisation of experimental conditions. $Ptc1^{-/-}$ MEFs and MCF7 cells were used at seeding densities of $6x10^5$ cells/mL and $4x10^5$ cells/mL respectively. The manufacturer protocol for creating the transfection complexes was followed, with the transfection volumes for each cell line and culture vessel used detailed in Table 2.4. Once transfection complexes were incubated for 15 min, one ‘well volume’ of cell suspension was added and pipette mixed gently before adding to the wells.

Cell line	Culture vessel	Culture volume (µL)	Tube 1		Tube 2		
			OptiMEM (µL)	L3000 (µL)	OptiMEM (µL)	DNA (ng)	P3000 (µL)
Ptc1$^{-/-}$ MEF	24 well plate	500	25	1.5	25	500	1
	4 well slide	1000	100	6	100	2000	4
MCF7	96 well plate	100	5	0.2	5	50	0.1

Table 2.4 Transfection volumes for reverse transfection with Lipofectamine 3000
Volumes of each reagent used for Lipofectamine 3000 reverse transfection of Ptc1$^{-/-}$ MEFs and MCF7s in each well size used for experiments in this thesis.

2.8 Shh conditioned media preparation and use

For immunoprecipitation experiments of Shh-treated cells, requiring a large number of cells , Shh or control conditioned media was used instead of recombinant Shh. To prepare conditioned media, 10cm dishes of HEK293 cells were transfected as described (2.4) with a control plasmid (pcDNA 3.1+) or Shh-expressing plasmid (pRK5-Shh), without changing the media back to 10 % FBS. After 48 h, conditioned media was collected in falcon tubes, centrifuged at 200 G for 5 min to remove any cell debris, and then syringe filtered. The resulting conditioned media was stored at 4 °C for up to 2 weeks. For use in experiments, conditioned media was diluted 1:5 in serum-free DMEM.

2.9 Chemicals

Where cells were treated with recombinant protein or chemicals, a standard concentration was used Table 2.5. However, the treatment time varied and is detailed in each experiment.

Chemical	Company	Cat. no.	Conc used
rShh	Bio-Techne	8908-SH-005/CF	100 ng/mL
Cycloheximide	Thermofisher Scientific	J66004.XF	100 µg/mL
Cmpd101	Cayman Chemical	26808	30 µM

Table 2.5 Chemicals used in experiments
Table details source of each chemical and concentrations used in experiments for this thesis. rShh (recombinant human Shh, high activity) contains a C-terminal cholesterol modification and an N-terminal palmitate.

2.10 Bacterial transformation

Chemically competent DH5α cells were prepared in-house with $CaCl_2$ and stored at -80 °C in 50 µL aliquots. For transformation, aliquots were thawed on ice for 10-20 min. Five µL DNA at a concentration of approximately 10 ng/µL was added per tube, gently flicked to mix, and placed on ice for 20 min. To heat shock, tubes were placed in a water bath at 42 °C for 30 seconds, and placed immediately back on ice for 2 min. Then 500 µL SOC media was added per tube, and incubated for 1 h at 37 °C with shaking (200-220 rpm). Generally, 200 µL of the inoculum (occasionally more or less if expecting a low or high efficiency) was spread on LB-Agar plates containing appropriate antibiotics, and once dried, placed in an incubator at 37 °C overnight.

2.11 DNA extraction and sequencing from bacterial preparations

DNA minipreps were prepared by picking single colonies from an LB-Agar plate, growing overnight in 10 mL LB broth + specific antibiotics, and pelleting at 3000 G for 10 min at 4 °C. DNA was extracted and purified using the Promega Wizard® Plus SV Minipreps DNA Purification System (A1330). Briefly, the pellet was resuspended, sequentially mixed with Cell Lysis, Alkaline Protease and Neutralisation Solutions, and centrifuged. The lysate was passed through a Spin Column, washed, and eluted with Nuclease-Free Water.

Where necessary, plasmid maxipreps were prepared using glycerol stocks or fresh bacterial transformations. Bacteria were grown for 16-20 h in 250 mL LB containing specific antibiotics, collected by centrifugation at 6000 G for 15 min at 4 °C, followed by DNA extraction and purification using the Qiagen HiSpeed® Plasmid Maxi Kit (12663). Briefly, the pellet was resuspended in Buffer P1, mixed sequentially with Buffers P2 and P3 and transferred to a QIAfilter Cartridge. After incubation, lysate was filtered into an equilibrated HiSpeed Tip, then washed and eluted. DNA was precipitated with isopropanol, filtered, washed with 70 % ethanol, and eluted with nuclease-free water. Plasmid concentration and purity was determined by A260/A280 using a Nanodrop spectrophotometer.

2.12 Site-Directed Mutagenesis

All PCR-based mutagenesis was performed with the Q5® Site-Directed Mutagenesis Kit (NEB, E0554S) with the exception of S1203A, S1280A, S1223A, and T1229A, for which the QuikChange II XL Site-Directed Mutagenesis Kit (Agilent Technologies, 200522) was used.

Most mutants were made from myc-tagged PTCH1 in pCS2+MT, either wild-type or previously mutated where indicated. The only exception to this was an mCherry-PTCH1 (SATA) construct, which was made by mutation of mCherry-PTCH1 (in a plasmid previously cloned from pEGFP-N3) for bioimaging, using the same primers as the myc-tagged PTCH1 (SATA) version.

Mutations were generated by PCR amplification using overlapping primers with a mutated sequence or primers that left a gap in the sequence (for generating deletions). PCR conditions used were those recommended by the manufacturers (Phusion® High-Fidelity PCR Kit, NEB, E0553S). Details of primers used for site-directed mutagenesis are listed in Table 2.6. Several colonies in selective LB agar were picked and miniprepped (Promega A1330). Mutagenesis confirmed via Sanger sequencing (Genewiz UK). Positive mutants were then maxiprepped (Qiagen 12643) for use in experiments.

PTCH1 mutation	**Template**	**Sequence 5'-3' (FW, RV)**
S1203A	Wild-type	CTGAGCCACCCCCCGCCGTGGTCCGCTTCGCCATG
		CATGGCGAAGCGGACCACGGCGGGGGGTGGCTCAG
ΔS1216-S1223	Wild-type	GTGCGTGTGGCCGGGCGGCATGGCGAAG
		GAGTATAGTTCCCAGACGACAGTGTCAGGCCTCAGC
ΔS1227-S1235	Wild-type	ACTATACTCCGAGTCGGAGGAATCAGACCCGCTGTG
		GAGGAGCTTCGGCACTACGAGGCCCAGCAG
S1280A	Wild-type	CATCACCCACCCGCCAACCCGAGACAGCAG
		CTGCTGTCTCGGGTTGGCGGGTGGGTGATG
ΔS1216-S1223, ΔS1227-S1235	ΔS1216-S1223	GAGGAGCTTCGGCACTAC
		ACTATACTCGTGCGTGTG
Δ1216-1235	Wild-type	GTGCGTGTGGCCGGGCGGCATGGCGAAG
		GAGGAGCTTCGGCACTACGAGGCCCAGCAG
S1223A, T1229A (SATA)	Wild-type	GTTCCCAGGCGACAGTGTCAGGCCTCA
		TATACTCCGCGTCGGAGGAATCAGACCC
S1223A	Wild-type	GAACTATACTCCGCGTCGGAGGAATC
		GATTCCTCCGACGCGGAGTATAGTTC
T1229A	Wild-type	CTGACACTGTCGCCTGGGAACTATAC
		GTATAGTTCCCAGGCGACAGTGTCAG
S1223E	Wild-type	TTCCTCCGACGAAGAGTATAGTTCCCAGACGACAG
		TCAGACCCGCTGTGCGTG
T1229E	Wild-type	TAGTTCCCAGGAAACAGTGTCAGGC

		TACTCCGAGTCGGAGGAA
S1223E, T1229E	Wild-type	TTCCCAGGAAACAGTGTCAGGCCTCAGC
		CTATACTCTTCGTCGGAGGAATCAGACCC
S1223D, S1226D, T1229E	T1229E	TATGATTCCCAGGAAACAGTGTC
		CTCATCGTCGGAGGAATCAGACCC
S1223A, S1226A, T1229A	S1223A, T1229A	CGCGGAGTATGCGTCCCAGGCGAC
		TCGGAGGAATCAGACCCG

Table 2.6 Primers used for site-directed mutagenesis
Table details the mutation of PTCH1, template used, and forward and reverse primer sequences.

2.13 Gli-Luciferase Assay

We used Promega's Dual-Luciferase® Reporter Assay System (E1960) to measure Gli transcriptional activity. For Gli-luciferase assays in Ptc1$^{-/-}$ MEFs, we used a Firefly-luciferase reporter plasmid under control by a minimum γ-crystalline promoter, with 8 tandem repeats of the HNF-3β gene Gli-binding site (p8XGBS-Luc). Luminescence of the sample reporter was normalised to a control plasmid encoding a Renilla-luciferase reporter under a strong constitutive SV40 promoter (pRL-SV40) to calculate the specific Gli activity. In addition to these constructs, we co-transfected WT or mutant PTCH1 variants as well as a Shh-expressing plasmid or empty plasmid to assess the effect of Shh.

Cells were reverse transfected in 96 well plates as described (2.5) with the different constructs comprising the following proportions of the total DNA added: 5 % pRL-SV40, 45 % p8XGBS-Luc, 25 % Shh or empty vector, 25 % PTCH1 test plasmid or empty vector.

After 24 h, cells were serum starved in DMEM + 0.5 % FBS for a further 16-24 h (overnight) to allow formation of primary cilia before assaying the Gli luciferase activity. Cells were lysed with 1x Passive Lysis Buffer (E1941) (30uL per well) at room temperature with orbital shaking for 15 min. Luciferase activity was measured according to the manufacturer's protocol. Briefly, 10 µl lysate was added to 50 µL LAR II reagent to measure Firefly luciferase activity, followed by addition of 50 µl Stop&Glo solution to measure Renilla-luciferase, using a Glomax 20/20 luminometer (Promega). Gli-luciferase activity was calculated as Firefly luciferase/Renilla luciferase to account for transfection efficiency, and reported as raw ratios of fold changes compared to empty plasmid (control).

2.14 Western Blotting

For western blotting, cells were either lysed directly in 1X Laemmli buffer, or in IP buffer, after which Laemmli buffer was added to a final dilution of 1X for whole cell lysates, or 2X for IP samples. Protein samples in Laemmli buffer were loaded into SDS-containing polyacrylamide:bisacrylamide (29:1 v/v) gels of 6-14 % acrylamide depending on separation required. Gels were run in 1X SDS-Tris-Glycine running buffer at 80 V, then at 120 V once all samples entered the resolving gel. Proteins were transferred to a PVDF membrane in ice-cold 1X transfer buffer (Tris-Glycine) containing 20 % methanol at 50-65 V for 2 h.

Membranes were washed in TBST (Tris-buffered saline with 0.1% Tween-20), and blocked for 1 h in 5% milk or BSA in TBST depending on antibody requirements. Primary antibodies were diluted in blocking buffer (Table 2.7), and incubated overnight at 4 °C with gentle shaking. Membranes were then washed 3 times with TBST for 5 min at room temperature.

Secondary HRP-conjugated and HRP-GAPDH antibodies were then incubated at RT for 1h, diluted in the same blocking buffer as primary antibody (Table 2.8). Membranes were washed again 3 times in TBST before imaging. Membranes imaged using Thermo Scientific SuperSignal substrate in a BioRad ChemiDoc XRS+ with ImageLab software. Densitometry analysis was performed using ImageJ.

Target	Species	Dilution	WB diluent	Company	Product code
myc	Rabbit	1:8000 (WB) 1:250 (IP)	5% milk in TBST	Proteintech	16286-1-AP
myc	Mouse	1:1000	5% milk in TBST	CST	2276
HA	Mouse	1:20,000	5% milk in TBST	Proteintech	66006-2-Ig
GFP	Mouse	1:5000	5% milk in TBST	Proteintech	66002-1-Ig
βarr1/2	Rabbit	1:1000	5% BSA in TBST	CST	4674
Erk1/2	Rabbit	1:1000	5% BSA in TBST	CST	4695
pErk1/2	Rabbit	1:1000	5% BSA in TBST	CST	4376
β-actin	Mouse	1:4000	5% BSA in TBST	Sigma	A2228
GAPDH	n/a (HRP-tagged)	1:10,000	5% milk in TBST	Proteintech	HRP-60004

Table 2.7 Primary antibodies used in western blots and IPs
Table contains details of each antibody target, species, dilution, and source. WB = western blot. CST = Cell Signalling Technology. Dilution is WB unless specified otherwise.

Anti-species	Dilution	Company	Product code
Rabbit	1:3000 (WB)	Bio-Rad	1721019
Mouse	1:3000 (WB)	Bio-Rad	172-1011
Conformation-specific rabbit	1:2000 (WB)	CST	5127S

Table 2.8 Secondary antibodies used in western blots
Table contains details of the target species, dilution used, and source.

2.15 βarr1/2-based co-immunoprecipitation assays

HEK293 cells were seeded in 6-well plates and transfected with indicated constructs using T5, as described in section 2.4. 24 h after transfection, cells were placed on ice and washed with PBS, then scraped in 200 µL IP buffer (50 mM Tris HCl pH 7.5, 150 mM NaCl, 1 % IGEPAL, 0.5 % sodium deoxycholate, 1 mM EDTA, 2.5 mM MgCl2, 1 % protease inhibitor cocktail (Abcam ab270055), 1 % phosphatase inhibitor cocktail 3 (Sigma P0044), 0.4 mM PMSF). Lysates were transferred to a pre-chilled tube and gently rotated at 4 °C for 30 min, followed by centrifugation at 17,000 G, at 4 °C for 15 min. A 50 µL aliquot of the supernatant was separated as "whole cell lysate fraction", supplemented with 10 µL 6X Laemmli buffer and heated at 45 °C for 30 min. The remaining 150 µL lysate was incubated with 0.75 µL βarr1/2 antibody (Cell Signalling, #4674) under rotation at 4 °C for 1.5h. Following formation of antibody-target complexes, 4.5 µL of Protein G Dynabeads™ (Invitrogen, #10004D) were added and rotated at 4 °C for a further 1 h. The magnetic beads were immobilised using a magnetic rack and washed 3 times with 300 µL IP buffer . After the last wash was removed, the beads were resuspended in 18 µL 2X Laemmli buffer and heated 45 °C 30 min. Samples were stored at -20 °C where necessary before being used for western blot analysis.

2.16 IP-MS/MS

Samples to be used for phospho-ID by mass spectrometry were first immunoprecipitated from cell lysates as described previously, with the following changes: cells were grown and transfected in 10 cm dishes, lysed in 700 µL IP buffer containing extra phosphatase inhibitor cocktail (5%) and incubated with 7 µL anti-myc antibody (Proteintech, #16286-1-AP) and 25 µL protein G dynabeads. The beads for phospho-ID were washed only once with 1 mL IP buffer and resuspended in 100 µL 2X Laemmli buffer before being processed for mass spec. Trypsin digestion and mass spectrometry performed by the mass spec staff at the University of Leeds using an Orbitrap Exploris 240 funded by the NIHR (NIHR200633). Analysis of MS data was performed using Peaks software by Dr. Sri Ranjani Ganji.

2.17 Co-localisation studies

For co-localisation studies, cells were reverse transfected (2.7) onto fibronectin-coated 4 well µ-Slides (IBIDI, 80426) with mCherry-tagged wild-type or mutant PTCH1 and βarr1-GFP (at a 90 % PTCH1 : 10% βarr1 ratio). 24 h after transfection, cells were serum starved in DMEM + 0.5 % FBS for a further 24 h. After this, cells were rinsed with PBS then 1 mL of serum-free media containing vehicle control or rShh at a concentration of 100ng/mL was added for 30min at 37 °C with 5 % CO_2. Then, cells were rinsed with PBS and fixed in 4 % paraformaldehyde for 15 min at room temperature.

Following another PBS wash, cells were incubated for 5 min with 300 nM DAPI diluted in 1 mL PBS . Cells were washed thoroughly and 1 mL PBS added for imaging or storage at 4 °C. Cells were imaged using a Zeiss LSM880 + Airyscan confocal microscope with ZEN (black edition) software (University of Leeds, Wellcome Trust WT104918MA), processed and analysed using Fiji.

For co-localisation analysis, GFP (βarr1-GFP) and mCherry (PTCH1-mCherry) channels were used. In the GFP channel, cells were traced using the selection tool, as close as possible to the membrane. The Coloc 2 analysis option was used to measure co-localisation between the two channels, and Pearson's R value (no threshold) recorded, since background was negligible and cells were outlined tightly to remove external factors.

2.18 WST-1 cell viability assay

Cell proliferation reagent WST-1 (Roche 5015944001) was used to assess cell viability following transfection with PTCH1 constructs. MCF7 cells were seeded and transfected in 6-well plates using Lipofectamine 3000 as described (2.6). At 6 h post-transfection, cells were trypsinised, counted, centrifuged and re-seeded at a density of $3x10^5$ cells/mL in four 96-well plates. One plate was prepared for assessing viability at each time point (0 h, 24 h, 48 h, 72 h).

At the indicated time point, 10 µL of WST-1 reagent was added per well to one plate, wrapped in foil, shaken for 30 s, and placed back in the incubator for 1 h. After 1 h, the plate was shaken again for 1 min, and the difference in absorbance at λ=450 minus λ=650 was measured using a HIDEX Sense microplate reader. Background (media only) was subtracted, and the absorbance of all wells was normalised to

empty plasmid (pcDNA) to allow comparison between time points and individual experiments.

2.19 Clonogenic assay

MCF7 cells were reverse transfected in a 12-well plate as described (2.6). After 24 h, cells were trypsinised, centrifuged, and resuspended to a single cell suspension by thoroughly mixing and passing through a cell strainer. Cells were seeded at a density of 750 cells/well in a 6-well plate in DMEM with 10 % FBS and 1 % P/S. Cells were incubated for 13 days to allow visible colonies to form. Wells were rinsed with PBS, fixed in 100 % methanol for 15 min, then stained with a 0.005 % crystal violet solution for 20 min. The solution was rinsed off with MilliQ water, wells allowed to dry, images taken, and colonies counted manually.

2.20 Apoptosis assay

Apoptosis was measured by assessment of caspase 3/7 activation using the Caspase-Glo 3/7 Assay System (Promega, G8091). Briefly, MCF7 cells were reverse transfected as described (2.7) in triplicate in a white opaque TC treated 96-well plate, including blank wells containing just media. After 6 h, when cells had attached, media was changed to DMEM + 10 % FBS containing either 100 ng/mL rShh or vehicle and incubated for further 16 h (overnight).

Caspase-Glo® 3/7 Assay was performed according to the manufacturer protocol, adding 100 µL Caspase-Glo® reagent per well, shaking for 30 s, incubating at room temperature for 1 h, then measuring luminescence in a HIDEX Sense microplate reader. Signal from wells containing only media was subtracted as blank.

2.21 End-point cycloheximide chase assay

MCF7 cells were transfected in 24-well plates as described in section 2.6, with myc-tagged wild-type PTCH1 and PTCH1 SATA. One plate was prepared for assessing protein levels at each time point (0 min, 30 min, 1 h, 2 h, 4 h). A day after seeding, serum was reduced to 0.5% FBS for a further 24h. On day 3, 100 µg/mL cycloheximide (CHX) was added to the wells and pre-incubated for 30 min, followed by addition of vehicle or 100 ng/mL rShh. At times 0, 30 min, 1 h, 2 h, and 4 h, a plate was removed from the incubator and placed on ice, wells rinsed with cold PBS, and lysed in 50 µL 1X Laemmli buffer. All samples were sonicated and heated at 45 °C for 30 min, before storing at -20 °C to be subsequently analysed by western blot.

2.22 Continuous cycloheximide chase assay

MCF7 wells were seeded in 96-well, TC-treated, black walled, clear bottom plates (PerkinElmer, 6005182) to be transfected according to section 2.6 with mCherry-tagged PTCH1 constructs using Lipofectamine 3000. After 24h, serum was reduced to 0.5 % FBS for 24 h. Before assaying, media was replaced with 80 µL phenol-red free, serum-free, CO_2-independent DMEM (Gibco, 18045-054) containing 100 µg/mL cycloheximide, and imaged using an ImageXpress Pico Automated Cell Imaging System to collect the 0 h time point. The imaging chamber is maintained at 37 °C. Then, 100 µg/mL cycloheximide with or without 100 nM Shh were added in a volume of 20 µL to total 100 µL in the wells. Plates were placed back inside the imager, and images were taken every 30 min for 6 h to monitor fluorescence changes.

Results were quantified using the Pico integrated software, CellReporterXpress® by Molecular Devices®, version 2.8.2.669. The '2 stained area' analysis was used. Parameters were defined as follows. Nuclei: DAPI channel, Segmentation parameters; Intensity = 15, Min Width = 5, Max Width = 30. PTCH1: TRITC channel, cytoplasm, Segmentation parameters; Intensity = 30, Min Width = 2, Max Width = 30. Data reported is Positive cell total integrated intensity, normalised by % Positive cells, expressed per well as a percentage of the 0 min time point.

2.23 AlphaFold 3 simulations

Protein-protein interaction simulations were run on the AlphaFold 3 server available at https://golgi.sandbox.google.com. Protein sequences were entered and post-translational modifications added where applicable. Files were downloaded, and crystallographic information files (cif) opened in PyMOL for visualisation, colouring, analysis, and image export. Values for ipTM and pTM were obtained from the 'summary confidences' text files (.json). Polar contacts were found via PyMOL, and counted manually.

Chapter 3

Identification of a novel interaction between PTCH1 and beta-arrestins

Chapter 3

Identification of a novel interaction between PTCH1 and beta-arrestins

3.1 Introduction

Hedgehog signalling is a highly regulated signalling network, with a multitude of downstream effects and phenotypic outcomes. The receptor SMO is a GPCR involved in HH signalling, canonically signalling through the GLI family of transcription factors, as well as having effects on other processes such as calcium oscillations, cytoskeletal regulation, and cAMP production (Belgacem and Borodinsky, 2011, Bijlsma et al., 2007, Ogden et al., 2008). βarrs are known to regulate several signalling pathways, generally by binding to and desensitising GPCRs. Naturally, βarrs have been studied in the context of SMO signalling and it has been documented that βarr2 binds to the SMO C-tail following GRK2 phosphorylation (Meloni et al., 2006).

The reaction centre for HH signalling is the primary cilium, an antenna-like organelle that controls many HH interactions through transport along the axoneme. Previous members of the lab investigated the role of cilia in Hedgehog signalling, which produced results leading to this project. The group used siRNA in various contexts to investigate the effect of βarrs, and found results that implicated βarrs in SMO-independent contexts including ERK activation and PTCH1 turnover in response to Shh (Figure 3.1, Figure 3.2).

ERK signalling has been linked to enhanced growth and migration via upregulated Hedgehog signalling (Lu et al., 2012, Liu et al., 2018). The mechanism of Hedgehog-mediated ERK upregulation is not fully understood. Some reports indicate a SMO-dependent mechanism that sees up- and down- regulation of ERK activity via SMO agonist purmorphamine and antagonist KAAD-cyclopamine respectively (Liu et al., 2018), most likely by changes in GLI-mediated gene expression. Others demonstrate a SMO-independent mechanism that functions in the presence of KAAD-cyclopamine and absence of SMO (Chang et al., 2010). This group proposes that a PTCH1 CTD interaction with Grb2 could mediate ERK activity through non-canonical Hedgehog signalling.

The best-known function of βarrs is their binding to the C-tails of active (ligand associated), GRK-phosphorylated GPCRs, and aside from G protein

desensitisation, signal for many processes including GPCR internalisation, degradation, and trafficking. As a GPCR, SMO is influenced by βarr2 in the same way. Internalisation of SMO has been blocked by siRNA of GRK2 or βarr2 (Chen et al., 2004), and overexpression of *Drosophila* orthologues of either GRK2 or βarr destabilises SMO (Cheng et al., 2010). It has also been shown experimentally (Kovacs et al., 2008) that βarrs are important for trafficking of SMO to the cilia, although later studies did not show the same, and instead suggest that SMO can accumulate in the cilia independent of βarrs (Pal et al., 2016).

There have been many non-GPCR proteins found within the βarr interactome (Xiao et al., 2007), so relating the non-canonical effects of βarrs to PTCH1-dependent signalling was plausible. Additionally, a study of GRK involvement in early development of zebrafish demonstrated an interaction between GRK2 and PTCH1 (Jiang et al., 2009), which does not require Shh but is enhanced by addition of ShhN. As the primary kinase for phosphorylation-dependent recruitment of βarrs to SMO and other GPCRs, this points to a similar mechanism potentially leading to recruitment of βarrs to PTCH1 through GRK2-mediated phosphorylation of the PTCH1 CTD. The specific role of phosphorylation in βarr recruitment to PTCH1 will be explored in Chapter 4.

One of the functions of GPCR-βarr interaction is the degradation of the receptor. GPCR degradation is coordinated by both binding of βarrs and ubiquitination of the receptor and the bound βarr. In the case of PTCH1, our lab has shown that the basal turnover is regulated by ubiquitylation of the PTCH1 CTD by the E3 ubiquitin ligase ITCH, which increases its internalisation and degradation (Chen et al., 2014). Therefore we postulate that βarrs may play a role in PTCH1 degradation through mediating its ubiquitination. Since both ITCH binding and PTCH1 ubiquitination both occur on the CTD, it is possible that there would be a relationship with a CTD-βarr interaction, and so this hypothesis was explored initially before gaining further insight into the binding mechanism of PTCH1-βarrs.

In this chapter, I will review preliminary work by previous members of the lab which uncovered a new interaction between PTCH1 and βarrs. This work will be built on by using co-immunoprecipitation studies investigating the role of PTCH1 ubiquitination on this interaction and uncovering further detail into the binding region of βarrs to PTCH1 through truncation of the PTCH1 CTD. Combined with the existing data, this will create a base to allow methodical interaction characterisation in further chapters.

3.2 Aims

1. Identify roles for βarrs in non-canonical Hedgehog signalling.
2. Investigate an interaction between PTCH1 and βarrs.
3. Assess the consequence of PTCH1 ubiquitination in this interaction.
4. Identify the βarr binding domain of PTCH1.

3.3 Results

3.3.1 βarr1 negatively regulates Shh-mediated ERK activation

This project was built upon preliminary work by previous members of our lab. While exploring the role of ciliary trafficking in non-canonical Hedgehog signalling, unusual results were obtained suggesting a role for βarrs independently of SMO. Previous results (Ho Wei et al., 2018) had shown that ERK and AKT are still activated in Kif3a knockout MEFs (without cilia), stimulated either by purmorphamine or purified ShhN (N-terminal Shh fragment, C25II). Furthermore, unpublished data shows ERK activation by SHH in $SMO^{-/-}$ MEFs and in the presence of KAAD-cyclopamine, a potent SMO inhibitor. Therefore, the possibility of PTCH1-dependent pathways of ERK activation through Shh stimulation was investigated.

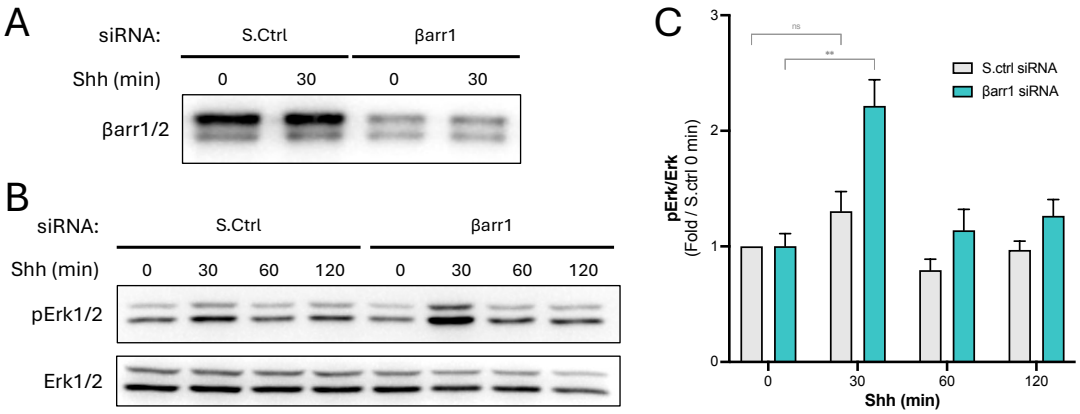

Figure 3.1 βarr1 silencing enhances Shh-mediated ERK activation
Experiments performed by Dr Mohammad Arastoo. (A) Depletion of βarr1 protein levels by siRNA treatment. (B) Kif3a-/- MEFs were treated with either control siRNA or siRNA targeting βarr1 before serum starving. Cells were stimulated with 0.25 μg/mL Shh at the indicated times before lysis. Prepared lysates were analysed for ERK and pERK protein levels by western blot. Densitometric analysis of n=3 independent experiments summarised in (C). 2-way ANOVA analysis: ns, not significant; ** P>0.005. Error bars= SEM.

Figure 3.1 shows that silencing of βarr1 increases Shh-mediated ERK activation. After confirming knockdown of βarr1 is significant and maintained following Shh treatment (panel A), ERK activation was observed over 2 hours (panels B and C). A

spike in ERK activity is observed at 30 min Shh treatment when βarr1 has been knocked down via siRNA. Since Shh binds to and inhibits PTCH1, and ERK activation in response to Shh is independent of SMO, this indicates a PTCH1-specific role for βarr1.

3.3.2 βarrs enhance Shh-mediated PTCH1 degradation

Since a key role for βarrs in other pathways is signalling for degradation of proteins, the group investigated the effect of βarr1/2 silencing on Shh-induced PTCH1 degradation. Using siRNA to knock down βarr1 and βarr2 or a scrambled control siRNA for 72h prior to the experiment, cells were stimulated with Shh and lysed over the course of 6 hours to monitor Shh-mediated degradation of PTCH1 and any effect of βarr1/2 suppression.

Indeed, Figure 3.2 shows decreased Shh-mediated degradation of PTCH1 when βarr1/2 protein levels are reduced. This result indicates a significant regulatory role for βarrs in Hedgehog signalling, negatively regulating the stability of PTCH1, potentially through a direct interaction similar to GPCR-βarr signalling.

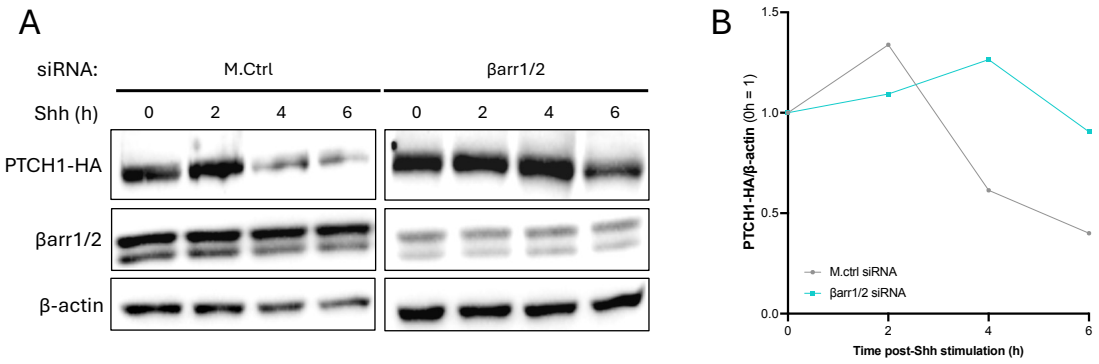

Figure 3.2 βarr silencing reduces Shh-mediated PTCH1 degradation
Experiments performed by Ioanna Georgiou. (A) siRNA-treated cells lysed at indicated time points following addition of Shh and western blotted to measure protein levels. (B) Densitometric analysis of A.

3.3.3 βarr1/2 bind to the PTCH1 C-terminal domain

Given the effect of βarrs on the degradation of PTCH1, and the reported finding that GRK2 interacts with PTCH1 (Jiang et al., 2009), the group hypothesised that there is a direct interaction, most likely to the large, disordered C-terminal domain of PTCH1, since βarrs typically bind to the C-tails of GPCRs to signal for receptor degradation in their well-studied canonical role. This was investigated using co-

immunoprecipitation of PTCH1 constructs overexpressed with βarrs in HEK293 cells.

Figure 3.3 A shows a very strong interaction between HA-PTCH1 and βarr1-GFP. There is also a weak signal for βarr2-YFP in the immunoprecipitate. We concluded that the primary interaction with PTCH1 is likely to be with βarr1. The βarr2-YFP construct did have less protein in the input, but the immunoprecipitation was still considered very weak. This reflects the well-documented finding that βarr1 and βarr2 have distinct functions but can functionally substitute for one another to some extent, for example in the case of single or double knockouts of mice (DeWire et al., 2007). Therefore βarr1 became the primary interest in the context of βarr interactions with PTCH1. This was later explored using protein-protein interaction prediction software in Chapter 6, where the weaker interaction of βarr2 with PTCH1 is explained by a lack of predicted binding *in silico*.

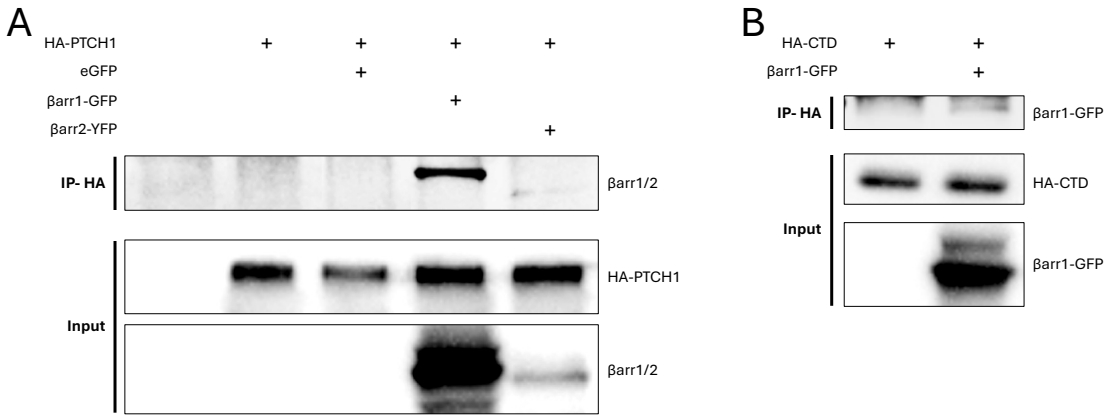

Figure 3.3 βarrs bind full length PTCH1 and PTCH1 CTD alone
(A, B) Indicated constructs were expressed in HEK293 cells and lysed 24h later. Proteins immunoprecipitated using HA antibody and analysed via western blotting. Assays performed by Ioanna Georgiou.

An additional co-immunoprecipitation of βarr1-GFP with a construct that expressed the PTCH1 CTD alone was performed to see if this domain is sufficient for βarr binding. Indeed, panel B shows that βarr1-GFP binds to the PTCH1 CTD when expressed as a separate construct. This CTD construct expressed the sequence of mouse Ptc1, but the human and mouse PTCH1/Ptc1 CTDs have very high sequence homology. Therefore, while this result is slightly limited to the constructs that were available, the results are comparable and are confirmed later in this chapter. From this, we were able to restrict the search for specific binding regions to the PTCH1 CTD.

3.3.4 Ubiquitination of PTCH1 is not required for βarr1 binding

Using the results from the previous members of the lab as a foundation, I began my project, which is to investigate the atypical role of βarrs in the regulation of Hedgehog signalling.

Ubiquitination often plays significant roles in βarr signalling. This ubiquitination can be to the receptor, the βarr itself, or both. Since this project is primarily focussed on the receptor PTCH1 and its binding site for βarr1, a role of receptor ubiquitination in the formation of the PTCH1-βarr interaction was investigated. Ubiquitination of βarr1 itself was not investigated here, but could form an additional branch of this project in the future.

For this, I used a different co-immunoprecipitation approach compared to the assays performed by previous members of the lab. First, to investigate the interaction at near endogenous protein level, the interaction of endogenous βarr1 and 2, which are highly expressed as shown before, with PTCH1 was measured. Myc-PTCH1 was transfected because endogenous levels are too low for detection with a specific antibody by western blot. Secondly, the reverse immunoprecipitation was performed, by pulling down endogenous βarr1/2 using a sensitive antibody (Cell Signalling, #4674), followed by detection of PTCH1 in the immunoprecipitate. After optimisation of this technique, I developed a protocol that was used in all of the βarr1/2-based co-immunoprecipitations in this project. Additionally, from this point onwards, only human PTCH1 constructs were used .

Figure 3.4 shows the co-immunoprecipitation of myc-PTCH1 variants via endogenous βarr1/2. Human PTCH1 is very efficiently immunoprecipitated by endogenous βarrs, as expected following the initial experiments using mouse PTCH1. In this experiment, two mutants were tested, both of which prevent PTCH1 CTD ubiquitination. The only ubiquitination site in the human PTCH1 CTD is K1426, so a point mutation of this site, K1426R, blocks its ubiquitination. Arginine is a common choice for ubiquitination-blocking mutations as it is a similar size to lysine and preserves the positive charge so causes minimal structural disruption, while blocking ubiquitination due to its lack of a free, reactive amino group. Additionally, the binding motif for ITCH, the E3 ubiquitin ligase responsible for ubiquitination of K1426, is the PPXY motif present at P1313-Y1316. To block ITCH binding, the tyrosine residue was mutated to threonine, Y1316T. Threonine maintains the polar properties of tyrosine through the hydroxyl group, and can form hydrogen bonds, so again blocks binding of the E3 ligase while minimising structural differences that

may be introduced by residues such as alanine, glycine, or phenylalanine. Preventing the binding of ITCH not only blocks K1426 ubiquitination, but ablates any processes that may occur if ITCH, while bound to PTCH1, ubiquitinates βarrs as they come into close proximity with PTCH1.

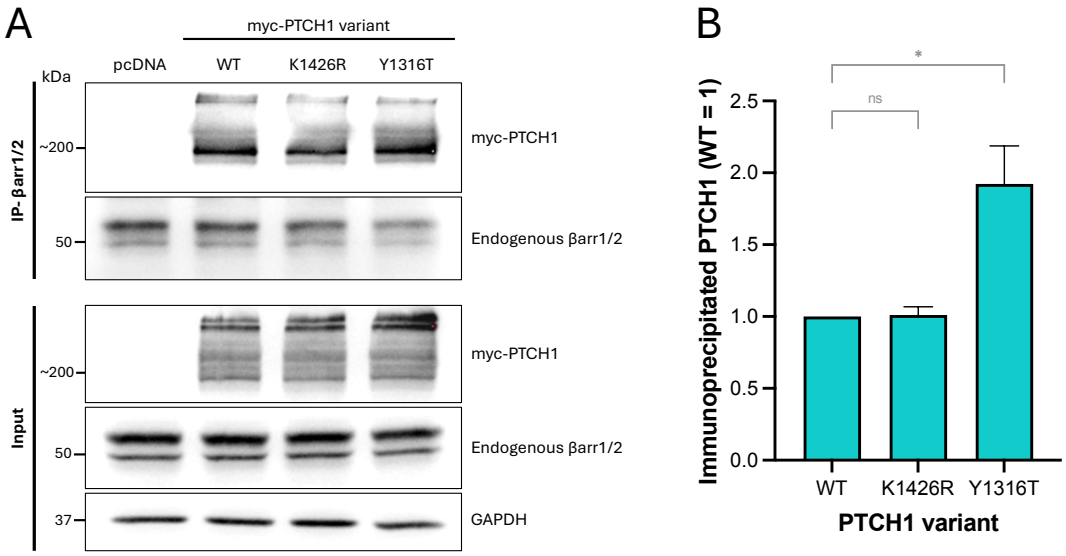

Figure 3.4 βarrs bind PTCH1 independently of CTD ubiquitination
Indicated constructs transfected into HEK293 cells for 24h, lysed, and immunoprecipitated with βarr1/2 antibody before western blotting. (A) Representative western blot with densitometric analysis of n=4 independent repeats shown in (B). Error bars= SEM.

As shown in Figure 3.4, disruption of the ubiquitination of the CTD of PTCH1 has no effect on βarr1/2 binding. The K1426R mutation very clearly does not affect βarr binding to PTCH1, indicating that PTCH1 ubiquitination is not required for interaction with βarr1/2. An increase in binding can be seen for the PTCH1 Y1316T mutant. Since the inhibition of PTCH1 CTD ubiquitination alone (K1426R) did not affect PTCH1-βarr interaction, I ruled out PTCH1 CTD ubiquitination as a requirement for the interaction itself. Therefore, the increased interaction to the PTCH1 Y1316T mutant could be explained by two mechanisms. Firstly, this increase could instead be due solely to ITCH binding and is ligase activity-independent. The binding of ITCH to the PTCH1 CTD may cause steric hindrance, partially blocking βarrs from binding the CTD. Alternatively, ITCH may ubiquitinate βarrs in addition to the PTCH1 CTD, particularly when brought into close proximity if both are able to bind to PTCH1 simultaneously. Ubiquitination of βarrs could have several functions, one being to signal for its release from the receptor (Shenoy and Lefkowitz, 2003), therefore preventing their ubiquitination might prolong interaction with PTCH1. Notwithstanding, we can conclude that neither ubiquitylation of K1426 nor ITCH binding at the PPXY motif is needed for PTCH1-βarr interaction. Given these findings, phosphorylation of the CTD as a requirement for PTCH1-βarr

interaction, similar to typical GPCR recruitment of βarrs, was later explored in Chapter 4.

3.3.5 βarrs bind in the region S1203-R1308 of PTCH1

Having established the lack of requirement of PTCH1 CTD ubiquitination for βarr binding, I aimed to further characterise the interaction in the CTD and identify the region of interest. Unlike the previous assays where a mouse CTD construct was shown to co-immunoprecipitate βarr1-GFP, the endogenous βarr1/2-based co-immunoprecipitation approach was used to explore the interaction of human PTCH1 with serial truncations of the CTD.

These truncations were based on mutations commonly seen in cancer (Caballero-Ruiz et al., 2023). They are denoted as 1316*, 1308*, and 1203*, where frameshift mutations truncate the PTCH1 protein at Y1316, R1308, and S1203 respectively. It can be seen in Figure 3.5 that residues Y1316-1447 are not required for βarr binding to PTCH1. In addition, the PTCH1 region 1308-1316 has only a minor role on βarr binding, as insignificant changes are observed in the levels of co-immunoprecipitation for 1316* and 1308* compared to wild-type. However, in a PTCH1 mutant truncated at S1203, almost all binding was lost. From this it was concluded that a region limited by residues S1203-R1308 is required for βarr binding to the PTCH1 CTD. This region became the region of interest for further experiments to identify a specific binding site in Chapter 4.

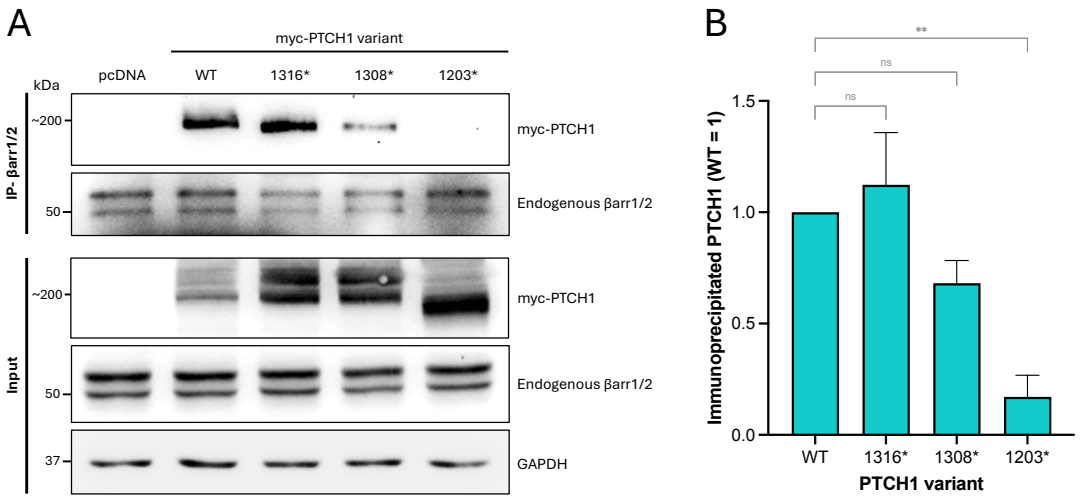

Figure 3.5 βarrs require PTCH1 region S1203-R1308 for binding
Indicated constructs transfected in HEK293 cells and lysed for βarr1/2-based immunoprecipitation 24h later for western blotting. (A) Representative western blot. (B) Densitometric analysis of n=3 independent repeats. Error bars= SEM.

3.4 Discussion

This chapter outlines a novel interaction of βarrs with PTCH1, which indicates new roles for βarrs in Hedgehog signalling and cancer. Here, I built on preliminary findings obtained by Dr Mohammad Arastoo and Ioanna Georgiou, previous members of our lab.

Investigations into extraciliary Hedgehog signalling produced data that suggested SMO-independent roles for βarrs. We observed increased Shh-mediated ERK activation upon knockdown of βarr1, even in $SMO^{-/-}$ cells. This indicates that βarr1 negatively regulates ERK signalling through PTCH1. Following this, the group found that knockdown of βarrs significantly increased the stability of PTCH1 following Shh stimulation. This further suggested a direct link between βarrs and PTCH1, where βarrs negatively regulate PTCH1 stability, increasing its Shh-mediated degradation.

It seems that binding of both Shh and βarrs to PTCH1 causes significant PTCH1 turnover, and it is possible that following βarr1 knockdown, the enhanced stability of PTCH1 could be the cause of the enhanced ERK signalling observed, rather than a direct PTCH1-ERK mechanism. However it is also plausible that adaptor proteins such as Grb2 may bind to the PTCH1 CTD in close proximity to βarr1, causing a competitive inhibition of one another and therefore enhanced ERK activation when βarr1 levels are decreased.

Guided by these findings and the reported interaction between PTCH1 and GRK2 (Jiang et al., 2009), the group hypothesised a direct interaction between PTCH1 and βarrs. They established that βarr1-GFP can bind to full length mouse PTCH1 as well as the CTD alone. This interaction is atypical, since PTCH1 is different from GPCRs, the canonical targets for βarrs, in many ways. It has distinct structural features and functional roles. PTCH1 is comprised of 12 TM helices where GPCRs have 7 TM domains. This results in a different topology, with 2 bulky extracellular domains and 3 large cytosolic domains, unlike the single extra- and intra-cellular domains formed by the N- and C-tails of GPCRs respectively. Additionally, PTCH1 is active under basal conditions and is inactivated by Hedgehog ligands DHH, IHH, or SHH, while GPCRs are activated by association to their ligands. Furthermore, where GPCRs have coupled G-proteins which are desensitised by βarr recruitment to the GPCR C-tail, PTCH1 is not known to couple to G proteins.

Despite these differences, PTCH1 also has characteristics that create parallels with other known βarr interactors. Firstly, βarrs have been found to experimentally bind

to other non-GPCR membrane-bound proteins, for example VE-cadherin and T cell surface glycoprotein CD3 zeta chain (CD247) (Hebda et al., 2013, Fernández-Arenas et al., 2014). Additionally, although active under basal conditions and inactive in the presence of ligand, the activity of PTCH1 is 'switchable', as is that of GPCRs. This would allow for tightly regulated activity-dependent recruitment of βarrs to the PTCH1 CTD, which in GPCR recruitment occurs when the receptor is active. Another similarity is the dynamic binding domains formed by the C-tails of both PTCH1 and GPCRs. Both are intrinsically disordered, and subject to PTMs, making them adaptable targets for effector proteins such as βarrs.

I built on this initial discovery by assessing the ability of human PTCH1 to interact with βarrs via endogenous βarr1/2-based co-immunoprecipitations. I found that human PTCH1 indeed interacts with endogenous βarrs, and this interaction is not dependent on ubiquitination of the PTCH1 CTD. Mutation of the ubiquitination site, K1426R, does not affect the level of interaction observed. A 2-fold increase in PTCH1-βarr binding can be seen when the binding motif for ITCH, the E3 ubiquitin ligase responsible for the ubiquitination of K1426, is disrupted via Y1316T mutation. However, this increase is not an effect of lack of PTCH1 ubiquitination , but instead likely caused by either lack of steric hindrance of ITCH binding or by decreased ITCH ubiquitination of βarrs and stabilisation of the βarr-PTCH1 interaction.

There is some evidence that the hypothesis of ITCH causing steric hindrance may be true. The interactions of PTCH1 with ITCH and βarrs is dynamic, and so they are not always in direct competition which is why we do not see a highly competitive 'one or the other' binding scenario, and βarrs are still able to bind to a significant extent when the ITCH binding motif is intact. However, ubiquitous disruption of the ITCH binding site and removal of the ligase from the PTCH1 CTD allows βarrs to freely bind without competition from ITCH and so an increased amount of PTCH1 in the immunoprecipitate is observed. It is therefore concluded that ubiquitination is not required for βarr binding to PTCH1; however, ITCH binding to an area proximal to the βarr binding site exerts a measurable inhibition which limits the extent to which βarrs are able to interact with PTCH1. To determine if this is the case, co-immunoprecipitation of ITCH could be performed using PTCH1 with a point mutation that prevents βarr binding, which would be expected to show increased ITCH binding compared to wild-type PTCH1, as this would demonstrate the competition between ITCH and βarrs for PTCH1 binding. However this was beyond the scope of this project.

I further narrowed down the region of interest for the binding of βarrs to the CTD of PTCH1. Truncation of the CTD revealed that residues S1203-R1308 are necessary for βarr binding, as truncation of residues downstream of R1308 did not affect the levels of interaction observed in co-immunoprecipitations, but removal of these residues significantly reduced binding to almost undetectable levels.

It could be argued that the previous speculation on the role of ITCH binding to the PTCH1 CTD and its steric inhibition of βarr binding does not apply following the results of the co-immunoprecipitations of truncated PTCH1. Truncation at R1308 removes the ITCH binding site (P1313-Y1316) so ITCH does not bind to this mutant, and truncation at Y1316 leaves the binding motif at the very end of the CTD meaning it is unlikely that ITCH binds as proteins often need stabilising residues surrounding their binding sites to form stable interactions. Despite this, these mutants show similar βarr binding levels as the wild-type, as opposed to the increased levels of binding seen from the Y1316T mutant. It could be true that the increase in βarr binding caused by Y1316T mutation is caused by a different process, however it is also likely that truncation of the CTD involves removal of many residues that could form stabilising structure upon binding of βarrs, and so the increase in binding from the absence of ITCH is negated by the removal of these stabilising segments of the protein, and instead we see a net neutral effect.

Together, this chapter has confirmed an interaction between PTCH1 and βarrs, primarily βarr1, in the region S1203-R1308 of the PTCH1 CTD. This is a novel interaction which implicates βarrs in non-canonical Hedgehog signalling and cancer. In Chapter 5, I will explore this further, isolating the specific binding motif for the PTCH1-βarr interaction, and the mechanism through which this occurs.

Chapter 4

The mechanism of β-arrestin recruitment to the PTCH1 C-terminal domain

Chapter 4

The mechanism of β-arrestin recruitment to the PTCH1 C-terminal domain

4.1 Introduction

In Chapter 3 I built on preliminary work to characterise a strong interaction between βarrs and the CTD of PTCH1. Through truncation of the CTD, I identified a region between PTCH1 residues S1203 and R1308 which is essential for binding. In this chapter, I aim to further characterise this interaction by identifying the specific binding site within PTCH1 and delving into the mechanism by which the two proteins are able to interact.

The identification of a PTCH1-GRK2 interaction (Jiang et al., 2009) suggests a potential role of GRK2 in βarr recruitment to PTCH1 though a phosphorylation-dependent mechanism. I developed the hypothesis that PTCH1-βarr recruitment mirrors that of GPCR-βarr recruitment, in which the "canonical" role of GRK2 is to phosphorylate active GPCRs for βarr binding and desensitisation.

There are three common factors involved in GPCR-βarr recruitment. Firstly, the receptor is activated by its ligand. Secondly, the GPCR C-tail is phosphorylated by a GPCR kinase (GRK). Finally, βarrs bind to the phosphorylated C-tail according to a common 'code' or motif described in a study that compared the phosphorylated sequences of 825 GPCRs (Zhou et al., 2017). This chapter will investigate the role of these processes in the PTCH1-βarr interaction to establish a binding mechanism.

In Chapter 3 I demonstrated that PTCH1 ubiquitination at K1426 by the E3 ubiquitin ligase Itch is not required for βarr binding. However, PTCH1 is known to be phosphorylated on the CTD (T1195, S1197) (Cross, 2023), and there may be other phosphorylation sites that exist within the CTD. It is entirely possible that the identified βarr binding region, S1203-R1308, is phosphorylated in a manner similar to GPCRs by GRK2 or another kinase to allow βarr recruitment.

For GRK-dependent phosphorylation to take place in GPCRs, the receptors must first be activated. GPCRs agonists binding to the receptors cause conformational changes in the TM domain that are translated to the C-tail, which are necessary for G protein activation. In contrast to GPCRs, PTCH1 is active under basal conditions in the absence of ligand, and is deactivated upon binding of any of the Hedgehog

ligands, for example SHH. We hypothesised that there is a relationship between SHH binding to PTCH and the level of βarr recruitment. Since both ligand (SHH) binding and PTCH1 activation are mutually exclusive, βarr recruitment is predicted to be induced either by SHH binding, or PTCH1 activation (absence of SHH).

The reported PTCH1-GRK2 association presents the likelihood that PTCH1 residues are phosphorylated by GRK2. This would reinforce the parallels proposed between GPCR and PTCH1 recruitment of βarrs. Jiang et al studied this interaction in the context of Cyclin B1 regulation by PTCH1 (Jiang et al., 2009). They reported that the GRK2-PTCH1 interaction is enhanced by SHH stimulation, and inhibits Cyclin B1 association to PTCH1 which increases nuclear accumulation of Cyclin B1.

Jiang reported that this function is independent of GRK2's kinase activity. However, a simple explanation of this is that kinase-dead GRK2 binds to the phosphorylation site that regulates βarr recruitment and simply prevents binding of other proteins in the vicinity that do not depend on phosphorylated motifs, such as Cyclin B1. Alternatively, other GRK isoforms, such as the closely related paralog GRK3, could also associate with PTCH1 and perform the separate role of phosphorylation for βarr recruitment.

The research of Zhou et al into the recruitment process of βarrs to GPCRs (Zhou et al., 2017) helped lead the investigation into their association with PTCH1. A key element of this process is the phosphorylation of the GPCR C-tail. They examined GPCRs to identify a common phosphorylation 'code' required for the high-affinity binding of βarrs. The code is based on the primary sequence of the protein, and includes phosphorylation at three key residues: *p*x(x)*pxxp*/E/D, where '*p* represents a phospho-serine or phospho-threonine and x any amino acid residue, except proline in the second xx occurrence'.

Their initial characterisation was based on 9 well studied GPCRs, through which they derived the set of phosphorylation codes. They then expanded their search to 825 GPCRs annotated in the UniProt GPCR proteome. Their analysis of phosphorylation codes found that 96% of these GPCRs contain possible instances of the code. Additionally, a search of the code in non-GPCR membrane proteins with C-tails found several proteins that had experimentally been shown to interact with βarrs.

They reported the consistency between the code they derived and studies *in vivo* and *in vitro* highlighting the requirement for three receptor-attached phosphates for arrestins to bind with high affinity (Mendez et al., 2000, Vishnivetskiy et al., 2007). Of the 9 initial GPCRs, all C-tails contained at least one complete phosphorylation code except that of β2AR, which instead contained multiple partial codes. This is consistent with the well documented observation that the β2AR C-tail binds arrestins with low affinity (Oakley et al., 2000, Shukla et al., 2014, Wisler et al., 2007). Analysis also showed a strong correlation between the classification of the GPCR superfamily based on their arrestin-binding abilities and the occurrence of complete phosphorylation codes, with the higher binding affinity found in class B receptors containing multiple complete phosphorylation codes, compared to the weaker binding class A receptors which contained a maximum of one complete phosphorylation code, or partial codes, or none at all.

In this chapter, I explore the recruitment process of βarrs to PTCH1. Guided by common mechanisms of GPCR recruitment, I assessed the requirements for the PTCH1-βarr interaction. I hypothesised that, similar to GPCR recruitment, βarrs are recruited to active PTCH1 following GRK-mediated phosphorylation of the CTD according to common phosphorylation codes, which in turn induces βarr binding.

4.2 Aims

1. Identify the minimal PTCH1 binding site for βarr1/2;
2. Assess the requirement of phosphorylation of the interaction site for binding;
3. Assess the effect of Shh, the inactivating ligand of PTCH1, on the PTCH1-βarr interaction;
4. Identify a candidate kinase that promotes the PTCH1-βarr interaction.

4.3 Results

4.3.1 The PTCH1 CTD contains many candidate motifs for βarr binding

Based on the hypothesis that βarrs are recruited to PTCH1 via a similar mechanism to GPCR recruitment, I began by looking at potential phosphorylation motifs in the CTD of PTCH1. I used a kinase prediction software (NetPhos 3.1 by DTU Health Tech) to generate a list of candidate residues for phosphorylation-dependent βarr binding. One caveat of this approach is that the software does not make predictions for GRK2 or GRK3, which are the lead candidate kinases for this phosphorylation based on the research by Jiang et al (Jiang et al., 2009). However, it does make 'unspecific' predictions for residues that are likely to be phosphorylated but does

not know by which kinase, so I continued with the current software with this in mind. Table 4.1 summarises kinase predictions made for all serine and threonine residues in the entire PTCH1 CTD, although the region of interest as identified in Chapter 3 is S1203-R1308.

Residue	Kinase(s)			Residue	Kinase(s)			
S1185	unsp			S1292	DNAPK			
T1195	unsp	GSK3		S1326	unsp	CKI		
S1197	unsp	CDK5	GSK3	T1327	-			
S1203	unsp			S1331	unsp			
T1214	-			S1334	PKC			
S1216	unsp			S1346	-			
S1218	unsp	CKII	CDK1	S1354	-			
S1220	CKII			T1355	-			
S1221	unsp	CKII	CDK1	S1359	-			
S1223	unsp	CDK1		S1360	-			
S1226	-			T1369	CDK1			
S1227	DNAPK	ATM		T1370	-			
T1229	unsp	CDK1		T1372	-			
T1230	unsp	CaM-II		S1374	unsp			
S1232	unsp			S1376	-			
S1235	unsp	CKI	CKII	T1378	PKC			
T1259	-			T1404	CKI	CKII		
S1267	unsp	CDK1		S1425	unsp	PKA	PKG	RSK
T1268	-			S1444	unsp	PKA		
S1274	unsp			S1445	PKB	unsp	PKA	RSK
S1280	unsp	PKC	GSK3	S1446	-			
S1290	-							

Table 4.1 Kinase predictions
Predictions of kinases that may phosphorylate serines and threonines in the PTCH1 CTD using NetPhos 3.1 by DTU Health Tech (Blom et al., 2004). Predictions are limited to the following kinases: ATM, CKI, CKII, CaM-II, DNAPK, EGFR, GSK3, INSR, PKA, PKB, PKC, PKG, RSK, SRC, CDK1, CDK5 and p38MAPK, and 'unsp' represents a non-specific prediction.

I focussed on the region between residues 1203-1308 given that previous experiments had demonstrated that βarrs bind in this region. This identified 20 predicted phosphorylated residues mainly constrained to the 1216-1235 region. To facilitate analysis of these potential sites, I decided to create small deletions to eliminate several predicted phosphosites at once. I made two small deletion mutants of full-length PTCH1 (ΔS1216-S1223 and ΔS1227-S1235), removing each

of these clusters of residues, and a third with both sites deleted. Hereafter, S1216-S1223 will be referred to as Site 1 and S1227-S1235 as Site 2. I also included two point mutations, S1203A and S1280A. S1203 is a residue affected in many cancer cases, usually as a frameshift mutation. S1280 has also been implicated in some cancer cases, and had multiple kinase predictions so I included this in the initial screening as well. Information on these mutations was found largely in the database generated by The Cancer Genome Atlas (TCGA) database: https://www.cancer.gov/tcga.

4.3.2 Deletions of putative phospho-residues reduces βarr1/2 binding

I assessed the effect of deleting these clusters of putative phospho-residues via co-immunoprecipitation of mutant PTCH1 variants with endogenous βarr1/2, using full-length wild-type PTCH1 as the positive control, and also including the two truncation mutants at either end of the section we have previously identified as the βarr-binding region, S1203* and R1308*. S1203* is a negative control as it loses almost all binding, and R1308* is essentially a secondary positive control.

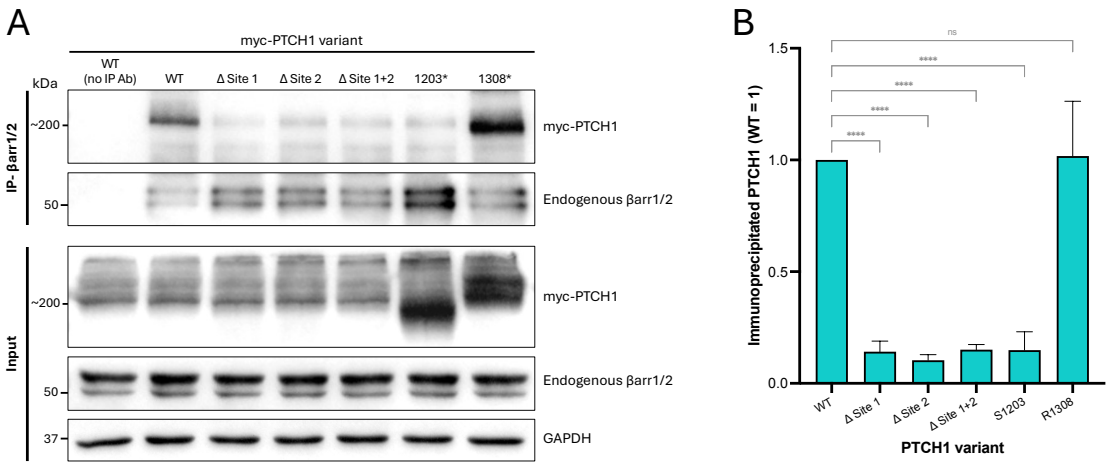

Figure 4.1 Small deletions of Ser/Thr clusters reduces βarr1/2 binding
Δ Site 1 has S1216-S1223 deleted, Δ Site 2 has S1227-S1235 deleted, and Δ Site 1+2 contains deletions S1216-S1223 and S1227-S1235. HEK293 cells were transfected with indicated constructs, and lysates immunoprecipitated with anti-βarr1/2 antibody for endogenous βarr1/2 and whole cell lysates and immunoprecipitates were probed for the presence of PTCH1 (anti-myc) and βarr1/2 by western blot. Negative control 'no IP Ab' had no anti-βarr1/2 antibody added to the lysates. Representative western blot (A) and densitometric analysis of n=4 independent repeats (B). 2-way ANOVA analysis: ns, not significant; ****P<0.0001. Error bars= SEM.

Figure 4.1 shows that all three deletion mutants show equal reduction in binding with endogenous βarr1/2 by co-immunoprecipitation, comparable to the S1203* mutant. This implies that at least one residue in each of the two deletion sites are

essential for βarr binding. Neither of the two point mutants, S1203A nor S1280A, showed a significant change in βarr binding (preliminary data, not shown), so these residues were not investigated any further.

4.3.3 A common βarr phosphorylation code exists in PTCH1 region of interest

The phosphorylation code identified by Zhou et al as crucial for high-affinity βarr binding in both GPCRs and non-GPCR βarr-binding membrane proteins led the next part of the search. As seen in Figure 4.2, the consensus GRK phosphorylation motif, *p*x(x)*pxxp*/E/D, can be found in several areas of the human PTCH1 sequence. It is also found in *Drosophila* Ptc, suggesting conservation of βarr recruitment to PTCH1 across species.

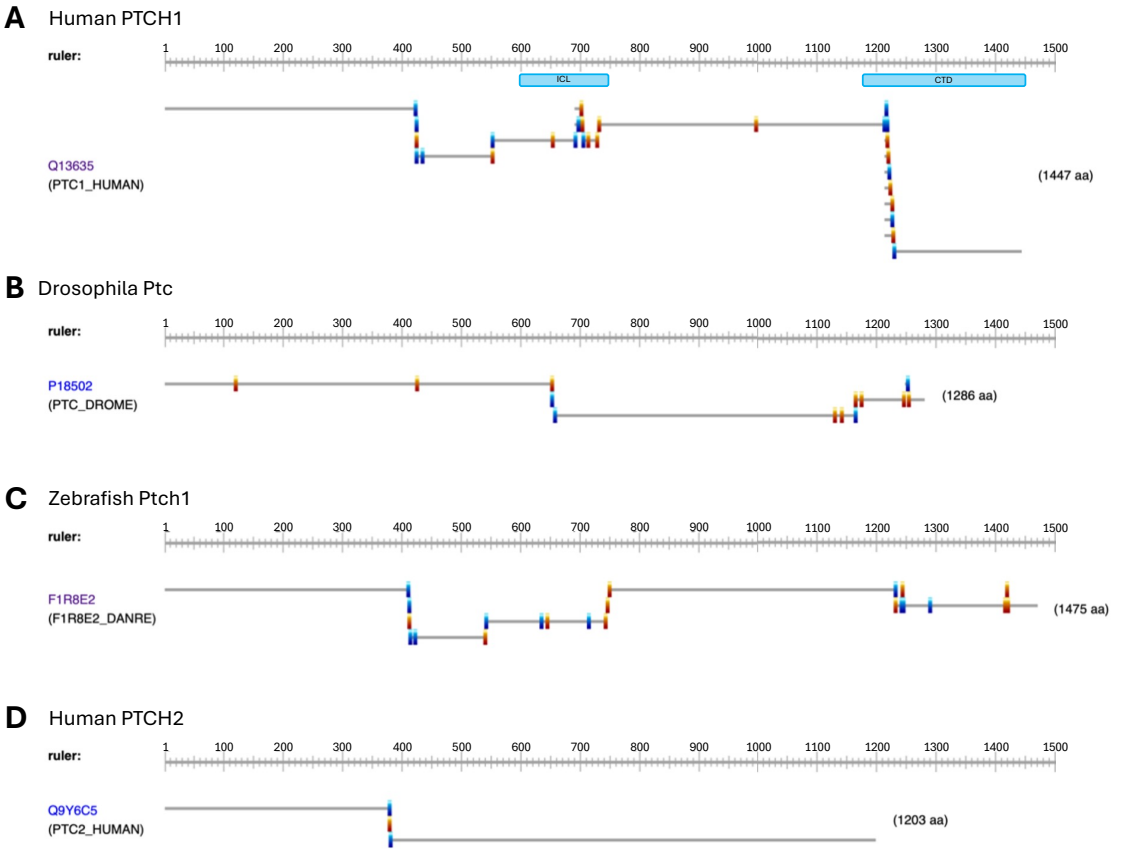

Figure 4.2 Occurrences of *p*x(x)*pxxp*/E/D motif in PTCH variants
Data collected 21.09.23 using the ScanProsite tool by Expasy. Ruler indicates length of primary sequence (amino acids). Blue or orange segments represent *p*x(x)*pxxp*/E/D motifs in the primary sequence (orange containing the optional second 'x'). ICL and CTD regions indicated by blue boxes for human PTCH1.

The same can be seen for zebrafish Ptch1, which corroborates research by Jiang et al (Jiang et al., 2009), where human PTCH1 and bovine GRK2 were shown to interact,

and the importance of this interaction was demonstrated in zebrafish embryos which experience developmental early arrest from GRK2 knockdown.

A search of the human PTCH2 primary sequence reveals no cytoplasmic occurrences of the *p*x(x)*p*xx*p*/E/D motif, the only 3 being within the first large extracellular loop. For this reason I did not include PTCH2 in my experiments.

Of the 28 hits of this motif in human PTCH1, 4 are in ECLI, one spans ECLI and TM2, 2 are in TM5, 9 in the large ICL, 1 in large ECLII, and 11 are in the CTD. The codes within extracellular loops and transmembrane helices can be ignored from this study as βarrs are intracellular proteins and are not found within the cell membrane, nor do they typically exist in extracellular space under normal physiological conditions.

All of the incidences in the human PTCH1 CTD cluster in the same small region, 1214-1235, as displayed in Figure 4.3. Interestingly, a single potential phosphorylation motif, comprising residues S1223-T1229, spans both deletion site mutants (green line). I hypothesised that this one motif is the binding site for βarrs as it would explain why there is an equal and almost complete loss of βarr binding when the deletion sites are removed either alone or together, as seen in Figure 4.1. This motif became my single candidate motif for the PTCH1-βarr interaction.

Figure 4.3 Occurrences of *p*x(x)*p*xx*p*/E/D motif in the human PTCH1 CTD
Primary sequence of human PTCH1 between residues 1211 and 1240. Blue lines above the sequence represent Site 1 and Site 2, corresponding to the small deletions of putative phospho-residue clusters. Black underlines denote all motifs that conform to the *p*x(x)*p*xx*p*/E/D sequence, with the green underlined motif representing the only occurrence that is disrupted in both site 1 and 2 deletion mutants.

4.3.4 Identification of the βarr binding motif in PTCH1

The candidate phosphorylation motif at S1223-T1229 has the sequence SEYSSQT, theoretically representing *p*xx*p*xx*p* in this instance if phosphorylated accordingly. I generated alanine point mutants of the two external S/T residues of the motif, S1223A and T1229A, both alone and together, to prevent their phosphorylation. The hypothesis of these 'phospho-dead' mutants was that they would cause a similar

level of binding disruption as the deletion mutants while altering the wild-type sequence as little as possible, therefore isolating the effect of the mutation to the SEYSSQT motif.

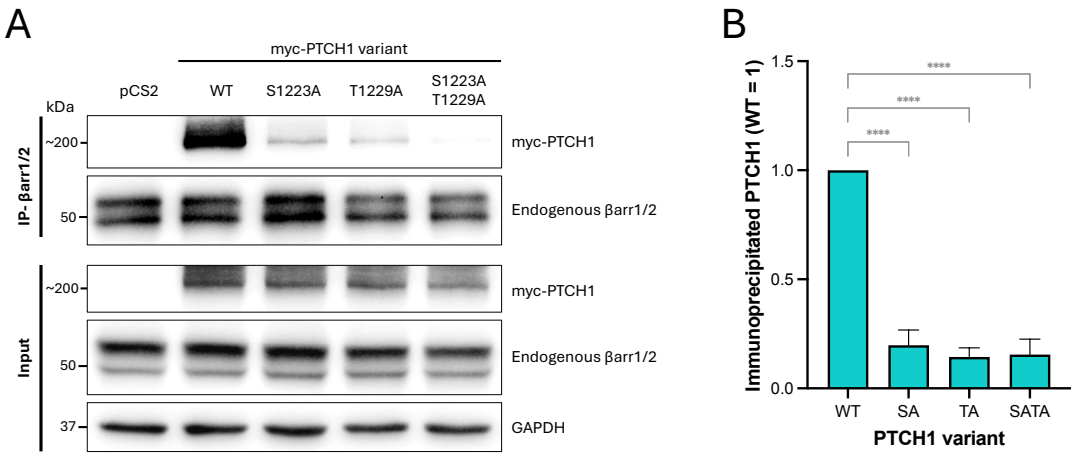

Figure 4.4 Mutations in the SEYSSQT motif prevent βarr1/2 binding
HEK293 cells transfected with indicated constructs were lysed, followed by co-immunoprecipitation of myc-PTCH1 with endogenous βarr1/2. Representative western blot (A) and densitometric quantification of n=5 independent repeats (B). 2-way ANOVA analysis: **** P<0.0001. Error bars= SEM.

Co-immunoprecipitation of these mutants with endogenous βarrs shows the expected result (Figure 4.4). Even when only editing one residue of the wild-type sequence, a significant reduction in βarr binding is observed, as with the double mutant (S1223A + T1229A, hereafter referred to as 'SATA'). Again, the level of this reduction is comparable between the single and double mutants, as well as the deletion and frameshift mutations previously shown (Figure 4.1) This indicates that the candidate motif at S1223-T1229 is indeed the binding motif for βarrs.

4.3.5 Phosphomimetic mutations do not enhance binding

Having identified the βarr binding motif, I sought to investigate the role of phosphorylation in the binding mechanism. It is predicted that the motif is phosphorylated at residues S1223, S1226, and T1229. A common way to identify the role of phosphorylation is to introduce a phosphomimetic mutation that creates a site with negative charge like a phosphate group. I generated 3 point mutations, mirroring the phospho-dead mutations, instead with glutamic acid (S1223E and T1229E, both alone and together).

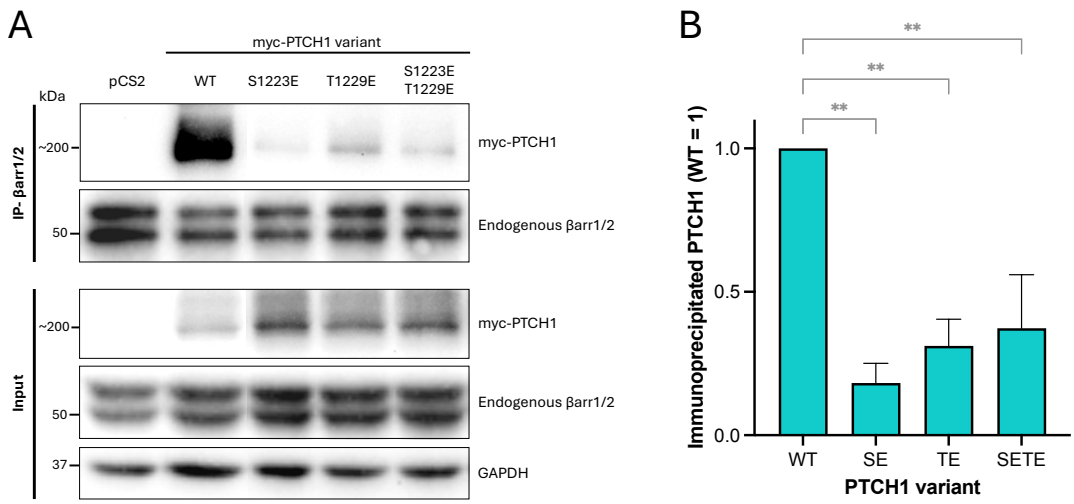

Figure 4.5 Phosphomimetic mutations of βarr binding site do not behave as expected

HEK293 cells were transfected with indicated constructs and lysates immunoprecipitated via endogenous βarr1/2 before preparation for western blotting. A representative western blot is shown in (A), and densitometric analysis of 3 independent repeats is shown in (B). 2-way ANOVA analysis: ** P<0.01. Error bars= SEM.

Figure 4.5 shows the endogenous βarr1/2-based co-immunoprecipitation of these phosphomimetic mutants compared to WT PTCH1. Surprisingly, where we expected the level of interaction to increase, we observed a significant decrease. Although the reduction of binding did not reach the same level of the phospho-dead alanine mutants, this finding was puzzling. However, these mutations do not completely reflect the effect of phosphorylation. While phosphomimetics are often a useful tool, they are not universal. Sometimes, wild-type primary sequence cannot be substituted as it may disrupt the structure or binding mechanisms to interacting proteins. This will be discussed later in this chapter and in investigated in Chapter 6. Because of the challenges of phosphomimetics, I decided to use other methods to investigate the role of phosphorylation in this interaction.

4.3.6 IP-MS/MS confirms phosphorylation of S1223, S1226, and T1229

To confirm phosphorylation of the three candidate PTCH1 residues S1223, S1226, and T1229 that form the βarr binding motif pSEYpSSQpT, mass spectrometry was used. In theory, mass spectrometry can identify PTMs on a protein and assign these modifications to their specific residues with high accuracy. To enrich the level of PTCH1 in the sample, IP-MS/MS was used where the exogenously expressed myc-PTCH1 was immunoprecipitated from a large sample of cells (10 cm dish) via an anti-myc tag antibody (Proteintech, 16286-1-AP). The final immunoprecipitated sample was digested via trypsin and analysed by the mass spec facility at the University of Leeds.

Preliminary data using wild-type PTCH1 was promising, reporting several putative phosphorylation sites along the PTCH1 CTD (Figure 4.6A). However, a closer look at the data revealed that is not the true phosphorylation state of PTCH1, which initially presents as a multi-phosphate peptide. Instead, the phosphates displayed are simply possibilities, since the phosphorylation detected by the software is very ambiguous, and the number of phosphates on a single peptide in this experiment did not exceed 2. The A-score for all detected phosphorylation events in this dataset is 0. This means that while the phosphates are detected, there is no confidence in the specific assignment of the phosphate group to the residues.

This lack of confidence in PTM assignment is likely due to the size of the peptide, and the low fragmentation achieved. The sequence of the fragment in question is as follows: FAMPPGHTHSGSDSSDSEYSSQTTVSGLSEELR. This is a 33-residue peptide, which is very large for this type of analysis. The length of the peptide can make it hard to fragment, in addition to the sequence itself. Residues that are small, polar, acidic, or cyclic can limit peptide fragmentation. This peptide contains many of these types of residues, such as Ser, Thr, and Glu.

Since the accurate assignment of phosphorylation events and preservation of phosphoester bonds in this peptide proved difficult to achieve, a different approach was used. In the same way as before, wild-type PTCH1 was immunoprecipitated for mass spec analysis, alongside 4 mutants. These mutants were the SA, TA, and SATA mutants previously described, as well as a 'DDE' mutant that had been developed for other experiments, and is a triple mutant: S1223D, S1226D, T1229E. These mutants sequentially eliminated the candidate phospho-sites, and therefore if all peptide phosphorylation is blocked when these residues are mutated, it would demonstrate that these are the only 3 residues in this peptide that are phosphorylated, supporting the hypothesis of the binding motif pSEYpSSQpT.

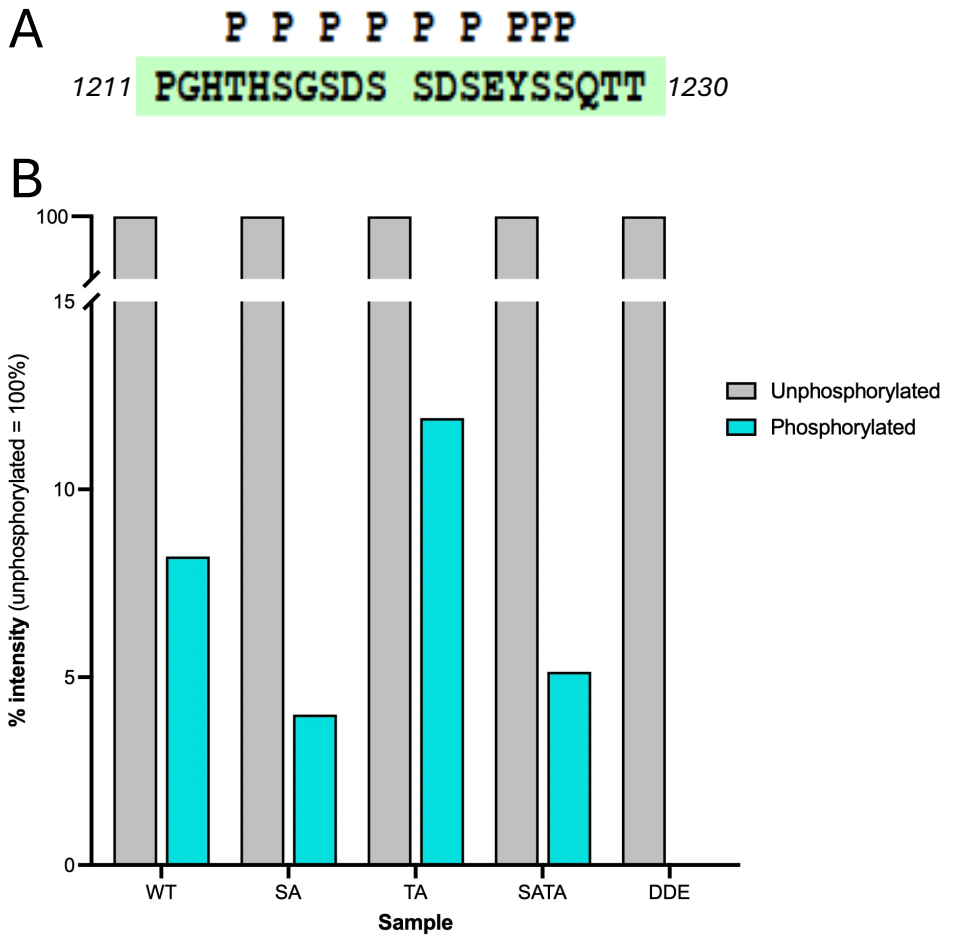

Figure 4.6 Phosphorylation reduced by mutation of S1223, S1226, and T1229
(A) Reported sequence PTM annotation from mass spec software before further analysis. (B) Quantification of peptide phosphorylation relative to the amount of unphosphorylated peptide (normalised to unphosphorylated = 100 %). N=1.

Figure 4.6B summarises the mass spec analysis of the PTCH1 mutants and their phosphorylation states. The abundances of each phospho-peptide recorded for each sample were totalled (since there were many variations), and normalised to the abundance of the unmodified peptide. This resulted in a measure of the percentage of peptide that is phosphorylated for each PTCH1 variant.

It can be seen that there are phosphate groups detected on the peptides formed from all PTCH1 variants except the triple mutant, DDE. This supports the hypothesis that residues S1223, S1226, and T1229 are phosphorylated, and phosphorylation of this region of PTCH1 is limited to these residues. There is less phosphorylation detected for the SA and SATA mutants compared to WT, which is in line with the removal of some of the phosphorylation sites, meaning that there is less overall phosphorylation. It is a little unusual that the level of phosphorylation apparently increases slightly for the TA mutant, as it would be expected that it decrease like

with the SA mutant. However this is a single experiment, and repeats may not show the same pattern, so speculation into the reasons why this may appear to happen is not recommended until more data has been gathered.

4.3.7 Conservation of the βarr1/2 interaction motif in PTCH1

Interestingly, when looking at evolutionary conservation of the identified βarr binding motif in PTCH across species, a significant consensus can be observed. In Figure 4.7, I selected PTCH1 sequences from species across animal classes, and conservation was observed in mammals, birds, and fish (human PTCH1 SEYSSQT motif outlined in pink). The three key phospho-residues, S1223, S1226, and T1229, have 62-69% conservation based on all sequences included.

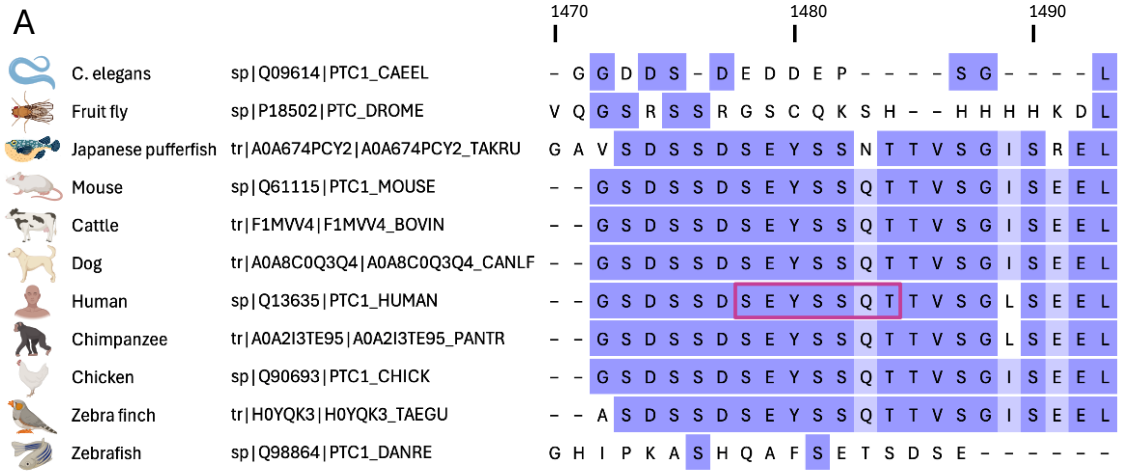

B

Residue	S	E	Y	S	S	Q	T
Consensus (%)	62	62	62	69	62	54	62

Figure 4.7 Conservation of βarr1/2 recruitment motif in PTCH1
Multiple sequence alignment performed using Clustal Omega by EMBL-EBI. A 24-position section of the sequence alignment is shown in (A) with residues coloured by percentage consensus range according to the key, and human PTCH1 SEYSSQT motif highlighted by a pink box. (B) Percentage consensus for each residue in the βarr binding motif.

In the case of βarr recruitment, exact conservation of the binding site for human PTCH1 is not an absolute measure of the conservation of the interaction in general. In the species with a PTCH1 ortholog that do not align or have high consensus to human PTCH1 βarr binding domain (C. elegans, Fruit fly, Zebrafish), the sequences contain multiple additional cytoplasmic *p*x(x)*p*xx*p*/E/D motifs. For Fruit fly and Zebrafish, this can be observed in Figure 4.2. Therefore, while the specific βarr

binding motif in human PTCH1 is considered to be significantly conserved, the PTCH1-βarr interaction in general is likely to be conserved to an even higher degree.

4.3.8 Shh-mediated inhibition of PTCH1 induces βarr1/2 dissociation

Having identified the minimal binding motif in PTCH1 needed for βarr interaction, I returned to the hypothesis that the recruitment process and binding mechanism reflects that of GPCRs. For βarr recruitment to GPCRs, the receptors must first be activated by ligand binding, which through conformational changes, allows phosphorylation of the C-tail and subsequent βarr recruitment. Unlike GPCRs, which are activated by agonistic ligands, PTCH1 displays constitutive activity and is inhibited by binding to HH ligands, such as SHH. In canonical HH signalling, this is necessary to release the repression PTCH1 holds over SMO to activate signalling through the GLI transcription factors. Therefore, it was necessary to investigate the relationship between PTCH1 ligand binding and PTCH1-βarr interaction, since it was unclear whether these would correlate positively or negatively.

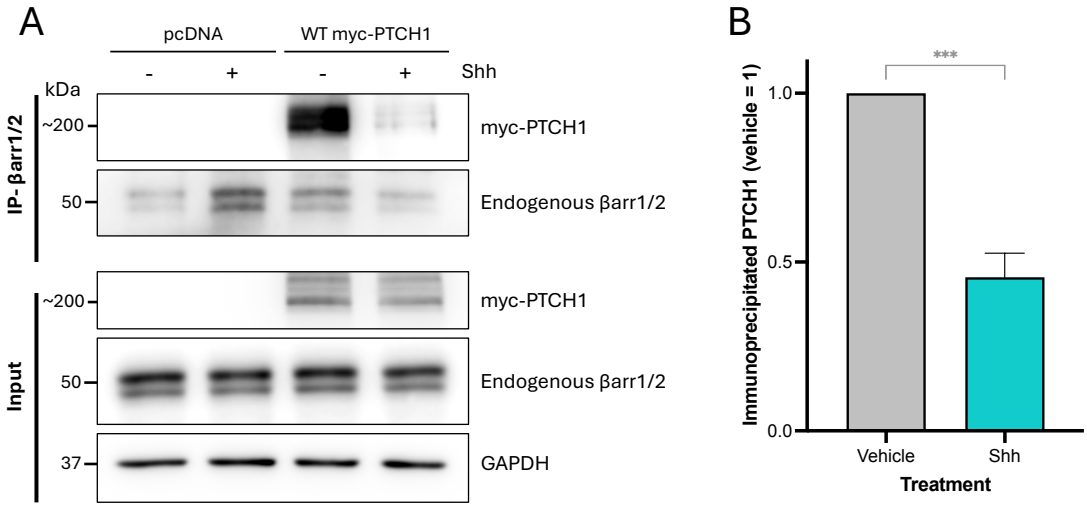

Figure 4.8 Treatment with rShh significantly reduces βarr binding
HEK293 cells were transfected with empty vector or wild-type PTCH1 using T5 as described with the exception of leaving the cells in DMEM + 2% FBS instead of changing media. Before lysis, cells were incubated with 100ng/mL rShh in serum-free DMEM for 30 min. Lysates were immunoprecipitated via endogenous βarr1/2 and prepared for western blotting. (A) A representative western blot, with densitometric analysis of 4 independent repeats summarised in (B). Two-tailed unpaired t test analysis: *** P<0.0005. Error bars= SEM.

When PTCH1 is co-immunoprecipitated with endogenous βarr1/2 as previously described, with the addition of 100 ng/mL rShh 30 min before lysis, I observed an average 55 % reduction in the amount of PTCH1 in the immunocomplex (Figure 4.8). This demonstrates that SHH binding to PTCH1 causes dissociation of βarrs after 30 min stimulation.

4.3.9 *In vitro* co-localisation of PTCH1 and βarr1 is reduced by SATA mutation or Shh stimulation

A negative correlation between Shh addition and βarr association with wild-type PTCH1 was observed via co-immunoprecipitation after 30 min SHH stimulation. While this is an effective measure of protein-protein interaction, it is important to confirm the interaction and its regulation by phosphorylation and/or Shh in live cells *in situ*. For this, I used fluorescence confocal microscopy to examine the localisation of PTCH1 and βarr1 fused to fluorescent tags under different experimental conditions (Figure 4.9). I compared wild-type PTCH1-mCherry and PTCH1 SATA-mCherry, each co-expressed with βarr1-GFP, and treated with 100 ng/mL rShh or a vehicle control for 30 min. I used Ptc1 homozygous knockout MEFs (Ptch1$^{-/-}$ MEFs) as host cells, as MEFs have intact Hedgehog signalling, and the Ptch1 knockout allows expression of PTCH1 and analysis of mutation effects without the confounding background from endogenous Ptch1.

In Figure 4.9, strong co-localisation of PTCH1 with βarr1 could be observed for wild-type PTCH in the absence of rShh. When wild-type PTCH1 stimulated with rShh for 30 min, co-localisation is reduced (Figure 4.9 B). The PTCH1 SATA mutant, as expected based on co-immunoprecipitations (Figure 4.4), did not show co-localisation with βarr1 regardless of the presence or absence of rShh. Panel B shows the Pearson's correlation (R value) of the mCherry and GFP signals in all cells imaged over 3 independent experiments. This reports a linear correlation between the two signals.

While not a perfect measure, as it creates a linear measure which is not generally the case in biology, a significant decrease in correlation between GFP and mCherry signal can be seen between wild-type PTCH1 in the absence of rShh and the other three conditions. This means that wild-type PTCH1 and βarr1 are statistically more likely to colocalise under basal conditions than in the presence of rShh or when the identified βarr interaction motif is mutated (SATA).

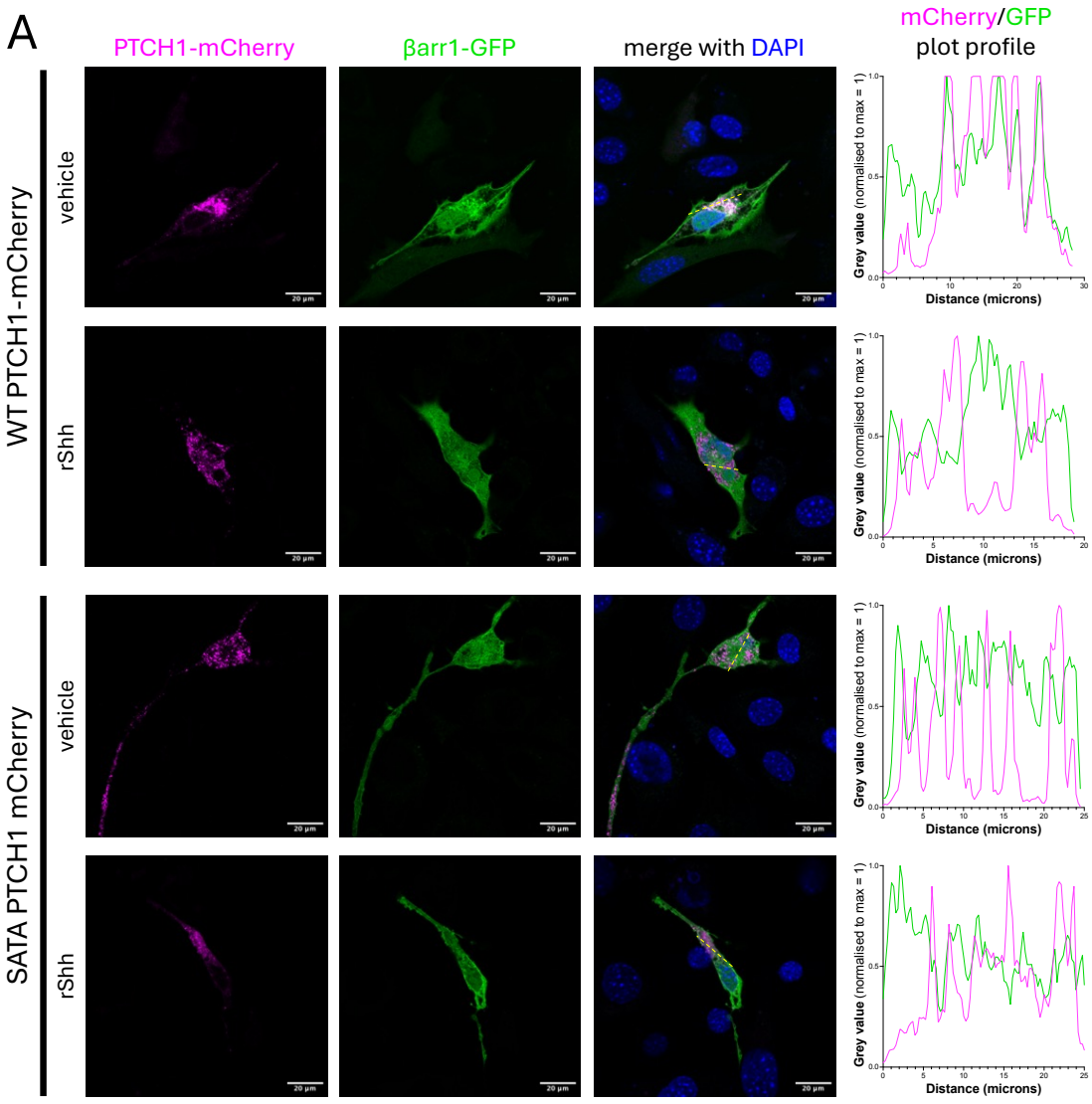
A
PTCH1-mCherry
βarr1-GFP
merge with DAPI
mCherry/GFP
plot profile
WT PTCH1-mCherry
vehicle
rShh
SATA PTCH1 mCherry
vehicle
rShh
Grey value (normalised to max = 1)
Distance (microns)

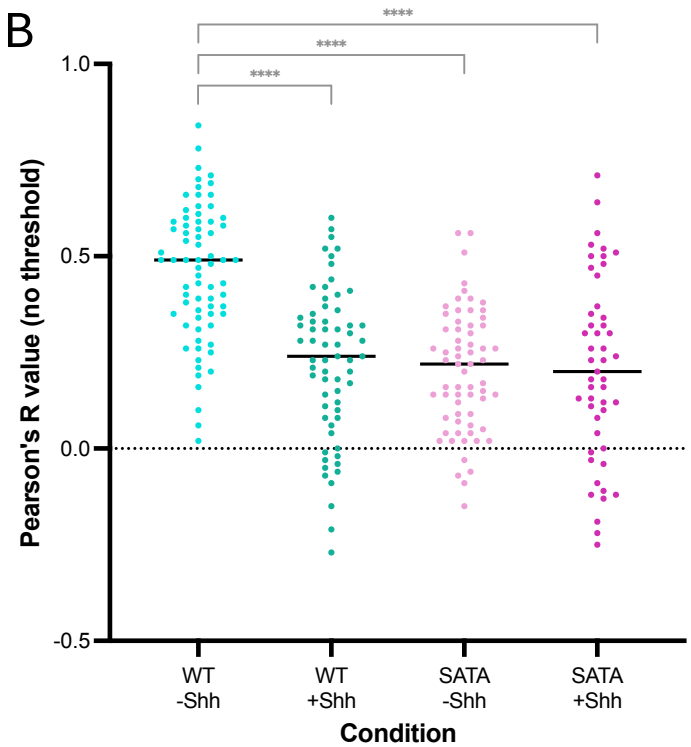
B
****
****
****
Pearson's R value (no threshold)
1.0
0.5
0.0
-0.5
WT
-Shh
WT
+Shh
SATA
-Shh
SATA
+Shh
Condition

Figure 4.9 Wild-type PTCH1 co-localises with βarr1 in the active state
Ptc1$^{-/-}$ MEFs were reverse transfected into coverslip chamber slides, serum starved for 24h, and treated with 100ng/mL rShh for 30 min before fixing and staining with DAPI. (A) PTCH1-mCherry (magenta) and βarr1-GFP (green) shown as separate channels and overlayed (white). Scale bar 20 μm. Right: Plot profiles of PTCH1-mCherry (magenta) and βarr1-GFP (green) signals across the yellow dashed line displayed on overlayed image. Values were normalised to a max of 1 for each channel. (B) Pearson's R value (no threshold) for individual cells is displayed as a single point with lines indicating the median (n=?? put the range of individual cells here). 2-way ANOVA analysis: **** P<0.0001.

For each of the representative images shown, a plot profile was generated along the yellow dotted line displayed in the merged image. Wild-type PTCH1 appears to co-localise with βarr1 under basal conditions, as seen by the white overlay between the magenta of PTCH1-mCherry and green of βarr-GFP. In this condition, the plot profile demonstrates a distinct correlation. As the mCherry signal peaks, the GFP signal also peaks, and vice versa as signal decreases, meaning the two profiles overlay for the majority of the line segment. In contrast, the other three conditions do not show this relationship. There is no consistent positive correlation between the two profiles, and in many instances, there is a negative correlation where one profile peaks while the other troughs in the same position.

These results together corroborate the co-immunoprecipitation results. Wild-type PTCH1 associates with βarrs under basal conditions via the S1223-T1229 region that conforms to the consensus phosphorylation motif *p*x(x)*pxxp*/E/D. Mutation of 2 of 3 predicted phosphorylation sites in that motif (SATA mutant) blocks the complex formation. Additionally, 30 min stimulation with the inactivating ligand, SHH, significantly reduces the interaction.

4.3.10 GRK2/3 inhibition decreases βarr1/2 binding to PTCH1

For the recruitment of βarrs to PTCH1, phosphorylation of the SEYSSQT motif was hypothesised to be necessary. There are be several kinases that may be involved in this; however, the lead candidate was GRK2, based on the interaction between PTCH1 and GRK2 previously reported (Jiang et al., 2009). To test this hypothesis, I co-immunoprecipitated PTCH1 with endogenous βarr1/2 in the presence of cmpd101, a known GRK2/3 inhibitor. Following transfection, HEK293 cells were incubated overnight with 30 μM cmpd101 before lysis, immunoprecipitation, and western blotting.

Figure 4.10 shows a significant decrease in the interaction between PTCH1 and βarrs following addition of cmpd101. While it is not a 100% reduction, the

interaction is reduced by an average of 50%, comparable to the effect of addition of SHH. While this results support the hypothesis that GRK2/3 phosphorylate PTCH1 promoting βarr1/2 association, it is possible that cmpd101 did not achieve full inhibition of GRK2/3 and/or that other kinases could phosphorylate the PTCH1 CTD to some extent, either in basal conditions, or as a backup mechanism when GRK2/3 are dysregulated. This result indicates that GRK2/3 are primarily involved in the phosphorylation of PTCH1's βarr binding motif at S1223-T1229 according to the *p*x(x)*pxxp*/E/D code and their inhibition disrupts the recruitment process.

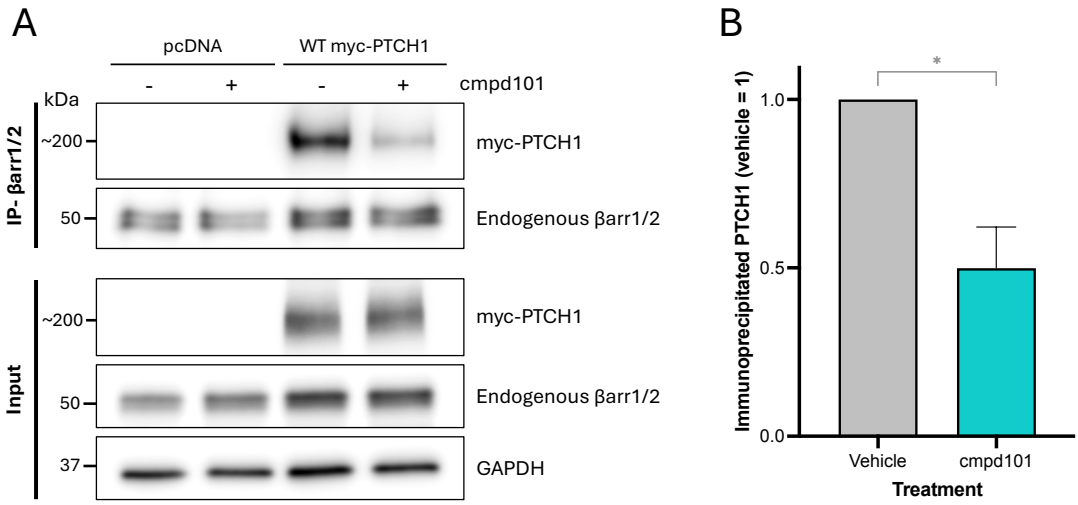

Figure 4.10 GRK2/3 inhibition decreases βarr1/2 binding
(A) Representative western blot of co-immunoprecipitation of wild type myc-PTCH1 with endogenous βarr1/2 in the presence and absence of a GRK2/3 inhibitor. HEK293 cells were transfected with myc-PTCH1 or pcDNA control, and after 6h 30 μM GRK2/3 inhibitor cmpd101 in DMEM + 10% FBS was added and incubated overnight before lysis, immunoprecipitation, and western blotting. Densitometric analysis of 3 repeats is shown in (B). Two-tailed unpaired t test analysis: * $P<0.05$. Error bars= SEM.

4.4 Discussion

In this chapter I have characterised the interaction of βarrs with PTCH1. A systematic approach was used to uncover the binding mechanism based on predicted parallels with GPCR recruitment of βarrs, and found that the process by which PTCH1 binds βarrs is consistent with this hypothesis. From the data so far I propose that Shh binding to PTCH1 causes a conformational change that allows enhanced GRK2/3-mediated phosphorylation of the CTD to increase βarr recruitment and signals for internalisation and degradation of PTCH1, during which βarrs become dissociated from PTCH1 as PTCH1 is trafficked to degradation machinery and βarrs are recycled for further use in the cell.

A bioinformatic search of the primary sequence of the PTCH1 CTD revealed multiple putative phosphorylation sites that may facilitate βarr binding. Co-immunoprecipitation with small deletion mutants showed that removing clusters of these residues blocked βarr binding to PTCH1. Deletion of these clusters (Site 1, S1216-S1223 and Site 2, S1227-S1235) blocks βarr binding to PTCH1 equally when deleted separately or together, and comparably to truncation at S1203. A further search of the CTD looking not just for phosphorylatable residues, but phosphorylation codes as described in literature (Zhou et al., 2017), revealed several overlapping occurrences of the *p*x(x)*p*x*x**p*/E/D code. I identified a single occurrence of this code that spanned the two small deletion sites.

This phosphorylation code which comprises residues S1223-T1229 of the PTCH1 CTD has been identified as the binding site for βarrs. Alanine point mutation of the two external phospho-residues S1223 and T1229, separately or together, blocks βarr binding equally and to the same level as the small deletion mutants, as shown via co-immunoprecipitation. This strongly suggests that it is phosphorylation according to the code at this specific site which allows βarrs to bind PTCH1. In this instance, the code is *p*x*x**p*x*x**p*, generating phospho-motif pSEYpSSQpT. This is visualised in Figure 4.11.

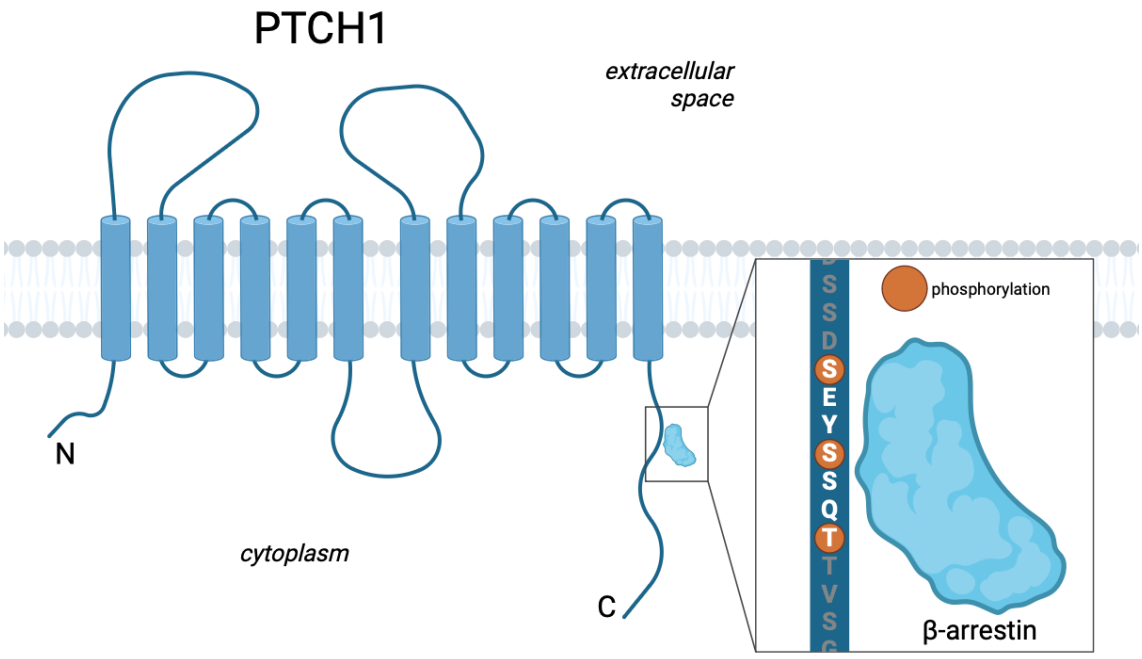

Figure 4.11 βarrs bind PTCH1 phospho-motif pSEYpSSQpT
Graphic showing βarr binding to phospho-motif pSEYpSSQpT at PTCH1 residues S1223-T1229. Not to scale. Created with Biorender.com.

The common method of using phosphomimetic point mutants to mimic phosphorylation of the pSEYpSSQpT motif was used. Essential residues S1223 and T1229 were replaced with glutamic acid to mimic phosphorylation at these sites, as is predicted to be necessary for PTCH1 recruitment of βarrs. However, these mutations did not enhance βarr binding, neither alone nor together. Table 4.2 summarises the variants of PTCH1 created and their ability to bind βarrs in co-immunoprecipitation assays.

Mutation	**Sequence (1211 – 1240, *pxxpxxp* underlined)**	**Binds βarr1/2?**
Wild-type	PGHTHSGSDS SDSEYSSQTT VSGLSEELRH	✓
ΔS1216–S1235	PGHTH----- ---------- -----EELRH	X
ΔS1216–S1223	PGHTH----- ---EYSSQTT VSGLSEELRH	X
ΔS1227–S1235	PGHTHSGSDS SDSEYS---- -----EELRH	X
ΔS1216–S1223 ΔS1227–S1235	PGHTH----- ---EYS---- -----EELRH	X
S1223A	PGHTHSGSDS SD**A**EYSSQTT VSGLSEELRH	X
T1229A	PGHTHSGSDS SDSEYSSQ**A**T VSGLSEELRH	X
S1223A & T1229A	PGHTHSGSDS SD**A**EYSSQ**A**T VSGLSEELRH	X
S1223E	PGHTHSGSDS SD**E**EYSSQTT VSGLSEELRH	X
T1229E	PGHTHSGSDS SDSEYSSQ**E**T VSGLSEELRH	X
S1223E & T1229E	PGHTHSGSDS SD**E**EYSSQ**E**T VSGLSEELRH	X

Table 4.2 Summary of PTCH1 variants and their ability to bind βarr1/2
Table details mutations made to myc-PTCH1 primary sequence and if that mutant was co-immunoprecipitated via endogenous βarr1/2. Data not shown for ΔS1216–S1235.

As discussed by Zhou et al, high-affinity arrestin binding generally requires three receptor-attached phosphates (Zhou et al., 2017), and so it is not entirely unexpected that phosphomimetic mutation of the βarr binding site was not able to enhance binding. There are several factors that may explain why this is the case.

Glutamic acid is often used for phosphomimetic mutations in the first instance as its larger side chain can better mimic the phosphate group in a spatial manner. However, it can be very context dependent, and the shorter side chain of aspartic acid can reduce steric hindrance in some contexts where this may be critical. Further to this, while aspartate and glutamate have a negative charge, compared to a phosphorylated serine or threonine the charge distribution is not absolutely comparable, which may lead to sub-optimal conditions for the binding interaction

to take place. Additionally, the length and flexibility of the D and E side chains are also not exact mimics, again potentially reducing the ability for βarrs to bind.

A study by Theillet et al reviewed the order- or disorder-promoting properties of each of the 20 natural amino acids (Theillet et al., 2013). Glutamic acid is the second-most disorder-promoting residue after proline. Serine closely follows, however the charge of a phosphate often adds significant order to proteins. Phosphorylation can induce conformational changes in proteins, proximally or distally, which may not be replicated by replacement with D or E, in fact the phosphomimetic mutation may even stabilise a different conformation that is not compatible with the binding partner. It is possible that in addition to electrostatic bond formation, a role of phosphorylation in this interaction is to create order within an intrinsically disordered region, the PTCH1 CTD, allowing docking of βarrs to a more stable conformation. Therefore it is possible that the glutamic acid substitution here is not accurately mimicking the effect of phosphorylation, and instead may be altering PTCH1's structure or charge distribution in a way that negatively impacts its interaction with βarrs.

Mass spectrometry was able to show that the three candidate residues, S1223, S1226, and T1229, are the only residues phosphorylated in the region of PTCH1 containing the *p*x(x)*p*xx*p*/E/D clusters. While there were limitations of the facilities used, for example the lack of confidence in phosphate group assignment, mutations of PTCH1 at these residues decreased levels of phosphorylation detected and therefore it can be concluded that the pSEYpSSQpT motif is phosphorylated as hypothesised.

Additionally, although it was not within the time constraints of this project, repeating this experiment would be beneficial since there is currently only n=1 repeats, and it would also be useful to change some variables to help improve the data collected. Firstly, some alternative or additional proteases could be used in the protein digestion to form different fragments, since the large size of the fragment of interest is likely to be causing a lot of the issues with this experiment. For example, chymotrypsin which cleaves at the C-terminal of aromatic residues such as Phe, Tyr, and Trp. Additionally, Glu-C cleaves the C-terminus of Glu and Asp ,and Asp-N at the N-terminus of Asp residues. Additionally, the method of fragmentation may offer better results. The method used was Higher-Energy Collisional Dissociation (HCD), which can be effective for large analyses, and can be effective in phosphoproteomics. However, Electron Transfer Dissociation (ETD) may be a more effective method, particularly for vulnerable phosphate groups, as it is much

better at keeping the phosphoester bond intact and producing more accurate data for phospho-peptides.

To further explore the role of phosphorylation in the PTCH1-βarr interaction, candidate kinase GRK2 and its closely related isoform GRK3 were inhibited using cmpd101 and the effects of this on PTCH1-βarr1/2 binding was measured via co-immunoprecipitation. It was found that inhibition of these kinases significantly reduced the binding ability of PTCH1 to βarrs, indicating the importance of GRK2/3 phosphorylation of the PTCH1 CTD in βarr recruitment. This supports the hypothesis that the recruitment of βarrs to PTCH1 mimics that of GPCRs, as GRKs are the main kinases that phosphorylate the C-tails of active GPCRs to allow arrestin binding.

While it has been shown that GRK2/3 are likely the main kinases involved in this recruitment process, there may be other kinases that can influence the phosphorylation of this region of PTCH1, however investigating other candidates was not within the scope of this project. To be more thorough, I would include investigation of other kinases in future work on this project. Other candidates include cyclin-dependent kinase 1 (CDK1), which was among the kinases predicted to phosphorylate S1223 and T1229 and has seen to be upregulated through hedgehog signalling in liver cancer (Cai et al., 2016), and casein kinase 2 (CK2) which is reported to drive hedgehog signalling in medulloblastoma (Purzner et al., 2018).

Treatment with rShh also caused a significant decrease in the level of PTCH1-βarr interaction observed in co-immunoprecipitations and co-localisation seen via fluorescent confocal microscopy. These decreases in PTCH1-βarr1 association were seen 30 min after Shh stimulation. However, in Chapter 3 it was shown that βarrs1/2 promote Shh-mediated PTCH1 degradation, seen at 4 h post-stimulation. This creates either an ambiguous relationship between Shh and βarrs in PTCH1 regulation, or that there are spatial and temporal processes involved in PTCH1-βarr1 association and dissociation. This will be explored further in Chapter 5, using the specific SATA mutant to specifically observe the effect of the PTCH1-βarr1 interaction on PTCH1 turnover.

Interestingly, the large number of *p*x(x)*p*x*x**p*/E/D codes found within the ICL of PTCH1 suggests a potential interaction with this large cytoplasmic looped domain. The PTCH1-βarr interaction is decreased to almost undetectable levels in a co-immunoprecipitation simply by alanine mutation of residues S1223 and T1229, as

well as truncation at S1203. However, a slight signal can still be seen in the aforementioned immunoprecipitates which does suggest a very weak interaction at an alternate binding site, which could be this cytosolic domain of the middle loop.

It has been observed in many examples that a sequential binding takes place between GPCRs and βarrs, firstly the binding to the C-tail which leads to activating conformational changes within the arrestin protein, and a second binding event of the 'finger loop' of arrestins to the transmembrane core of the GPCR which is weaker and likely to be important for the desensitisation of GPCRs from their G-proteins (Shukla et al., 2014, Gurevich and Gurevich, 2004). While PTCH1 does not have coupled G-proteins that could be desensitised by a receptor core interaction, it has been shown that deletion of the majority of the PTCH1 middle loop (with a small number of residues left to form a short loop for correct protein folding) increases PTCH1 stability and membrane localisation (Timmis, 2021). This could indicate a role of this secondary interaction with βarrs, which are known to internalise receptors and enhance their degradation. Therefore I have a hypothesis that the similarity between the PTCH1-βarr interaction continues beyond the initial binding to the CTD, and this GPCR core interaction may be paralleled by an interaction with the PTCH1 middle loop. In any further work in this project, I would explore the role of the middle loop in the PTCH1-βarr interaction as this indicates a potential secondary binding event, not one required for the initial binding of βarrs to PTCH1, but one that may have a stabilising or functional role.

Together the work in this chapter has shown that βarrs are recruited to the CTD of PTCH1 via the wild-type expression and GRK2/3-mediated post-translational phosphorylation of the βarr binding motif, S1223-T1229, to pSEYpSSQpT. This novel interaction is atypical given PTCH1's size and its absence of coupled proteins when compared to GPCRs, which it resembles in recruitment. In Chapter 5, I will explore the functional consequences of this interaction, assessing whether the similarities with GPCRs continue or if βarrs have a distinct function in the context of PTCH1.

Chapter 5

Exploring the functional consequences of the PTCH1-βarr interaction

Chapter 5

Exploring the functional consequences of the PTCH1-βarr interaction

5.1 Introduction

Previously, I characterised the recruitment of βarrs to PTCH1 via a GRK2/3-phosphorylated motif spanning PTCH1 CTD residues S1223 to T1229, pSEYpSSQpT. In this chapter I will assess the functional consequences of this interaction *in vitro*, using the SATA mutant (S1223A, T1229A), which does not bind βarrs, to compare results to wild-type PTCH1.

Canonical Hedgehog signalling regulates GLI activity through SMO, which is itself regulated by PTCH1. It is thought, although not fully understood, that PTCH1 inhibits SMO via its cholesterol transport mechanism. SMO is activated by binding of cholesterol or cholesterol derivatives (Nedelcu et al., 2013), while PTCH1 is able to transport cholesterol (Zhang et al., 2018). In this way PTCH1 reduces the amount of accessible cholesterol within close proximity to SMO, and therefore prevents its activation. This process is blocked by SHH binding to and inactivating PTCH1 and therefore restoring free cholesterol to SMO-activating levels.

The role of the CTD in canonical signalling is a little unclear. There is evidence that there are tissue-specific effects, where truncation of the CTD results in altered canonical signalling in adipose tissue (Li et al., 2008), but no change is reported in epithelial cells nor fibroblasts (Okolowsky et al., 2014, Nieuwenhuis et al., 2007). The CTD has shown to be dispensable for canonical signalling in vitro via a Gli-luciferase reporter assay in MEFs (Fleet et al., 2016), where PTCH1 with a truncated CTD represses canonical signalling and is rescued by addition of SHH, in the same way as wild-type PTCH1. It is therefore unlikely that the PTCH1-βarr interaction, which takes place on the PTCH1 CTD, influences canonical Hedgehog signalling through GLI.

Typically, aside from desensitisation, βarrs regulate GPCRs through internalisation, trafficking, and degradation. Since their interaction with PTCH1 is similar, it is possible that they regulate PTCH1 in a similar way. The PTCH1 ligand SHH, while inhibiting PTCH1, also increases its turnover (Denef et al., 2000, Rohatgi et al., 2007). Preliminary work with βarr siRNA discussed in Chapter 3 (Figure 3.2) identified that SHH-mediated PTCH1 degradation is enhanced by βarrs. This

combined with the known function of βarrs degrading GPCRs via a direct interaction points to the PTCH1-βarr interaction being necessary for this degradation, therefore I will use the SATA PTCH1 mutant to confirm this.

Other roles of PTCH1 include regulating apoptotic signalling and cell proliferation. PTCH1 overexpression increases cell death via caspase-3 activation, unlike SMO activation or inhibition by small molecule compounds, and is blocked by addition of SHH (Thibert et al., 2003). Silencing of SHH using siRNA also increases caspase-3 activity, which again is blocked by addition of recombinant SHH (Bissey et al., 2020). Therefore the pro-apoptotic activity is thought to depend on active PTCH1. It was reported that the CTD of PTCH1 binds to a pro-apoptotic complex containing DRAL, TUCAN, and caspase-9 which cleaves PTCH1 at D1392 in mouse Ptc1 (Mille et al., 2009), or D1405 in human PTCH1 (Caballero-Ruiz et al., 2023). This cleavage is crucial for cell death via apoptosis; however, the downstream signalling has not yet been fully elucidated.

PTCH1 is also able to modulate cell proliferation via cell cycle regulation. The large intracellular loop (ICL) can bind to cyclin B1, sequestering it in the cytosol and preventing its nuclear accumulation (Barnes et al., 2001). This prevents cyclin B1-CDK1 complex formation and nuclear function of phosphorylation of mitotic substrates including histones and nuclear lamins (Porter and Donoghue, 2003).

In addition, overexpression of PTCH1 has been shown to downregulate BMI-1. BMI-1 is a member of the Polycomb group (PcG) proteins and is known for its oncogenic activity via promoting self-renewal and proliferation of cells. Therefore PTCH1 reduces clonal growth of cancer cells (Bhattacharya et al., 2008).

Together, through promoting apoptosis, and reducing proliferation and clonogenicity, PTCH1 negatively regulates cell growth and survival. Many *in vivo* studies have demonstrated the tumour suppressor function, for example heterozygous knockdown of PTCH1 in mice creates BCC precursor lesions, which progress to aggressive BCCs in irradiated mice (Mancuso et al., 2004) or in combination with Dsg2 overexpression (Brennan-Crispi et al., 2019). Additionally, addition of peptides that competitively inhibit SHH binding to PTCH1 reduces pancreatic cancer cell proliferation and GLI1 expression *in vitro* and *in vivo* in mice (Nakamura et al., 2012).

The role of PTCH1 as a tumour suppressor has clearly been demonstrated through *in vitro* and *in vivo* studies. This makes those proteins that mediate PTCH1 tumour suppressor function of interest for novel cancer therapies, especially given the current limitations of existing drugs which target Hedgehog-related cancers via SMO inhibition. In this chapter I will investigate functional consequences of the PTCH1-βarr interaction to assess its relevance in the tumour suppressor function of PTCH1.

5.2 Aims

1. Use PTCH1 mutants to assess the functional effects of the PTCH1-βarr interaction on non-canonical Hh signalling

5.3 Results

5.3.1 Canonical signalling is unaffected by the PTCH1-βarr interaction

To test the influence of the PTCH1-βarr interaction on canonical Hedgehog signalling, a Gli-luciferase reporter assay was used in Ptch1-deficient cells. These cells show high basal GLI transcriptional activity, which is inhibited by re-introduction of PTCH1. $Ptc1^{-/-}$ MEFs were co-transfected with luciferase reporter plasmids (pRL-SV40 and p8XGBS-Luc), a SHH-expressing plasmid or empty vector control, and PTCH1 variants as indicated. Cells were serum starved overnight to promote ciliogenesis. Results were obtained using Promega's Dual-Luciferase® Reporter Assay System, reported as Gli-luciferase reporter activity (Firefly/Renilla luciferase ratio), and normalised to the unstimulated pcDNA control. It can be seen in Figure 5.1 that under basal conditions, expression of WT PTCH1 almost completely blocks Gli-luciferase reporter activity. Additionally, while addition of SHH has no effect without PTCH1 (pcDNA), when WT PTCH1 is present, SHH restores GLI activity to almost the same level as the pcDNA control. These results are expected and confirm that co-transfection of a SHH-expressing construct is an effective method for stimulating the cells in this model, as opposed to addition of recombinant SHH.

Here, PTCH1 mutants were used to assess the influence of its interaction with βarr1/2 on canonical Hh signalling through quantification of GLI transcriptional activity. The previously described PTCH1 SATA mutant was compared to WT PTCH1 to specifically measure any influence on the PTCH1-βarr interaction, since the SATA mutation blocks this interaction. The 3 truncation mutants 1316*, 1308*, and 1203* were also included to determine if these sections of the CTD plays any role in GLI

transcriptional activity. None of the mutations to PTCH1 tested in this experiment had any effect on Gli-luciferase reporter activity either under basal or SHH-stimulated conditions when compared to wild-type PTCH1. This demonstrates that the PTCH1-βarr interaction does not influence canonical signalling in these conditions.

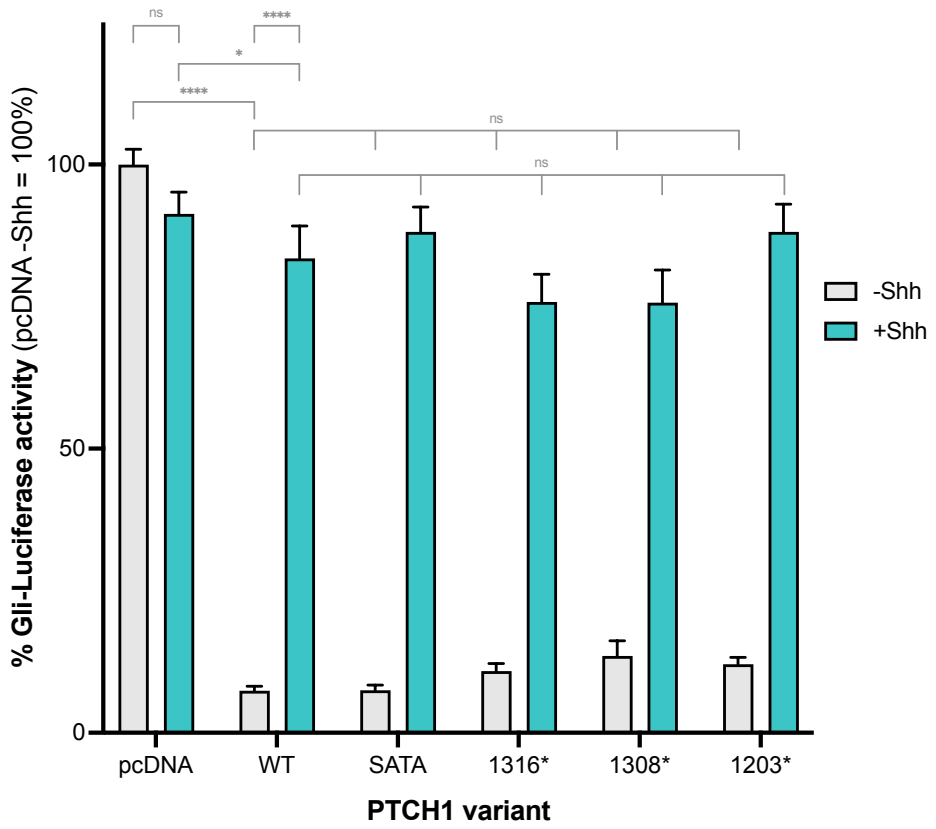

Figure 5.1 Mutation of the PTCH1-βarr binding site does not affect Gli-luciferase reporter activity
Ptc1$^{-/-}$ MEFs were co-transfected with empty plasmid (pcDNA) or the indicated PTCH1 constructs and with SHH-expressing plasmid or empty vector control, together with luciferase plasmids. After 24h cultured in 0.5% FBS, cells were lysed for Gli-luciferase activity assay. N=3. 2-way ANOVA analysis: ns, not significant; * P<0.05; **** P<0.0001. Error bars= SEM.

5.3.2 βarrs enhance SHH-mediated degradation of PTCH1

The previous finding that knockdown of βarrs via siRNA increases the stability of PTCH1 after SHH treatment (Figure 3.2) implies a role of βarrs in PTCH1 degradation. Since silencing of βarrs is expected to have effects on many biological processes which could indirectly affect PTCH1 turnover, a similar experimental setup was used to test the stability of the PTCH1 SATA mutant to isolate the effect of the PTCH1-βarr interaction. MCF7 cells were treated with cycloheximide to block

protein synthesis, followed by treatment with rSHH or vehicle and then lysing cells at various time points to observe the decay of PTCH1 protein levels over time.

In unstimulated cells, the levels of wild-type PTCH1 or the PTCH1-SATA mutant remained stable over 4 h (Figure 5.2). As previously reported, when treated with SHH, wild-type PTCH1 protein levels decrease over the course of 4 hours to 65 % of the initial amount. Interestingly, level of the PTCH1-SATA mutant was stable even after addition of SHH (Figure 5.2). This finding, combined with the βarr siRNA data, demonstrates a direct effect of the PTCH1-βarr interaction in SHH-mediated PTCH1 degradation.

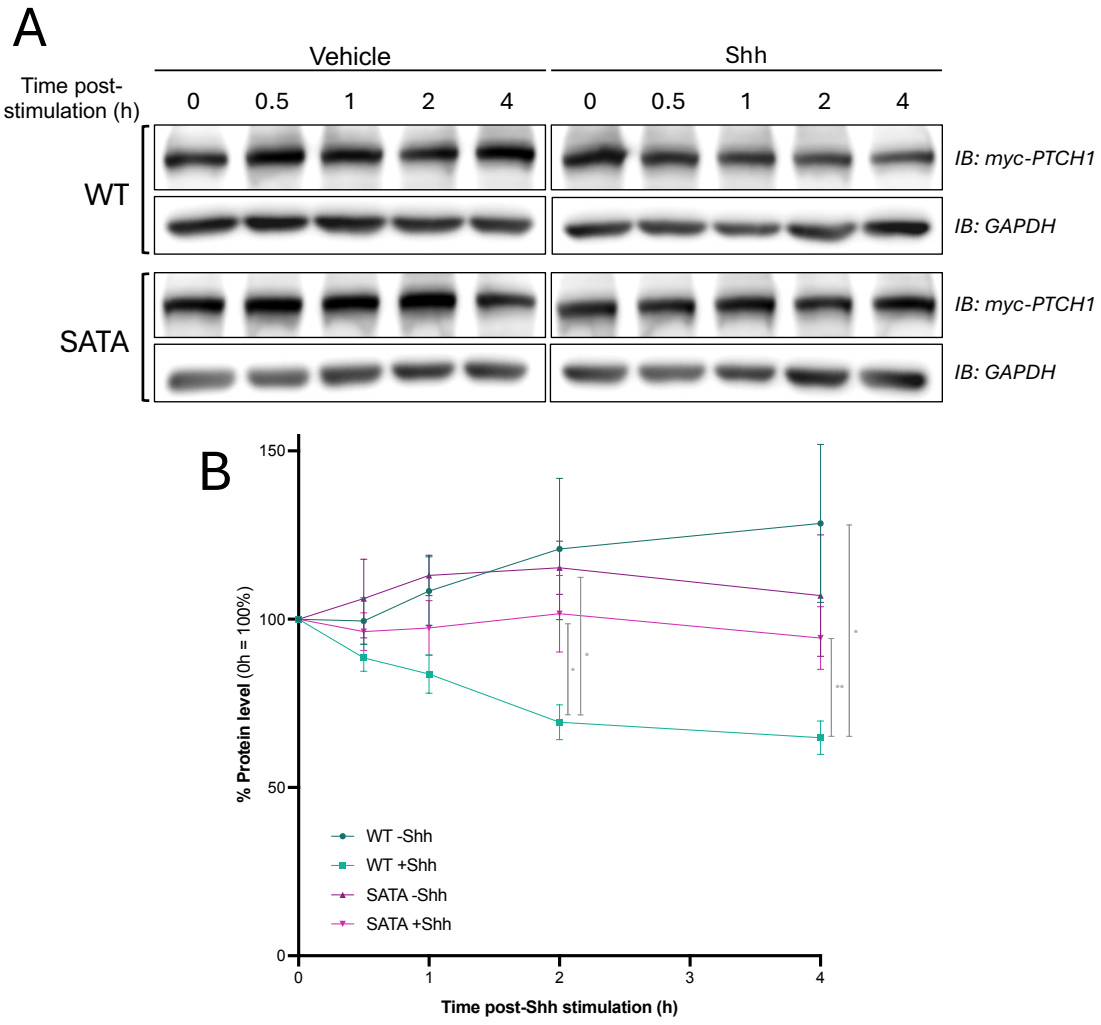

Figure 5.2 Mutation of the βarr binding site enhances PTCH1 stability
(A) MCF7 cells were transfected with WT myc-PTCH1 or SATA myc-PTCH1 for 24h. Cells pre-incubated 1h with 100 µg/mL CHX, then 100 ng/mL rSHH added and cells lysed at indicated time points. (B) Densitometry of n=4 independent experiments. 2-way ANOVA analysis: * P<0.05; ** P<0.01. Error bars= SEM.

It is possible that the experimental conditions did not completely inhibit protein synthesis, since the WT -SHH condition shows a slight increase in protein levels over the 4 time period. However the amount of CHX added was optimised based on cell health, since it is toxic to cells so adding too much can significantly increase apoptosis which would negatively effect the results. Therefore, 100 µg/mL was the concentration used since it was the highest amount that could be added that would not cause excess cell death over the course of this experiment.

5.3.3 Live cell cycloheximide chase assay requires further optimisation

Having used western blotting to monitor βarr- and SHH-mediated PTCH1 degradation both by silencing of βarrs and by point mutation of the βarr binding site of PTCH1, I proposed the use of live cell imaging to observe the PTCH1 degradation in real time. For this, an mCherry-tagged PTCH1, both wild-type and carrying the SATA mutation to block βarr binding, were used. MCF7 cells were reverse transfected with these constructs into opaque walled, clear bottomed 96-well plates to image using an ImageXpress Pico Automated Cell Imaging System (Pico), which takes fluorescent images of cells in 96-well plates while incubating at 37 °C. A 40x magnification was used to obtain detailed images of the cells while still covering a significant area of the well to include many cells for quantification (~2000 cells imaged per well). For this assay, 24h after transfection, the cells were pre-incubated for 1h with Hoechst and 50 µg/mL cycloheximide. These were diluted in CO_2-independent media since the Pico incubator was not equipped to maintain an atmosphere of 5% CO_2. Following this, treatments (100 ng/mL rSHH or vehicle) were added, and cells imaged over the course of 6 hours (images taken every 30min).

Figure 5.3 presents the results from these assays. Panel A shows representative images from each condition at times 0 and 6 h (following addition of rSHH or vehicle). It is worth noting that since MCF7 cells are cancer cells, they have a high rate of migration, so the changes in positions of the cells seen in this figure is not a concern. From the images, a loss of PTCH1-mCherry can be seen between 0 h and 6 h for wild-type PTCH1 treated with rSHH. In all other conditions, the level of PTCH1 protein indicated by mCherry signal appears to be more stable, reflecting the results from the western blots in Figure 5.2.

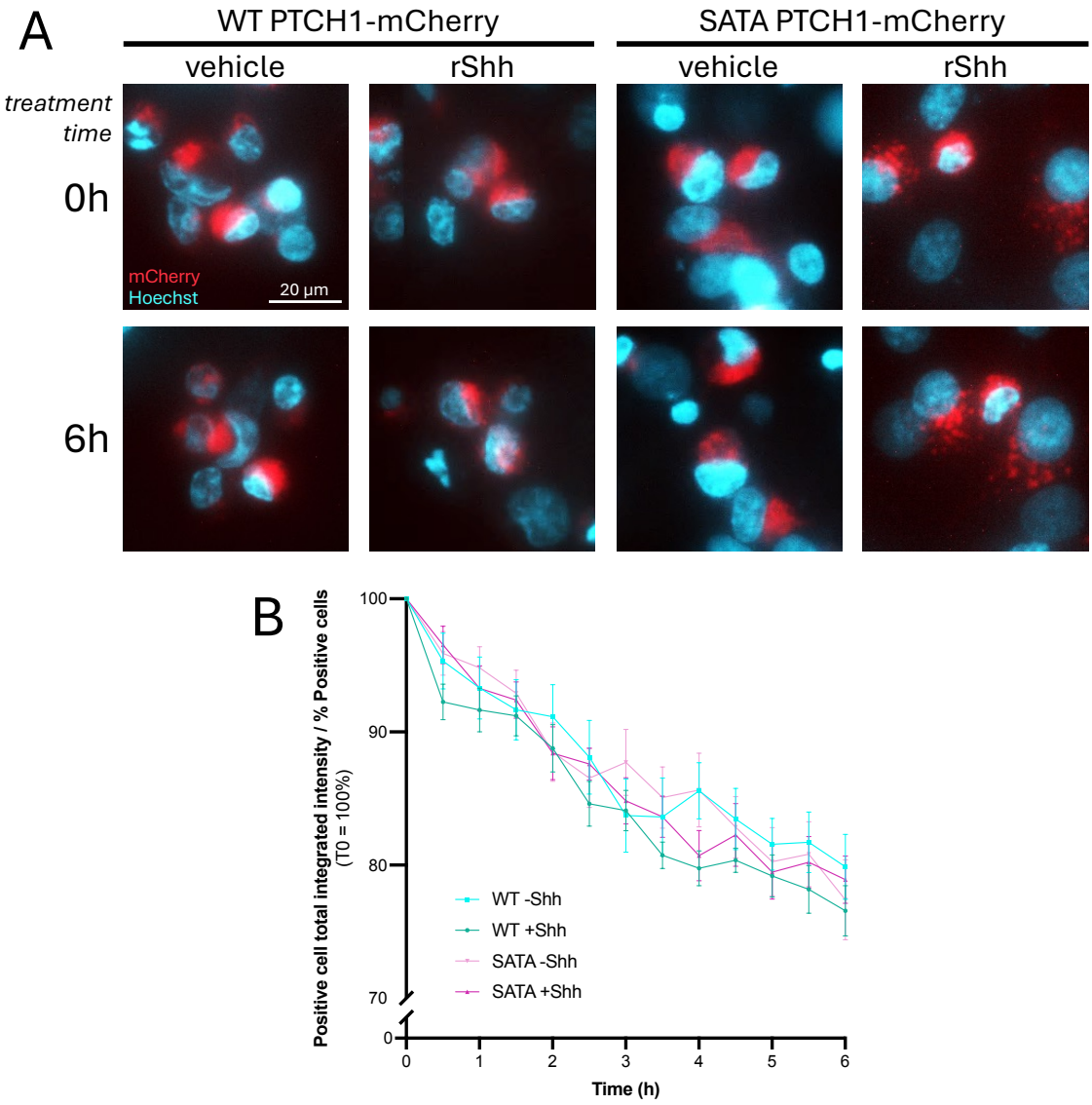

Figure 5.3 Continuous cycloheximide-chase assay with fluorescently tagged PTCH1

MCF7 cells were seeded in opaque-walled 96-well plates and transfected with indicated constructs. After 24 h, cells incubated with CHX 1h before addition of 100 ng/mL rSHH and imaging in an incubated Pico imager. Images taken every 30 min for 6 h. pcDNA control included for mCherry fluorescent background, none detected. (A) Representative images from time points 0h and 6h observing PTCH1-mCherry degradation. Hoechst= cyan, mCherry= red. Scale bar: 20 µm. (B) Software analysis of 'Positive cell total integrated intensity'/'% Positive cells', reporting relative intensity of mCherry marker in cells detected via Hoescht staining, normalised to proportion of live and transfected cells per well. Error bars= SEM.

Panel B shows the combined results from 3 independent experiments. The images were analysed with the instrument's built-in software CellReporterXpress®. The cell scoring function, which can quantify the fluorescence signal of markers (i.e. mCherry) in cells which have been detected by nuclear staining (Hoechst). The programme only detects live cells via nuclear staining of a specified minimum

width, and minimum and maximum intensity, which ensures only healthy cells are used in the analysis. Positive cells were selected if mCherry signal was detected in the cytoplasm, again with specified minimum width and minimum and maximum intensity. Of these mCherry-positive cells, total integrated intensity was reported, which is a sum of the intensities of each pixel in all positive cells. To control for variation in both total live cells per well and the number of positive cells among these, each well's total integrated mCherry intensity value was normalised to the percentage of positive cells per well.

This analysis did not appear to work optimally for this experiment. There is a lot of variation and the differences between the conditions are not statistically significant. While wild-type PTCH1 in the presence of SHH showed the lowest values, as expected, the difference to untreated condition is not significant, precluding drawing conclusions. I believe that the biggest limiting factors for this analysis are, firstly, a low transfection efficiency, as there are not enough positive cells to quantify and therefore any changes will be more variable. Secondly, the conditions for this experiment were not optimal, as there was evidence of significant cell death, which interferes with the imaging and analysis since dying or dead cells have very bright Hoechst (and sometimes mCherry) staining, and their overexposure can both hinder the imaging of other cells in their vicinity and skew the analysis. This experiment would require further optimisation to produce conclusive results; however, given the time constraints of this project and the fact that sufficient data had been produced from the western blot experiments, this was not taken further at this stage.

5.3.4 Caspase activity is enhanced by disruption of the PTCH1-βarr binding site

PTCH1 has been shown to trigger apoptosis through interaction of the CTD with a pro-apoptotic complex which includes DRAL, TUCAN, and pro-caspase 9 (Mille et al., 2009). PTCH1 induces apoptosis in the absence of SHH, acting as a dependence receptor, and addition of SHH ligand blocks the pro-apoptotic activity of PTCH1 (Thibert et al., 2003). Thus, the consequence of PTCH1-βarr interaction on its pro-apoptotic activity was measured using the Caspase-Glo® 3/7 Assay System by Promega, which provides a luminescent signal proportional to caspase-3/7 activity. Following transfection with test constructs, MCF7 cells were incubated overnight with 100 ng/mL rSHH. This model is slightly limited by the low transfection efficiency of MCF7 cells and that they express endogenous PTCH1, so the response seen is limited but still significant.

For wild-type PTCH1, I expected to observe an increase in apoptotic signalling compared to empty vector control under basal conditions, and for this increase to be blocked upon addition of SHH. This has been well studied, so this outcome is effectively a control for this system. When testing the effect of the PTCH1-βarr interaction in this model using the PTCH1 SATA mutant which blocks this interaction, several alternative outcomes were considered . Firstly, there could be no effect at all, with the same pattern of caspase activity in wild type and mutant PTCH1. Secondly, since addition of SHH reduces PTCH1-βarr binding, it could be possible that dissociation of βarrs from PTCH1 is linked to reduction in apoptotic signalling. In this scenario, the PTCH1 SATA mutant would have the same levels of caspase-3/7 activity as wild-type PTCH1 in the presence of SHH, since it would mimic the SHH-mediated dissociation of βarrs from wild-type PTCH1. Finally, since the SATA mutation increases PTCH1 stability, I would simply see the same trends in caspase-3/7 activity as wild-type, but enhanced by the higher levels of PTCH1 protein.

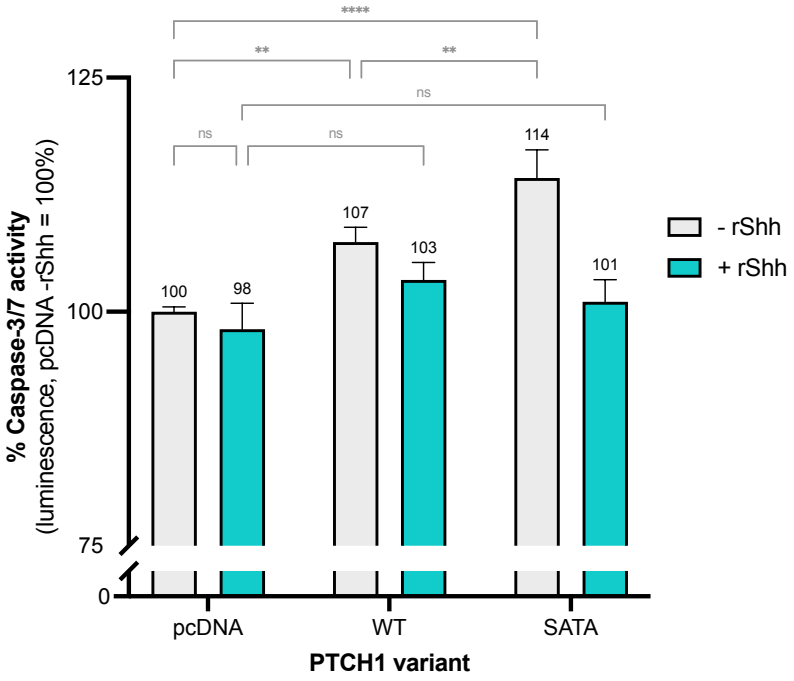

Figure 5.4 Caspase activity is enhanced by mutation of the PTCH1-βarr binding site, but is still blocked by SHH

MCF7 cells reverse transfected with indicated constructs and treated overnight with 100 ng/mL rSHH before assaying in the Caspase-Glo® 3/7 Assay System by Promega. N=4. 2-way ANOVA analysis: ns, not significant; ** P<0.01; **** P<0.0001. Error bars= SEM.

As expected, addition of SHH has no effect on the empty vector (pcDNA) control since MCF7 express very low levels of endogenous PTCH1 (Figure 5.4). In the absence of SHH, overexpression of wild-type PTCH1 increases caspase-3/7

activity, and SATA mutation increases this even further. Addition of SHH reduces caspase-3/7 activity to the level of pcDNA control in cells expressing either wild-type or mutant PTCH1. Therefore, while confirming the expected results of wild-type PTCH1 which increases apoptosis in the absence of SHH, an effect which is blocked by addition of SHH, I observed a clear negative effect of βarr binding to PTCH1 on its pro-apoptotic activity.

βarrs appear to negatively regulate PTCH1-dependent apoptotic signalling, most likely by enhancing the degradation of PTCH1. It also becomes apparent that the SHH-mediated blockade of apoptotic signalling is through a βarr-independent mechanism, since there is a significant decrease of caspase-3/7 activity when adding SHH to cells expressing PTCH1 SATA, which cannot bind βarrs in either condition.

5.3.5 Cell viability is decreased by disruption of the PTCH1-βarr binding site

Having observed an increase in PTCH1 stability and apoptotic signalling by mutation of its βarr interaction site, I expected that cell viability would be decreased in cells expressing wild-type PTCH1 and be enhanced further by SATA mutation. For this, I used a cell viability assay that uses WST-1 to give a colorimetric readout.

In live cells, the tetrazolium salt WST-1 is cleaved to formazan, a soluble dye which can be quantified by colorimetric measurement. This is catalysed by the succinate-tetrazolium reductase system which is active in the mitochondria of viable cells, requiring the production of NAD(P)H. This reagent therefore is commonly used to measure cell viability by addition to the media of cultured cells, where the amount of formazan produced positively correlates with the number of metabolically active cells. Following incubation, absorbance (450 nm - 650 nm) is measured and reported relative to the control.

MCF7 cell viability measured over 72 h decreased in cells overexpressing wild-type PTCH1 compared to an empty vector control. The PTCH1 SATA mutant induced a much larger decrease in viability (Figure 5.5), in agreement with the higher pro-apoptotic activity of that mutant. These results indicate that PTCH1-βarr interaction negatively regulates its stability and pro-apoptotic activity; i.e. reduces its tumour suppressor function.

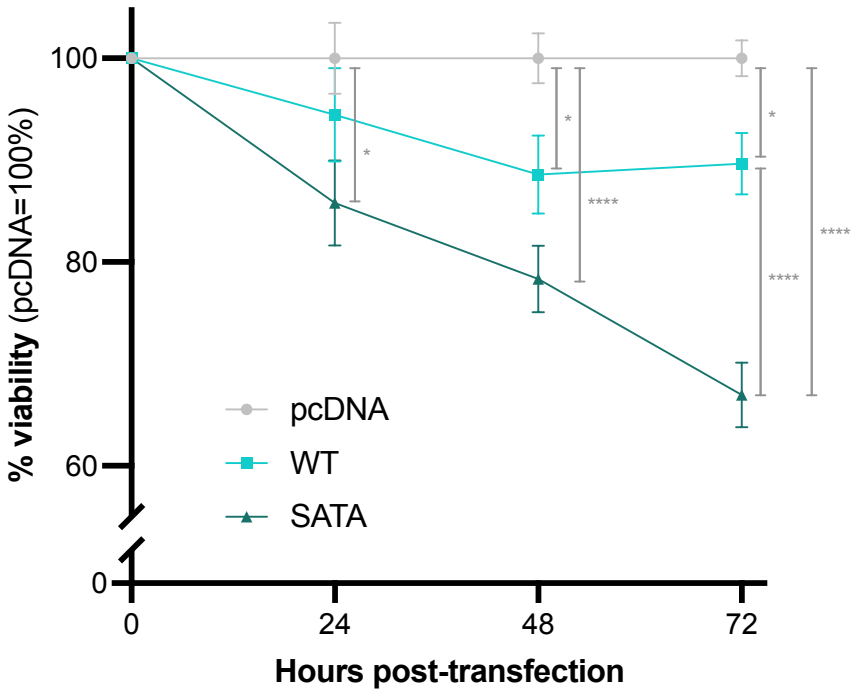

Figure 5.5 WST-1 assay shows disruption of the PTCH1-βarr binding site further decreases cell viability caused by PTCH1
MCF7 cells were transfected with indicated constructs and re-seeded after 6h into 96-well plates, 30,000 cells per well. WST-1 incubated for 1h at each time point and measured in a HIDEX plate reader. This is not an end-point assay so values from each time point normalised to pcDNA to reduce variability from development time differences. N=4. 2-way ANOVA analysis: * P<0.05; **** P<0.0001. Error bars= SEM.

5.3.6 Clonogenicity of PTCH1 is decreased by disruption of the PTCH1-βarr binding site

Overexpression of PTCH1 is known to decrease clonogenicity of cancer cells (Bhattacharya et al., 2008, Thibert et al., 2003), so to test any effect of βarrs on this process, MCF7 cells were transfected with either empty vector, wild-type PTCH1 or PTCH1 SATA. Figure 5.6 shows reduced colony formation by MCF7 cells overexpressing wild-type PTCH1, and a further decrease by the PTCH1 SATA mutant.

A clear trend can be seen, with pcDNA, WT, and SATA having the most, less, and least colonies, respectively. There was variability in the extent of this decrease between repeats which meant that statistical analysis did not show significance. However, a clear trend can be observed amongst independent experiments (as shown by the coloured lines in panel B). Therefore, a conclusion can be drawn that mutation of the βarr binding site in PTCH1 increases the tumour suppressor

function of PTCH1. If further repeats of this experiment were performed, statistical analysis would likely confirm this conclusion.

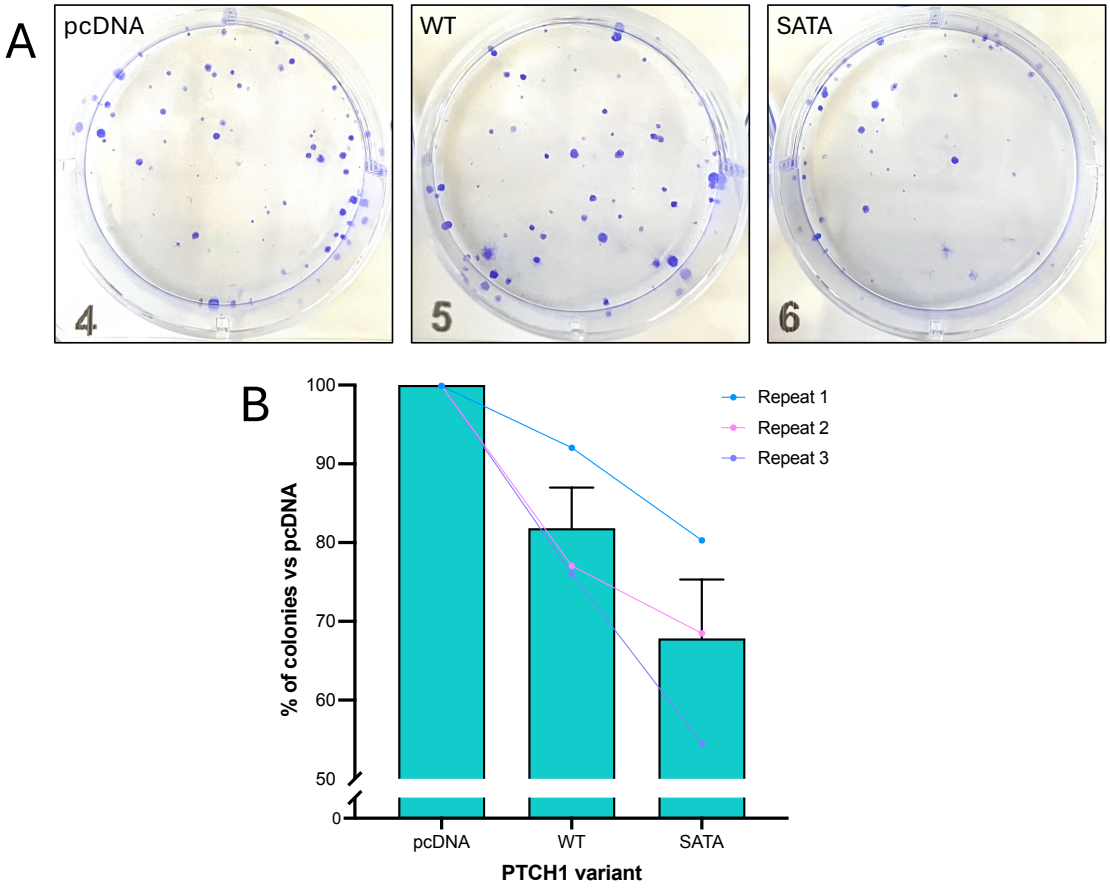

Figure 5.6 WT PTCH1 reduces clonogenic ability of MCF7 cells, which is further reduced by disruption of the PTCH1-βarr binding site
MCF7 cells were reverse transfected with indicated constructs and 24h later seeded in 6-well plates at a density of 750 cell per well. After 13 days, cells fixed with methanol and stained with crystal violet before manual counting. (A) Representative images of wells for each condition. (B) Summary of n=3 independent repeats. Error bars= SEM.

5.4 Discussion

In this chapter, I performed various assays to characterise the functional effect of the interaction between PTCH1 and βarrs based on known downstream signalling of PTCH1.

Firstly, the effect of the PTCH1-βarr interaction on canonical Hh signalling was assessed by measuring Gli-luciferase reporter activity under basal and SHH-stimulated conditions. Wild-type PTCH1 inhibits GLI transcriptional activity, which is rescued by inhibition of PTCH1 by addition of SHH. The same behaviour was

observed with the PTCH1 SATA mutant, as well as the three PTCH1 truncation mutants 1316*, 1308*, and 1203*. From this it was concluded that βarr recruitment to PTCH1 does not affect canonical signalling under these experimental conditions.

Since these PTCH1 mutants are more stable, it would have been reasonable to assume that they could further repress GLI activation through SMO. To thoroughly investigate this, I would repeat the experiment using recombinant SHH to include controls of incubation time and dose, since in this model the cells were under SHH-producing conditions for 24h, which is a long incubation, and the SHH produced is in a large excess. It would be interesting to see if a dose-response or time course of SHH addition would change the results and indicate an effect of PTCH1 stability on GLI transcriptional activity.

Using an end-point cycloheximide chase assay where cells transfected with wild-type PTCH1 or PTCH1-SATA were stimulated or not with SHH, I was able to reproduce results from preliminary work on this project discussed in Chapter 3 (Figure 3.2). The previous results showed a decrease in SHH-mediated PTCH1 degradation when βarrs were knocked down by RNA interference. Using PTCH1 mutants, a decrease in wild-type PTCH1 protein levels was observed under SHH-stimulated conditions unlike the stable levels seen in the absence of SHH; however, the PTCH1 SATA mutant level remained stable in the presence or absence of SHH. Therefore the interaction of βarrs accelerates SHH-mediated degradation of PTCH1. This indicates a combined role of both SHH and βarrs in the degradation of PTCH1.

Combining this with the findings described in Chapter 4, I propose that SHH binding to PTCH1 causes a conformational change that increases GRK2/3-mediated phosphorylation of the CTD to enhance βarr recruitment, and that this recruitment signals for the internalisation and degradation of PTCH1, during which βarrs become dissociated from PTCH1 as PTCH1 is trafficked to degradation machinery and βarrs are recycled for further use in the cell.

This result could of course mean that further functional effects of the PTCH1-βarr interaction may be due to differences in PTCH1 stability between wild-type and PTCH1 SATA mutant, rather than any direct complex formation between PTCH1, βarrs, and/or other adaptor and effector proteins. I therefore approached the results and conclusions of the remaining experiments with this in mind, debating both this and alternative explanations for effects observed.

While using live-cell imaging to monitor the degradation of PTCH1 would be beneficial, the experimental setup achievable within this project period was not optimal. To use the same equipment, further optimisation would be required to increase the percent of PTCH1-positive cells and reduce cell death. However, the cell death is quite unavoidable when transfecting with PTCH1, as demonstrated by enhanced apoptotic signalling observed in the Caspase-Glo® assay. The transfection efficiency of MCF7 cells was optimised to be as high as possible with reagents available, so optimising this may require the testing of different transfection reagents. Alternatively, a different cell line could be used, however was limited to what was available within the lab. HEK293 transfect a little better, but these cells do not have intact Hedgehog signalling so should not be used for phenotypic study. Another potential cell model are $Ptc1^{-/-}$ MEFs; however, their transfection efficiency for these cells is equally low, so the results obtained were not conclusive.

The aim of using the Pico live imaging system was to gather data from a high number of cells to generate a large dataset. However it seemed that this may have slightly sacrificed the quality of the data I was able to collect, therefore an alternative method may be to use live-cell confocal imaging. This would restrict the dataset produced, as confocal imaging is only usually able to capture one transfected cell at a time due to the low transfection efficiency. However the increase in quality would create a more accurate depiction of the degradation of PTCH1 within the cell. It would also generate more detail in terms of changes of localisation of PTCH1 over time following addition of SHH. Given more time, I would explore this next.

Using Promega's Caspase-Glo® 3/7 Assay, I was able to measure the increase in apoptotic signalling caused by overexpression of wild-type PTCH1, and the blockage of this by addition of SHH. The prevention of PTCH1-βarr binding by SATA mutation further increased the levels of apoptotic signalling under basal conditions, but this was reduced to the same level as wild-type PTCH1 following addition of SHH. Therefore, βarrs negatively regulate PTCH1-induced caspase-3/7 activation, most likely via enhanced degradation of PTCH1. The reduction of caspase-3/7 activity upon addition of SHH to the same level as control in both wild-type and PTCH1 SATA suggests that SHH blocks apoptotic signalling independently of the PTCH1-βarr interaction. This could be via a conformational change that prevents the binding of the pro-apoptotic complex and therefore the subsequent cleavage at D1405 to expose the PTCH1 pro-apoptotic domain. The increase in apoptotic signalling by the PTCH1 SATA mutation could also be due to a steric effect. It is possible that βarr binding competes for binding of the pro-apoptotic

complex containing caspase-9, and therefore PTCH1 is not cleaved as effectively to induce apoptosis when bound to βarrs. Removal of the βarrs binding site from the PTCH1 CTD by SATA mutation would allow binding of the pro-apoptotic complex.

After observing that prevention of βarr binding to PTCH1 enhances PTCH1 stability and apoptotic signalling, it is unsurprising that the WST-1 assay showed a larger reduction of cell viability over 72 h in cells transfected with PTCH1 SATA compared to cells expressing wild-type PTCH1. These results could be due to an increase in apoptosis, and therefore fewer live cells survive over time, as well as to increased blockage of cell cycle progression. PTCH1 is a cell cycle gatekeeper, interacting with cyclin B1 and preventing its nuclear accumulation to block cell cycle progression (Barnes et al., 2001). The overexpression of PTCH1 reduces cyclin B1-mediated cell proliferation, and it is possible that the enhanced stability of the PTCH1 SATA mutant causes a greater reduction. Therefore, I speculate that these two effects combined cause a greater reduction in cell viability over time through blocking the PTCH1-βarr interaction and enhancing PTCH1 stability.

Study of the effect of PTCH1-βarr interaction on the colony formation capacity of breast cancer cells showed that overexpression of the PTCH1 SATA mutant reduces colony formation to a greater extent than wild-type PTCH1. The pro-apoptotic function of PTCH1 is the key candidate that may cause this effect, which is increased by overexpression of wild-type PTCH1, and further by PTCH1 SATA.

The low transfection efficiency of cells with intact Hedgehog is a common caveat to the functional experiments performed in this chapter. I considered that generating stably transfected cell lines would solve this problem, however since PTCH1 is pro-apoptotic, it is likely that this would prove extremely difficult if not impossible, as cells consistently overexpressing PTCH1 would struggle to grow. Therefore given the time scale of this project this was not a route I explored.

I also explored the use of fluorescence-activated cell sorting (FACS) to enrich a population of cells positive for PTCH1 expression. For this I used $Ptc1^{-/-}$ MEFs to avoid interference of endogenous PTCH1 with experiments. Following transfection of the PTCH1-mCherry constructs, were detached, prepared for FACS, and sorted via mCherry. This technique was unsuccessful, as the cells were not able to tolerate the harsh conditions of the FACS process, especially following PTCH1 transfection. Any cells collected were seeded into tissue culture plates, but did not survive overnight to allow any testing of viability. Again, this could be optimised using different conditions or cell lines but this was outside the scope of this project.

The results suggest that the best route to solve the issue of low transfection efficiency in these functionally relevant cells would be viral transduction, for example using lentivirus, adenovirus, or adeno-associated virus. These generally are much more effective for inducing construct expression; however, require more time investment for generation and purification of the viruses as well as optimisation of cellular infection, and can carry the risk of insertional mutagenesis. However, if I was to continue with this project, I would explore this route to generate better datasets comparing the wild-type and PTCH1 SATA constructs.

In addition, the debate between more direct effects of the PTCH1-βarr interaction and indirect effects from the βarr-mediated degradation of PTCH1 creates some uncertainty in the conclusions from these results. I would propose a couple of techniques to investigate this and confirm or rule out an effect of differing rates of degradation between wild-type and PTCH1 SATA. One method would be to include inhibitors of protein degradation such as MG132 or Bafilomycin A1, which inhibit the proteasomal and lysosomal degradation pathways respectively. This would prevent degradation of both PTCH1 proteins and theoretically even out the levels of each mutant. However this could present other problems such as off-target effects due to being broad inhibitors, as well as increases in cell stress and toxicity. It may be effective for short-term assays but longer time scales may be negatively affected. Additionally, while this would prevent degradation, it wouldn't prevent internalisation, which is a key step and may be the main effector for changes in signalling efficacy between wild-type and SATA PTCH1, rather than the degradation itself which happens further downstream. Instead, inhibiting receptor internalisation may be a better way to equalise accessible protein levels. Since βarrs internalise GPCRs via clathrin-mediated endocytosis, I would start there. Chlorpromazine prevents the formation of clathrin-coated pits and would therefore prevent PTCH1 internalisation if that is the method used. If this did not work, other methods of internalisation could be investigated such as caveolin- or lipid raft-mediated endocytosis.

This project did not explore the effects of the PTCH1-βarr interaction on non-canonical type 2 signalling, for example calcium oscillations and cytoskeletal regulation. Since no effect was observed on canonical signalling, it is unlikely that there would be any effect on other signalling downstream of SMO. However, given the speculation on regulation of SMO signalling as a result of PTCH1 stability regulation by βarrs, these pathways may be worth exploring in future work.

The main open question regarding function of the PTCH1-βarr interaction is if it mediates ERK signalling. Initial work described in Chapter 3 (Figure 3.1) demonstrated a combined role of SHH and βarrs in negatively regulating ERK activation, since siRNA knockdown of βarrs enhanced ERK activation after 30 min of SHH stimulation. During the later stage of my project, after characterising the binding interaction and generating the SATA mutant, I attempted to investigate this, isolating the effect to the PTCH1-βarr interaction by comparing wild-type and SATA PTCH1 on ERK activation by SHH, rather than the global effect of βarr knockdown. Unfortunately, within the time scale of this project, I was not able to optimise experimental conditions that generated reproducible results to draw conclusions from. I believe the main problem was once more the low transfection efficiency, which is common across the cell lines to study Hedgehog signalling (e.g. MCF7, MEFs). I would suggest in any further work on this project to generate a high-expressing system using viruses as discussed, which should generate more conclusive results when investigating the effect of the PTCH1-βarr interaction on ERK signalling.

Together, this chapter highlights phenotypic effects of the PTCH1-βarr interaction. To summarise so far, βarrs reduce the tumour suppressor function of PTCH1 by enhancing PTCH1 degradation and reducing PTCH1-mediated apoptotic signalling. These effects indicate that targeting the interaction therapeutically may provide alternate routes to increasing PTCH1 tumour suppressor function for treatment of Hedgehog-related diseases and cancer, separate to SMO inhibitors, and may provide a way to modulate alternative signalling pathways that are PTCH1-dependent.

Chapter 6

Using AlphaFold 3 interaction simulations to confirm experimental results

Chapter 6

Using AlphaFold 3 interaction simulations to confirm experimental results

6.1 Introduction

In the previous chapters, *in vitro* experiments were used to identify the binding site and characterise the interaction between PTCH1 and βarr1. It has been determined that βarr1 binds to PTCH1 CTD residues S1223-T1229 in a GRK2/3-dependent manner, likely through the phospho-motif pSEYpSSQpT. In this chapter, AlphaFold 3, an artificial intelligence (AI) based tool which can be used to predict structures of macromolecules including proteins, both as monomers and multimers, was used to gain insight into the predicted binding interface between these two proteins.

The logical next direction of this project would be to solve the structure of the PTCH1-βarr1 heterodimer using X-ray crystallography or cryo-electron microscopy (cryo-EM). X-ray crystallography often produces higher resolution structures (<2 Å), although requires the protein to be crystallised which can be difficult to achieve with proteins that are membrane-bound or intrinsically disordered, both of which are elements of PTCH1. Cryo-EM flash-freezes the proteins to visualise them instead of requiring crystallisation, which is ideal for these kind of proteins that adopt multiple conformations, but often at the expense of resolution, which is important to investigate details of a binding interface. Although, in recent years the technique has advanced and higher resolution can be more readily achieved. Unfortunately, structural characterisation of the PTCH1-βarr1 interaction was beyond the scope of this project. However, this chapter comprises a preliminary structural study using *in silico* predictive tools to assess how PTCH1 and βarr1 might interact *in vitro*.

AlphaFold is a deep learning tool developed by DeepMind, which uses an AI-enhanced version of machine learning to predict protein structures from their amino acid sequences. The revolution of protein structure prediction that AlphaFold brought is evidenced by the recent Nobel Prize in Chemistry to Demis Hassabis and John Jumper. AlphaFold uses algorithms which integrate large datasets of known protein structures and sequences to model proteins and complexes based on user-input sequences. A feature of the newest version of AlphaFold, AlphaFold 3 (AF3) (Abramson et al., 2024), is the ability to add post-translational modifications to proteins, unlike AlphaFold 2 or Multimer. Since

phosphorylation has been shown to be such an integral part of the PTCH1-βarr1 interaction, this version of the software was the only feasible option for this study.

The AF3 server is available to the public, and generates structural models based on simple sequence input. It is also able to predict structures of DNA, RNA, ligands, and ions, however the focus here is proteins. For each simulation, it produces 5 models, each accompanied by 3 important metrics which are crucial for interpreting their accuracy and reliability: the predicted local distance difference test (pLDDT), predicted template modelling (pTM), and interface predicted template modelling (ipTM) scores.

The pLDDT score is assigned to each atom in the model, ranging from 0 to 100, with higher scores reflecting greater confidence in the predicted position of the atom within the structure. Colouring of the models according to AF3 pLDDT scores (AF pLDDT) used in this chapter is as follows: very high (pLDDT > 90) coloured dark blue; confident (90 > pLDDT > 70) coloured light blue; low (70 > pLDDT > 50) coloured yellow; very low (pLDDT < 50) coloured orange. The pTM score is derived from the traditional template modelling (TM) score, which measures the similarity between two experimentally solved protein structures. Here, the pTM score reflects the predicted global similarity between the generated model and the true structure of the protein. Finally, the ipTM score is specific to multimeric models and indicates the confidence in the predicted interactions at the interface between proteins in a complex.

In this chapter, AF3 was initially used to perform a broader superficial evaluation of predicted structures to assess whether βarr1 could bind to PTCH1 via any of the 10 other *p*x(x)*p*xx*p*/E/D motifs in the CTD cluster described in Chapter 4 aside from the identified SEYSSQT motif, as well as the number of phosphorylated residues required for βarr1 to bind to the SEYSSQT motif. Following this, the focus was shifted to a detailed analysis of the predicted PTCH1-βarr1 structure formed by SEYSSQT phosphorylation, including some variants of PTCH1 to isolate the study to the SEYSSQT-βarr1 interaction interface. For these critical structures, more models were generated – 50 instead of the initial 5 – allowing for a more detailed examination and increasing confidence in the accuracy of the models chosen for visual analysis.

The key structures that will be seen throughout this chapter are shown in Figure 6.1. These are experimentally solved structures, available on the RSCB Protein Data Bank (PDB). Panel A shows the structure of human βarr1 obtained by X-ray

crystallography, recognisable by two domains of beta sheets. Some loop sections appear to be missing however this is due to intrinsic disorder so these regions cannot be resolved experimentally. Panel B shows the structure of the human PTCH1 monomer, which experimentally does not show any cytosolic domains since these intrinsically disordered regions cannot be solved by cryo-EM and so were partially truncated to improve protein expression. The 12-transmembrane helical bundle can be seen spanning the membrane (grey lines), with the two large extracellular loops (ECLs) above this, where the Hedgehog ligands bind. The AF3-predicted structures in this chapter will contain these two recognisable structures, with the addition of the unsolved disordered cytosolic regions, often appearing as large 'strings' in the models.

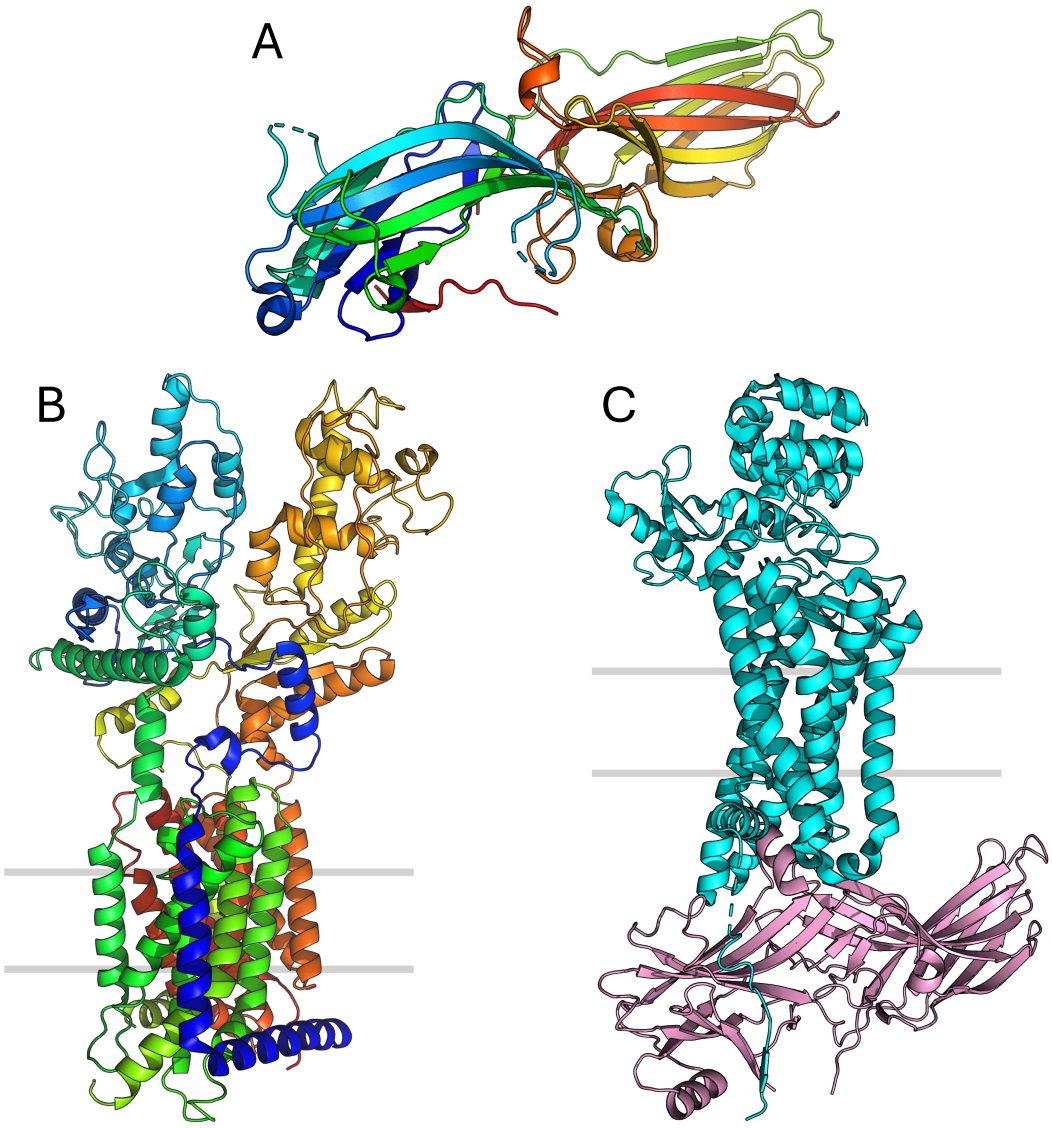

Figure 6.1 Key structures for this chapter
PyMOL-generated images. (A) Human βarr1, PDB ID: 8AS4. (B) Human PTCH1, PDB ID: 6DMB. Grey lines indicate plasma membrane. (A, B) Rainbow colouring from blue N-term to red C-term. (C) Rhodopsin-arrestin structure from Zhou et al, PDB ID: 5W0P. Rhodopsin in cyan, arrestin in pink (Zhou et al., 2017). Grey lines indicate plasma membrane.

Panel C shows the rhodopsin-arrestin structure solved in the paper identifying the *p*x(x)*pxxp*/E/D motif (Zhou et al., 2017), where the C-tail of human rhodopsin interacts with mouse visual arrestin-1. This study focussed on visual arrestin since rhodopsin is primarily found in rod cells; however, its structure is similar to βarrs and their interactions with GPCRs, for example βarr1 with vasopressin-2 receptor (V2R) (Shukla et al., 2013), and therefore represents a common interface between GPCR C-tails and βarrs.

6.2 Aims and hypotheses

1. Use AlphaFold 3 to model PTCH1-βarr1 interaction
2. Compare the predicted models to *in vitro* results
3. Analyse the models using confidence scores and existing experimental information

6.3 Results

6.3.1 Truncating PTCH1 ECLs will allow study of CTD-βarr binding

For predictions of βarr binding to PTCH1 in this chapter, AF3 simulations frequently predict βarr binding at the large ECLs of PTCH1. This is likely due to the higher confidence in ECL predictions, as they are more ordered and their structures have been experimentally resolved through X-ray crystallography and cryo-EM, providing AF3 with more reliable data for structure prediction. Because the CTD is intrinsically disordered, it is not favoured over the ECLs for binding. The ECLs do contain *p*x(x)*pxxp*/E/D motifs so it is unsurprising that a binding interface is predicted here. However, βarrs are intracellular, so this prediction is not supported by the biology of the system and was ignored. To circumvent this and to focus on CTD binding predictions, a truncated PTCH1 sequence, lacking all ECL residues except for five at each end to preserve small loops, ensuring proper folding between transmembrane helices, was tested.

The difference between the predicted models for full-length PTCH1 and PTCH1 with deleted ECLs (ΔECL) can be seen in Figure 6.2, panels A and B. As shown by the pLDDT colouring, the transmembrane core and ECLs in full-length PTCH1 have high confidence scores. The ΔECL version maintains high confidence in the transmembrane core, while both models have equally low confidence of the disordered cytosolic domains, as expected. This also means the pTM score is reduced from 0.7 to 0.59 by removal of the ECLs, but this is expected since the

percentage of intrinsic disorder (N-terminal domain, middle loop, and CTD) increases from 36% to 58% by removing the ECLs.

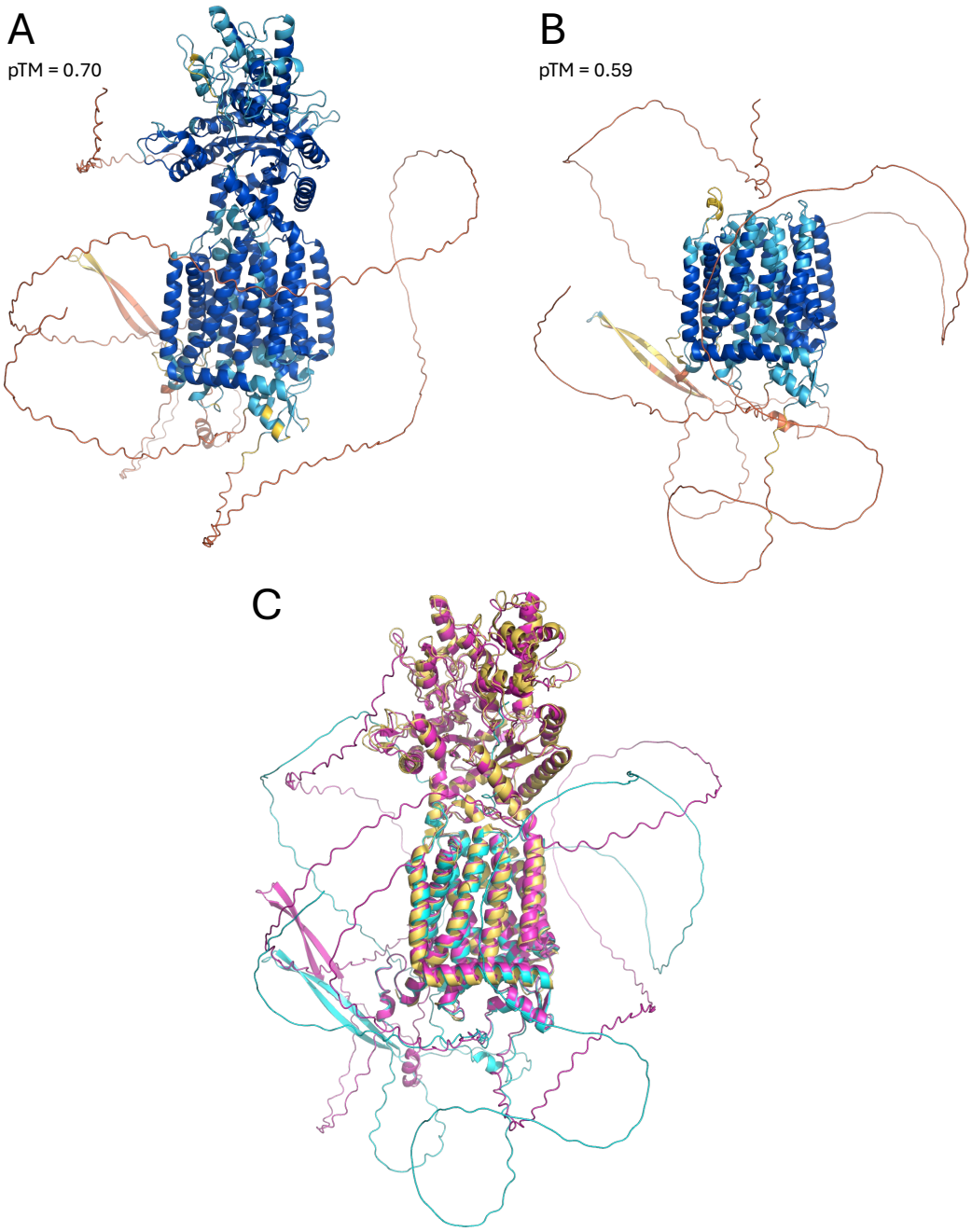

Figure 6.2 Removing PTCH1 large ECLs does not disrupt the remaining structure
(A) Full-length PTCH1 coloured by AF pLDDT. pTM= 0.7. (B) PTCH1 with ECLs removed coloured by AF pLDDT. pTM= 0.59. (C) Aligned structures of A (full-length PTCH1, magenta), B (ECLs removed, cyan), and human PTCH1 solved by cryo EM (PDB ID: 6DMB, yellow).

To confirm that removal of the ECLs does not disrupt the remaining structure, specifically the ordered transmembrane core, the two models were aligned together along with the cryo EM-solved structure of human PTCH1 (PDB ID: 6DMB). Panel C shows the full length PTCH1 model in magenta, truncated model in cyan,

and the cryo EM structure in yellow. The ordered parts of each structure align well, with the full length model matching the solved structure of the extracellular domains, and all 3 demonstrating very similar structure in the transmembrane core. Of course the disordered cytosolic domains do not align tightly, but importantly, little change can be observed in the transmembrane core by removing the ECLs. Therefore this truncated model can be used to study predicted CTD binding of βarrs with the knowledge that the absence of the ECLs does not affect the transmembrane or cytosolic structures.

6.3.2 AlphaFold 3 hallucinates order in disordered regions

In the 6 months since the release of AF3, many have observed an issue that it creates believable structure from disordered regions. The cytosolic domains of PTCH1 are intrinsically disordered, which leaves it susceptible to this effect. Indeed, when phosphates are added to the SEYSSQT motif (pS1223, pS1226, pT1229), AF3 models often create helical bundles from the cytosolic domains, which are shown in Figure 6.3, panel A being the unmodified full length PTCH1, and panel B the same full length sequence with the three phosphates added. Both of these models have a pTM score of 0.70.

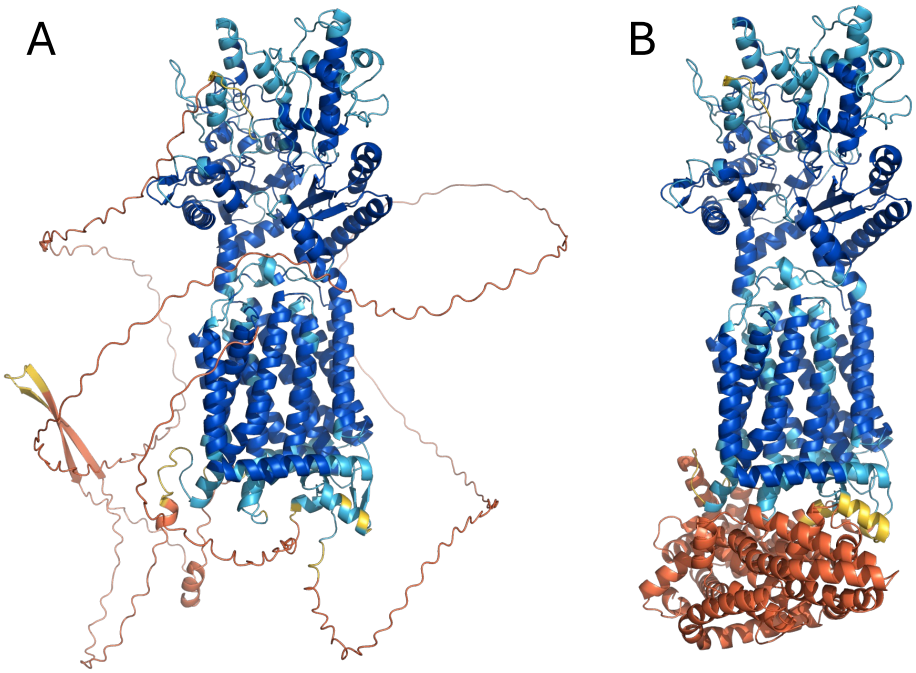

Figure 6.3 Hallucinated helical bundle created by phosphorylation of the SEYSSQT motif
(A) Full length unmodified PTCH1 coloured by AF pLDDT. (B) Full length PTCH1 modified with phosphorylation at S1223, S1226, and T1229, coloured by AF pLDDT.

The pLDDT score for residues in this helical bundle are very low, as seen by the orange colouring, which reinforces the idea that this structure has very low confidence. It is important to take this into consideration when analysing models for the interaction with βarrs.

6.3.3 Phosphorylation-mediated PTCH1-βarr1 binding is predicted by AlphaFold 3

With the conditions for AF3 simulations optimised and key caveats established, interactions were analysed using the truncated (Δ ECLs) PTCH1. Figure 6.4 shows representative models generated for interactions between PTCH1 and βarrs. Panels A and B are with βarr1, and E and F with βarr2, both with unmodified PTCH1 (A and E) or with the three key phosphates added to the βarr1 binding site pSEYpSSQpT (B and F).

These predictions suggest that neither βarr can bind to unmodified PTCH1, and that βarr2 does not interact with PTCH1 even when the SEYSSQT motif is phosphorylated (pSEYpSSQpT). Since the algorithm has been told to create a multimer, it will force an interaction between the two proteins, creating an interface it calculated to be the most likely. Where the model shows an interaction between βarrs and the small ECLs above the plane of the membrane with low ipTMs (here 0.23-0.26), it was concluded that an interaction with the CTD does not occur and that the predicted interaction is not physiologically possible. Mirroring the *in vitro* studies, βarr2 was not investigated any further in this chapter. Importantly, as expected from experiments discussed in Chapter 4, the CTD of PTCH1 is predicted to bind to βarr1 only when phosphorylated at S1223, S1226, and T1229 (Figure 6.4 B).

While the CTD helical bundle predicted by AF3 when the βarr binding motif phosphorylated is most likely the result of forced and unrealistic folding, the model has higher confidence at the triple phosphorylated SEYSSQT motif and generates a binding interface with βarr1. Panel C shows a zoom of the interface between phosphorylated PTCH1 and βarr1, with βarr1 set to 80% transparency to allow for clearer visualisation. The colouring of the SEYSSQT motif, as highlighted by the arrow, shows a higher pLDDT score for these residues compared to the unmodified PTCH1 model, and these scores are shown graphically in panel D.

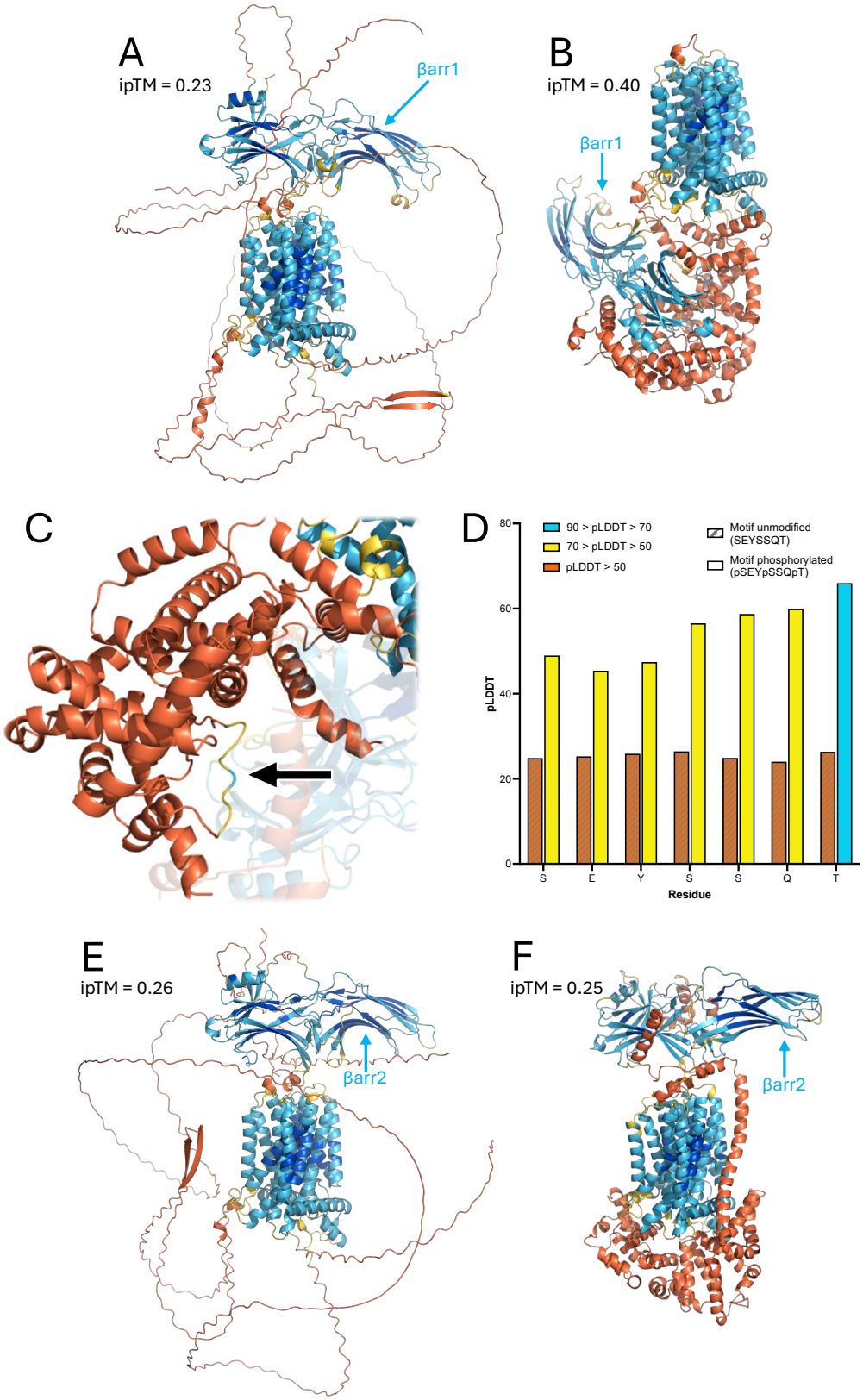

Figure 6.4 βarr1 is predicted to bind to phosphorylated motif pSEYpSSQpT
All models use PTCH1 with truncated ECLs, and are coloured by AF pLDDT. (A) Unmodified PTCH1 with βarr1. ipTM= 0.23. (B) PTCH1 phosphorylated on SEYSSQT motif (pS1223, pS1226, pT1229) with βarr1. ipTM= 0.4. (C) Zoom of PTCH1 CTD in B, βarr1 80% transparent. Arrow indicates SEYSSQT motif with higher pLDDT. (D) Bar chart showing pLDDT scores for each residue of SEYSSQT motif in A (unmodified) and B (phosphorylated). Bars coloured by AF pLDDT. (E) Unmodified PTCH1 with βarr2. ipTM= 0.26. (F) PTCH1 phosphorylated on SEYSSQT motif (pS1223, pS1226, pT1229) with βarr2. ipTM= 0.25.

6.3.4 βarr1 is not predicted to bind to other *p*x(x)*p*xx*p*/E/D motifs

As discussed in Chapter 4, there are 11 regions in the PTCH1 CTD that conform to the the *p*x(x)*p*xx*p*/E/D motif. Since *in vitro* analysis of point mutants demonstrated the necessity for the SEYSSQT motif at S1223-T1229 for βarr1 interaction, the other motifs were not investigated any further. However, to assess the potential role of the other motifs in this interaction, simulations were run mimicking each of the motifs in their phosphorylated state.

Table 6.1 contains the details of each of these simulations, where for each phosphorylated motif, the number of models which create a binding interface between that motif and βarr1 is listed, as well as the highest ipTM score for these models. As previously seen (Figure 6.4), an interface is created when the SEYSSQT motif is phosphorylated at S1223, S1226, and T1229. Interestingly, none of the remaining 10 motifs are predicted by AF3 to interact with βarr1, and instead the models are more similar to the non-interacting models shown in Figure 6.4 (panels A, E, and F). This increases the confidence in the conclusion that the PTCH1 SEYSSQT phospho-motif is the sole binding site for βarr1.

Region	Sequence	Phosphorylated residues	βarr1-motif complex?	ipTM
1214-1219	THSGSD	T1214, S1216, (D1219)	0/5 models	0.24
1216-1221	SGSDSS	S1216, S1218, S1221	0/5 models	0.27
1218-1223	SDSSDS	S1218, S1220, S1223	0/5 models	0.19
1218-1224	SDSSDSE	S1218, S1221, (E1224)	0/5 models	0.22
1220-1226	SSDSEYS	S1220, S1223, S1226	0/5 models	0.21
1221-1226	SDSEYS	S1221, S1223, S1226	0/5 models	0.20
1223-1229	SEYSSQT	S1223, S1226, T1229	4/5 models	0.40
1226-1232	SSQTTVS	S1226, T1229, S1232	0/5 models	0.22
1227-1232	SQTTVS	S1227, T1229, S1232	0/5 models	0.20
1229-1235	TTVSGLS	T1229, S1232, S1235	0/5 models	0.25
1230-1235	TVSGLS	T1230, S1232, S1235	0/5 models	0.22

Table 6.1 Predictions of *p*x(x)*p*xx*p*/E/D motifs binding to βarr1
Table details variations of PTCH1 (truncated ECLs) input into AF3 to mimic phosphorylation of each *p*x(x)*p*xx*p*/E/D motif identified. Number of models reported where complex formed between βarr1 and the PTCH1 CTD motif of that row, rather than small extracellular loops as described. Highest interface predicted template modelling (ipTM) score for each run listed.

6.3.5 βarr1 binding to the SEYSSQT motif requires triple phosphorylation

Experimentally, mutating only one of the three phosphorylated residues in the SEYSSQT motif significantly reduces the PTCH1-βarr interaction observed via co-IP (Figure 4.4). This reinforces the reported conclusion that high-affinity βarr binding requires three receptor-attached phosphates (Zhou et al., 2017). This concept was tested computationally using AF3, assessing the predicted interaction of βarrs with the PTCH1 CTD when phosphorylating one, two, or all three of the key residues in the SEYSSQT motif (S1223, S1226, and T1229).

The only condition that predicted an interaction between the SEYSSQT motif and βarr1 was where the 3 key residues were phosphorylated to form the full phospho-motif, pSEYpSSQpT (Table 6.2). Again, all other models created the forced interaction with the small extracellular loops, suggesting that no interaction with the CTD occurs.

Sequence	Phosphorylated residues	βarr1-SEYSSQT complex?	ipTM
SEYSSQT	-	0/5 models	0.23
SEYSSQT	S1223	0/5 models	0.24
SEYSSQT	S1226	0/5 models	0.24
SEYSSQT	T1229	0/5 models	0.23
SEYSSQT	S1223, S1226	0/5 models	0.21
SEYSSQT	S1226, T1229	0/5 models	0.18
SEYSSQT	S1223, T1229	0/5 models	0.25
SEYSSQT	S1223, S1226, T1229	4/5 models	0.40

Table 6.2 Predictions of PTCH1 CTD-βarr1 interaction with varying levels of phosphorylation
Table details PTCH1 (truncated ECLs) with combinations of 0, 1, 2, or 3 phosphates on the SEYSSQT motif input into AF3 with βarr1. Number of models reported where a complex was formed between βarr1 and the SEYSSQT motif rather than small extracellular loops as described. Highest interface predicted template modelling (ipTM) score for each run listed.

Together, the results so far corroborate the findings from Chapter 4 which identified the PTCH1 binding motif for βarr1 at CTD residues S1223-T1229, phosphorylated according to Zhou et al's phosphorylation code to form pSEYpSSQpT. The AF3 predictions additionally suggest that βarr2 does not form an interaction to this motif, and that this is the only motif in the CTD that βarr1 is able to bind to, requiring

phosphorylation of all 3 residues in the motif. Having established this, this study was continued by looking more closely at this identified interaction.

6.3.6 Phospho-motif pSEYpSSQpT binds to a positively charged pocket in βarr1

A closer look at the interaction between the PTCH1 motif pSEYpSSQpT and βarr1 reveals a specific structure- and charge-based interface. The PTCH1 CTD section containing the pSEYpSSQpT motif sits within a positively charged pocket of βarr1 rich in lysine and arginine residues. The PyMOL APBS (Adaptive Poisson-Boltzmann Solver) Electrostatics plugin is able to determine electrostatic potential of a protein and display this as a surface representation with a coloured scale, red being negative, white being neutral, and blue being positive.

This is visualised in Figure 6.5, where PTCH1 is represented by cartoon in cyan, and βarr1 by surface, coloured by electrostatic potential. Panel A shows the full heterodimer as in Figure 6.4 B, except with the aforementioned representations instead of pLDDT colouring. Panel B shows how the phosphorylated SEYSSQT motif fits tightly into the pocket of βarr1 which is coloured blue indicating positive electrostatic potential. Polar contacts found by the PyMOL software are shown in panel C, indicated by yellow dashed lines, which includes some electrostatic bonds between the phosphorylated PTCH1 residues and the positively charged βarr1 residues, although since electrostatic bonds can be longer in range, there may be some additional contacts not detected by the PyMOL software here. The negatively charged phosphate groups of the pSEYpSSQpT motif are predicted to create electrostatic bonds with the lysine and arginine residues of βarr1 (K11, R25, K160, R161, R165, K294).

Interestingly, some contacts are made between βarr1 and non-phosphorylated residues in the SEYSSQT motif. This could provide some reason as to why the PTCH1-βarr1 appears to be specific to this motif, and not the other *p*x(x)*p*xx*p*/E/D motifs in the PTCH1 CTD. For example tyrosine (Y1225) is known to be important for mediating protein recognition and smaller residues such as serine provide conformational flexibility, so together these non-phosphorylated residues can create favourable contacts for binding (Koide and Sidhu, 2009).

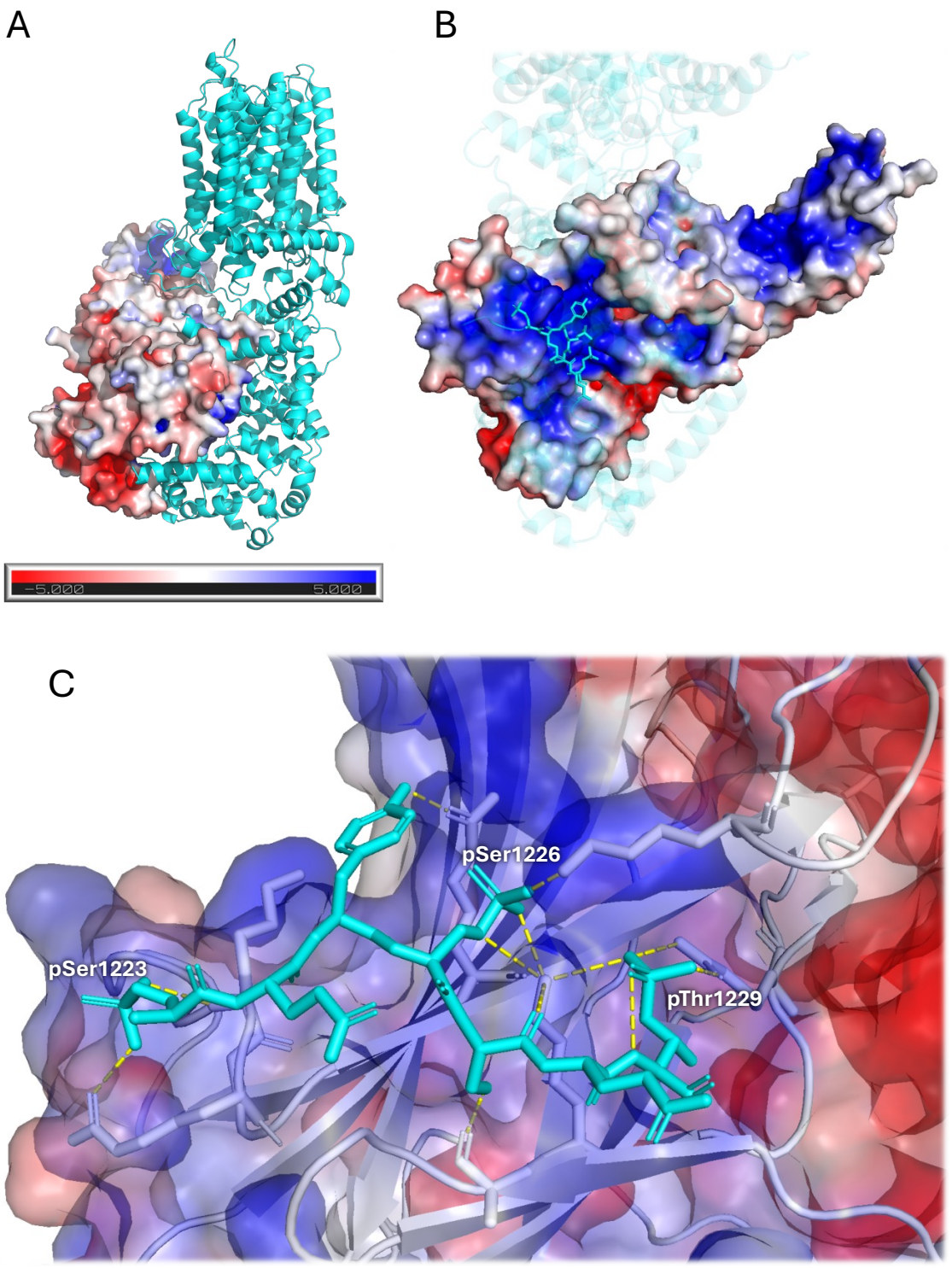

Figure 6.5 Interface between PTCH1 phospho-motif pSEYpSSQpT and βarr1
Colouring scale of electrostatic potential is as follows: red – white – blue corresponds to -5 kT/e – 0 kT/e – +5 kT/e. Scale shown in A but applies to A, B, and C. ipTM 0.40. (A) PTCH1 in cyan. βarr1 shown as surface coloured via electrostatic potential. (B) Rotate and zoom of A, PTCH1 at 80% transparency, except pSEYpSSQpT motif shown with sticks. (C) Zoom of interface between pSEYpSSQpT motif and βarr1. Key PTCH1 phosphorylated residues labelled in white. βarr1 cartoon in white, with surface at 60% transparency coloured by electrostatic potential. Contact-forming βarr1 residues shown as sticks. Yellow dashed lines indicate polar contacts.

6.3.7 The SEYSSQT motif alone is sufficient for βarr1 binding

While the models discussed thus far are supported by the experimental results, the ipTM scores are low (0.40 for the model discussed in section 6.3.6). Generally, scores this low are not accepted in the field, as the confidence in the model and the binding interface is not sufficient to create conclusions. However, I suggest that a large reason for the low score is the amount of disorder in this complex. PTCH1 has many large intrinsically disordered regions, as discussed, and even βarr1 has some small disordered sections in the structure.

As previously discussed, the helical structures created from the cytosolic domains of PTCH1 in these models is possibly hallucinated by the AF3 algorithm. I suggest that for the PTCH1-βarr1 interaction to take place, the only crucial part of PTCH1 is the phosphorylated SEYSSQT motif. To determine this, two artificial sequences were created to input into AF3, which should create similar binding interfaces if this hypothesis is correct. Firstly, a 'scrambled' version of PTCH1 (SCR). Specifically, the sequence of the N-terminal domain, large middle loop, and CTD were separated except the phosphorylated SEYSSQT motif. Keeping this motif in the same sequence and position, and maintaining the methionine at the start of the N-terminal domain, a random sequence rearranger was used to scramble the remaining cytosolic sequence. Then this scrambled sequence was re-inserted back into the PTCH1 construct, maintaining the original lengths of each section. This created a construct where the large, intrinsically disordered cytosolic domains are completely rearranged, leaving only the SEYSSQT motif in its original place. Should this construct maintain an interaction with βarr1 with a similar interface and either equal or higher ipTM, this shows that there is no specific role for the rest of the cytosolic domains of PTCH1 in this interaction.

Additionally, to reinforce this hypothesis further, an additional input sequence consisting of a short peptide of the PTCH1 CTD was used. It contains the phosphorylated SEYSSQT motif plus the 4 flanking residues at either side for stability, creating a 15-residue peptide. Again, should this peptide create a similar binding interface between the SEYSSQT motif and βarr1, it would demonstrate the lack of necessity of the rest of PTCH1 in this interaction, and an ipTM of higher value would further reinforce this, having removed much of the disordered region which ordinarily brings down the ipTM score.

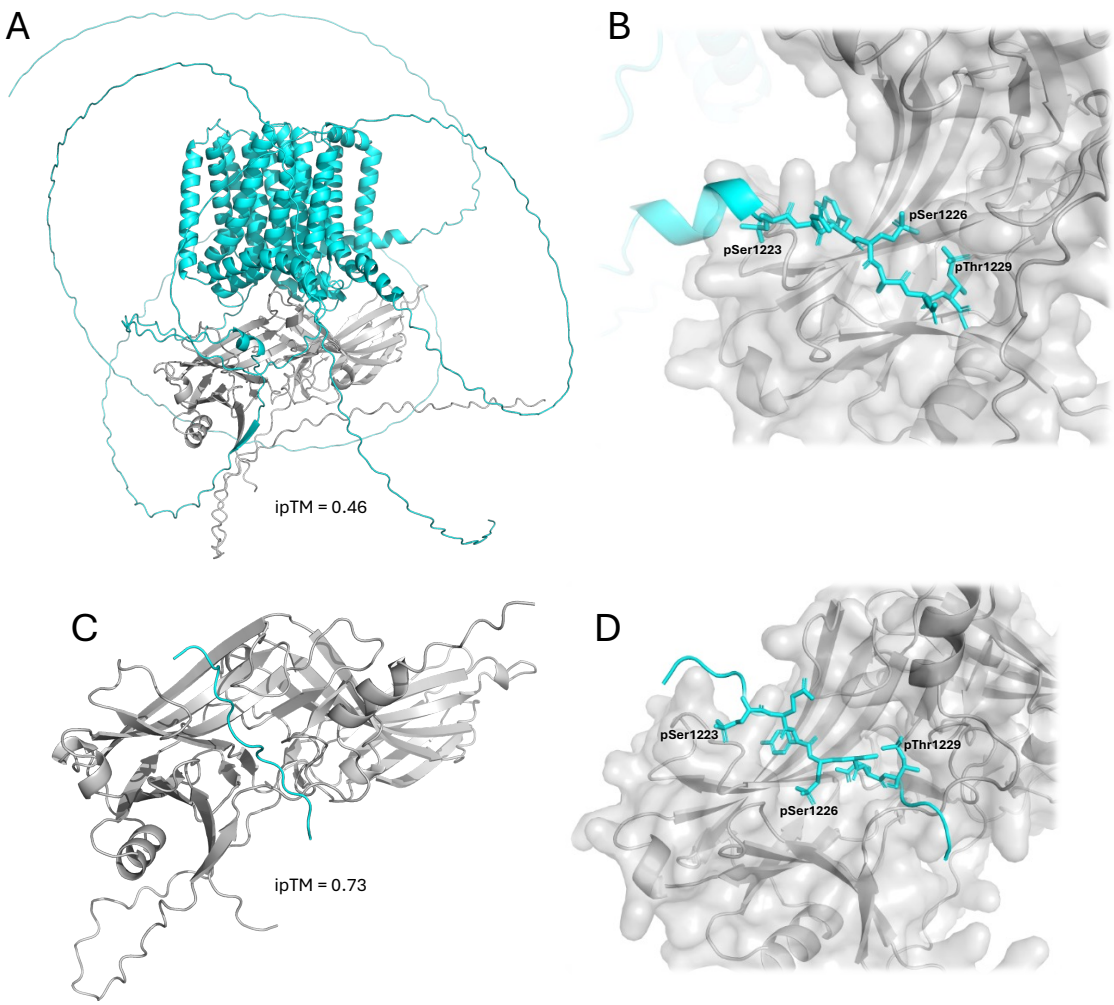

Figure 6.6 Models of scrambled PTCH1 and PTCH1 peptide with βarr1
(A) PTCH1 SCR in cyan, βarr1 in grey. ipTM: 0.46. (B) Zoom of A with SEYSSQT motif shown as sticks, with phospho-residues labelled and βarr1 surface added at 60% transparency. Remaining PTCH1 sequence faded to 90% transparency for clarity. (C) PTCH1 peptide in cyan, βarr1 in grey. ipTM: 0.73. (D) Zoom of C with SEYSSQT motif shown as sticks, with phospho-residues labelled and βarr1 surface added at 60% transparency.

The PTCH1 SCR construct is shown in Figure 6.6 A. The scrambled cytosolic domains maintain the string-like structure of disordered regions as wild-type PTCH1, unlike the phosphorylated or βarr1-bound version of wild-type PTCH1 with the 'hallucinated' helical bundle. However, a closer look (panel B) shows that the pSEYpSSQpT motif binds to the same groove of βarr1 in a very similar manner. Additionally, the short peptide also maintains this interaction but with higher confidence (ipTM = 0.73), shown in panels C and D. In both cases, if the SEYSSQT motif is not phosphorylated, no CTD-βarr1 interaction is formed.

When looking in more detail at these interactions, more models should be used to have higher confidence in the predictions generated and conclusions made from them. For interactions between βarr1 and these two PTCH1 constructs (SCR and

peptide), as well as wild-type PTCH1 (without ECLs) both unmodified and phosphorylated at S1223, S1226, and T1229, 50 models of each were generated in AF3. These 4 simulations were then compared, assessing differences in ipTM scores, the number of polar contacts made between the SEYSSQT motif and βarr1, and how closely aligned their binding interfaces are.

To more closely look at the binding interface and if it is maintained between the models using different PTCH1 constructs, their structures were compared directly. The best and most representative models from each set were aligned based on the βarr1 structure, since that is the most uniform part of each of the structures (Figure 6.7). The rhodopsin-arrestin structure from Zhou et al's study was also included to compare the binding interface between PTCH1 and βarr1 to that considered to be universal for GPCR-arrestin binding (Zhou et al., 2017). The key region for the three PTCH1 constructs remains the SEYSSQT motif, and in rhodopsin is a slightly different variation of the *p*x(x)*pxxp*/E/D code, with the phosphorylated sequence of pTVpSKTE at residues 336-341.

The WT and SCR versions of PTCH1 align very closely, with each of the 3 key residues, S1223, S1226, and T1229 residing in the same location for both models. The short peptide PTCH1 model is also very similar, except the T1229 residue does not quite follow the same direction as the others. This is most likely because there are very few residues either side of the motif, so the protein is less constrained to fit into tighter spaces that may not be possible for the full length versions. However, the fact that the SEYSSQT motif still binds to the same groove in βarr1 and that the first two key residues align very well is encouraging, and reinforces the hypothesis that the rest of the cytosolic domains of PTCH1 are not necessary for βarr1 binding.

Additionally, the rhodopsin structure from Zhou et al sits within the same βarr1 groove as the PTCH1 constructs, which again suggests that these predicted interfaces are reflective of the true interactions. The specific alignment is very close but slightly shifted, where the T1229 of PTCH1's SEYSSQT aligns with S338 of rhodopsin's TVSKTE (Figure 6.7 B). Whether or not these predicted differences in positioning between rhodopsin and the PTCH1 constructs are reflective of the true interface would need to be assessed experimentally using X-ray crystallography or cryo-EM. AF3 does not provide definitive structures, so it is possible that the PTCH1-βarr1 interfaces predicted are not exactly correct. However, it could be that these models do reflect the true binding interfaces, and perhaps the slight differences in positioning are there to provide substrate specificity. For example different 'x' residues within the *p*x(x)*pxxp*/E/D motifs, as well as whether or not there is a second

'x' in the motif, will differ between targets. This specificity may be the basis for arrestins' ability to elicit different cellular responses depending on its protein target.

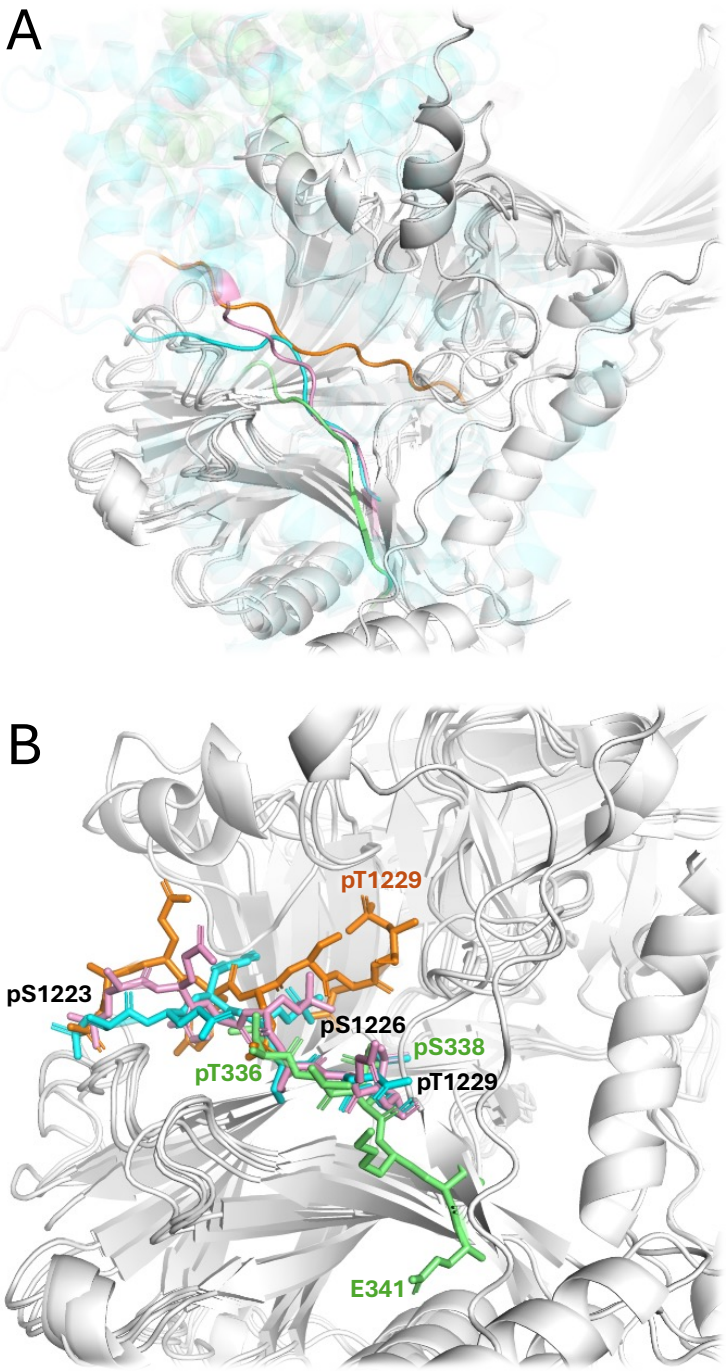

Figure 6.7 Aligned models show similar binding interfaces
Four models aligned by βarr1 structure. PTCH1 WT in cyan, SCR in pink, peptide in orange, and rhodopsin in green (PDB ID: 5W0P). βarr1 is shown in white. (A) Cartoon representation, SEYSSQT or equivalent rhodopsin motif are opaque, and the remaining structures fade out to 95% transparency. (B) Same alignment as A, with only the phosphorylated SEYSSQT motif of PTCH1 or equivalent rhodopsin motif shown in sticks and all other PTCH1 or rhodopsin structure removed. Labels indicate residues, either coloured to match each model, or in black when representing the same residue in multiple structures.

6.3.8 Comparison of multiple models increases confidence in the predicted binding interface

As previously mentioned, 50 models were generated for interaction between βarr1 and 4 PTCH1 constructs. These were the wild-type PTCH with ECLs truncated, either unmodified or phosphorylated at pSEYpSSQpT, PTCH1 SCR, where the cytosolic domains had been scrambled except the pSEYpSSQpT motif, and the 15-residue peptide with 4 residues either side of the pSEYpSSQpT motif.

Quantitative information was obtained for each of the models (Figure 6.8). The ipTM scores for each model were recorded and displayed, as shown in panel A. Additionally, the number of polar contacts found by PyMOL between the SEYSSQT motif and βarr1 was counted for each model, and displayed in panel B. The relationship between these two parameters is shown in panel C, with each model represented by a point of the corresponding colour to its construct, to visualise the distribution of models based on these variables.

The ipTM graph (panel A) shows that the ipTM for the unmodified version of PTCH1 is consistently low, and as previously mentioned there is no CTD binding as displayed in panel B. The phosphorylated version of PTCH1 has a greater distribution of ipTM scores, with many higher than the unmodified version. Generally, those with the lowest ipTMs do not form an interaction between SEYSSQT and βarr1 (panel C). Those with higher ipTMs (≥ 0.4) have between 7 and 11 polar contacts. These higher ipTM models are more reliable than the cluster with lower scores. Interestingly, scrambling the cytosolic domains besides the SEYSSQT motif increases the ipTM of the models. Additionally, all models create an interaction between pSEYpSSQpT and βarr1. It is possible that the scrambled sequence creates an easier protein for AF3 to interpret and predict, possibly removing some potential clashes or unfavourable interactions, which provides more consistent outputs and so higher-scoring models. The wild-type interaction is likely to be stringent, to allow for proper regulation and specificity of the interaction, which makes it more difficult for AF3 to predict.

The distribution of the number of polar contacts does not greatly differ between the three phosphorylated constructs. However, as expected, the ipTM scores for the PTCH1 peptide are generally much higher. Removing the rest of the PTCH1 sequence takes away a lot of the disorder in the complex, which improves the confidence of the structures and interaction predicted. Since the peptide construct creates a very similar binding interface to wild-type and SCR, and has higher ipTM

scores, it can be concluded that the pSEYpSSQpT motif is necessary and sufficient for βarr1 binding, and the local interface predicted by AF3 is likely to be accurate despite the lower global confidence in the models.

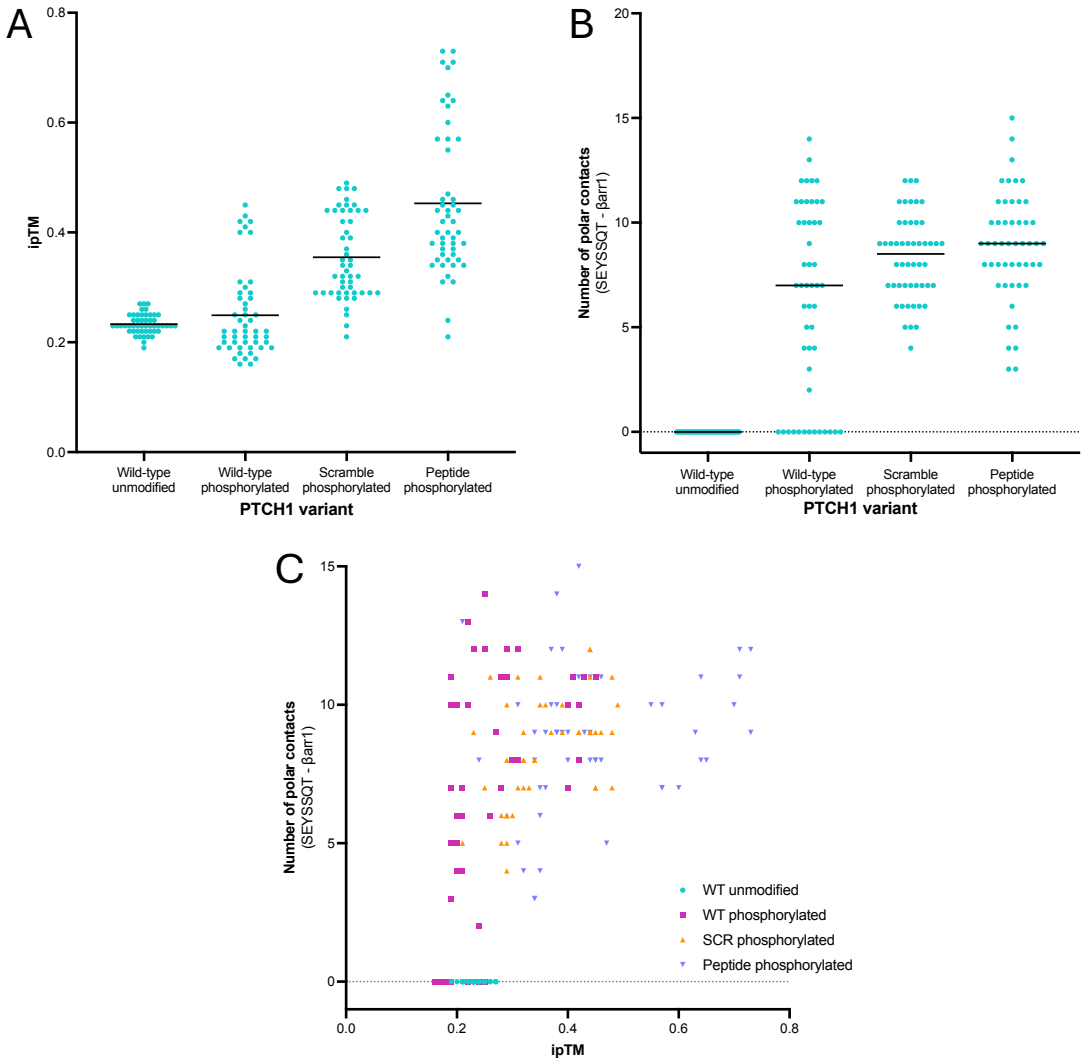

Figure 6.8 Quantification of ipTMs and polar contacts for PTCH1 models
Comparing 4 models: wild-type unmodified (no ECLs PTCH1 with no PTMs), wild-type phosphorylated (no ECLs PTCH1 with phosphorylation at S1223, S1226, and T1229), scramble phosphorylated (cytosolic domains scrambled as described, pSEYpSSQpT phosphorylated), peptide phosphorylated (15-residue peptide as described, phosphorylated to pSEYpSSQpT). (A) ipTM of each of the 50 models for each construct with βarr1. (B) Number of polar contacts detected by PyMOL between SEYSSQT and βarr1. (C) Combined A and B to show distribution of models for each construct.

6.4 Discussion

Together, AF3 was used to corroborate the results from previous chapters, where βarr1 binds to PTCH1 via a phosphorylation code, pSEYpSSQpT, spanning PTCH1 CTD residues 1223-1229, via a similar mechanism to GPCR recruitment of βarrs.

Throughout this chapter, the limitations of AF3 in accurately predicting structures, particularly for proteins with intrinsically disordered regions, have been highlighted. For example the helical structures generated that are likely to be hallucinated were mostly ignored, and instead we looked specifically at the small interaction interface. As such, the conclusions drawn here are approached with caution, fully acknowledging the inherent weaknesses of this AI-based tool for IDRs. However, since these simulations serve to support experimentally demonstrated findings, and align with *in vitro* results, they can be interpreted with greater confidence than if this were a solely theoretical study.

As mentioned previously, AF3 was the chosen tool for this study based on the ability to input post-translational modifications, since phosphorylation plays such a crucial role in the PTCH1-βarr1 interaction. Other versions, including AlphaFold 2 and AlphaFold multimer do not have this option. In fact, during preliminary investigations before the release of AF3, simulations of complex formation between PTCH1 and βarr1 were attempted using phosphomimetic mutation as was attempted *in vitro* in Chapter 4 (Figure 4.5). However, similar to the *in vitro* results, no interaction was generated even when trialling different versions of phosphomimetic mutation, including both aspartate and glutamate in the substitutions.

The results from AF3 reflect those from previous chapters. Investigation into the effect of phosphorylation of the CTD of PTCH1, specifically of the Ser/Thr residues involved in the *p*x(x)*pxxp*/E/D motif clusters described in Chapter 4 (Figure 4.3) show that the pSEYpSSQpT motif characterised experimentally is the sole βarr1 binding motif among the other candidate motifs in the PTCH1 CTD. Phosphorylation of all 3 key residues (S1223, S1226, T1229) is required for βarr1 binding, and no interaction is formed by triple phosphorylation of any of the other 10 *p*x(x)*pxxp*/E/D motifs.

The models from AF3 suggest that βarr2 does not bind to the SEYSSQT motif, unlike βarr1. However, the initial co-immunoprecipitations performed (Figure 3.3) showed some interaction between PTCH1 and βarr2. The *in vitro* PTCH1-βarr2 interaction seen in that experiment does appear to be weaker than PTCH1-βarr1, but it is still significant. It is possible that βarr2 is able to bind PTCH1 at a different site than βarr1, perhaps one of the other *p*x(x)*pxxp*/E/D motifs in the CTD, or even in the large intracellular loop, where there are some occurrences of this phosphorylation code. However, further investigation of this effect was not within the scope of this project, and given the low pLDDT and ipTM scores of these AI-generated structures, would

additionally require *in vitro* experiments to verify the models generated as with the PTCH1-βarr1 results.

A closer look at the predicted interface between PTCH1 and βarr1 shows several bonds between the negatively charged section of the PTCH1 CTD created by phosphorylation of the SEYSSQT motif, and a positively charged groove of βarr1 which has a significant number of lysine and arginine residues. The bonds formed between negative phosphate groups and positive lysine or arginine residues are likely to be the driving forces in creating and maintaining the PTCH1-βarr1 interaction. There are additional polar bonds predicted in many of the models involving the main chains or other residues, for example the tyrosine at PTCH1 position 1225. These are not likely to be as important for the interaction, however highlight a potential role of the non-phosphorylated residues of the SEYSSQT motif which could be spatial, the larger residues such as tyrosine, and smaller serine side chains creating a precise shape which fits specifically within the landscape of the βarr1 groove, and creates specificity for this motif only.

A comparison of the PTCH1-βarr1 interface using different versions of PTCH1 shows that the rest of the cytosolic domains of PTCH1 are not required for binding, instead only the SEYSSQT motif is necessary. Creating a PTCH1 construct where the sequence of the large cytosolic domains is scrambled, except for the pSEYpSSQpT motif, does not affect the binding interface. Additionally, very little change is seen in the interface when PTCH1 is reduced to a 15-residue peptide including the phosphorylated SEYSSQT motif with 4 residues either side. Furthermore, the ipTM scores for the peptide models are increased significantly, which is consistent with the hypothesis that the low scores of the full-length models are mainly due to the large regions of intrinsic disorder, and therefore removing a lot of this disorder increases the confidence of the model. Together, these suggest that for this specific interaction, only the triple phosphorylated SEYSSQT motif is required, and no other part of the cytosolic regions of PTCH1 are required for βarr1 binding. It is possible that, as previously mentioned, βarr1 makes a secondary interaction with the large middle loop of PTCH1, which may have a functional role similar to the core interaction βarrs form with GPCRs. However when focussing on the primary interaction, the SEYSSQT motif is both necessary and sufficient for βarr1 binding to PTCH1.

Interestingly, these models using PTCH1 variants, which align closely to each other, also align closely to the rhodopsin-arrestin complex solved by Zhou et al in their paper describing the *p*x(x)*pxxp*/E/D motif (Zhou et al., 2017). This supports the

hypothesis that the recruitment of βarrs to PTCH1 is similar to their recruitment to GPCRs. There are some small shifts in the precise location of the aligned residues, which may be an inaccuracy in the predictions, or alternatively may be true and these minor differences may create the specify of these interactions, allowing differentiation between βarr1 and βarr2, and GPCRs, PTCH1, and other receptors that may form similar interactions.

While these results are encouraging and provide further insight into the PTCH1-βarr1 interaction, the next step in this project should explore generating *in vitro* structural models of the interface. The models generated by AF3 should be approached with a level of caution, and methods such as X-ray crystallography or cryo-EM would provide much more certainty, particularly regarding the fine details of the interaction such as the orientation of key residues and bonds formed between the two proteins. However, the models described in this chapter corroborate the findings described in earlier chapters and indicate that further structural investigation into the PTCH1-βarr1 interaction would be beneficial.

Chapter 7

General discussion

Chapter 7

General discussion

7.1 Discussion

Hedgehog signalling orchestrates crucial biological processes, including embryonic development and adult tissue homeostasis. PTCH1 acts as a negative regulator of the pathway by inhibiting SMO, preventing canonical signalling. Recent insights highlight the multifaceted roles of PTCH1 beyond its canonical function, which is what was further investigated in this project. A phosphorylation-dependent interaction was uncovered between PTCH1 and βarr1. βarrs are traditionally associated with GPCR signalling; however, emerge here as modulators of PTCH1's stability and downstream effects.

This study comprised systematic characterisation of a novel interaction between PTCH1 and βarr1, which, with PTCH1 being a 12-transmembrane receptor around twice the size of most GPCRs, was slightly unexpected. The classical mechanism of βarr recruitment to GPCRs involves ligand-mediated GPCR activation, GRK phosphorylation of the GPCR C-tail, and subsequent βarr binding. Using those elements to guide this investigation, as well as a universal GPCR-βarr phosphorylation code, *px*(x)*pxxp*/E/D (Zhou et al., 2017), the PTCH1 binding motif for βarrs was identified.

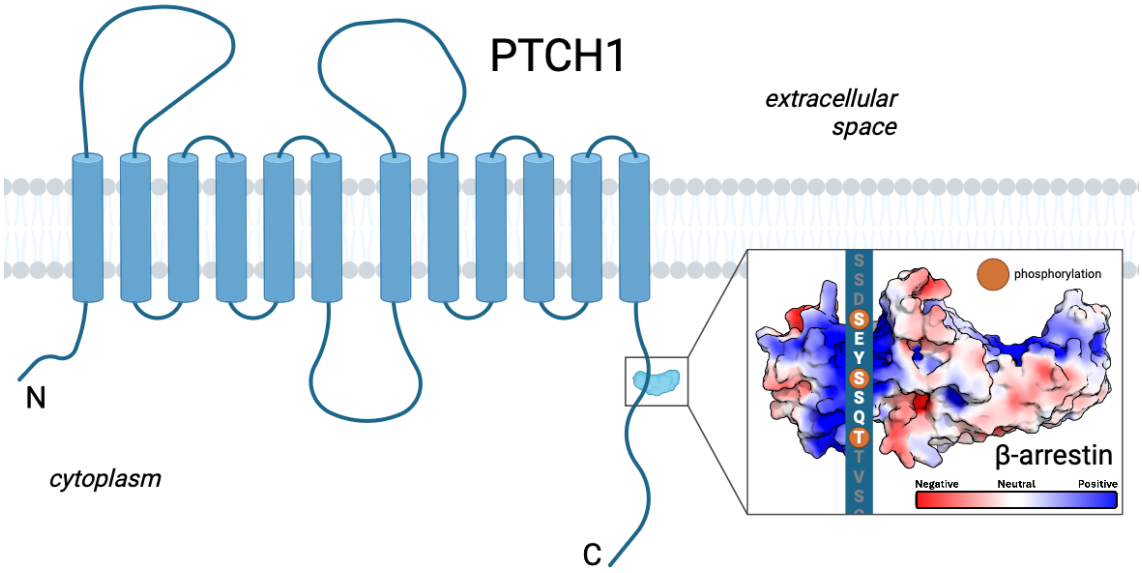

Figure 7.1 Schematic of the PTCH1-βarr1 interaction
Created in BioRender.com. Schematic of PTCH1 topologically spanning the plasma membrane, and βarr1 binding to the SEYSSQT motif of the CTD. Not to scale.

Residues S1223-T1229 of the PTCH1 CTD are phosphorylated by GRK2/3 to form the motif pSEYpSSQpT, to which βarr1 binds (Figure 7.1). Mutation of either S1223 or T1229 to alanine individually or both together blocks βarr1 binding as seen by co-immunoprecipitation of these PTCH1 mutants with endogenous βarrs. Using mass spectrometry, we observed that only residues S1223, S1226, and T1229 are phosphorylated. Significant reduction of PTCH1-βarr binding by addition of GRK2/3 inhibitor cmpd101 identifies these kinase(s) as the principal mediator(s) of this interaction via phosphorylation of the motif. Additionally, these conclusions were supported by *in silico* studies using AlphaFold 3 to predict the binding interface, which also highlights the necessity of the phosphorylation of S1223, S1226, and T1229. This creates a negatively charged section of the PTCH1 CTD which sits within a positively charged groove in βarr1, creating multiple electrostatic bonds and precise spatial arrangement for a stable interaction.

The function of the PTCH1-βarr1 interaction has been shown to primarily regulate the stability of PTCH1. PTCH1 has a high turnover rate, but its degradation is accelerated by binding to SHH. SHH-stimulated PTCH1 degradation is reduced by siRNA knockdown of βarrs, as well as by the SATA mutation of PTCH1 (S1223A and T1229A) which blocks βarr1 binding. Together, these results demonstrate the requirement for βarr recruitment to PTCH1 for its SHH-mediated degradation. This role of βarr1 in ligand-receptor complex degradation is consistent with its primary role in GPCR desensitisation and signal termination. However, internalised PTCH1-βarr1 complex could also trigger βarr-dependent signalling like in GPCRs (Shukla et al., 2011).

Addition of the PTCH1 inhibitory ligand SHH also reduces PTCH1-βarr1 binding as determined by co-immunoprecipitation; however, the mechanism for this is uncertain. Treatment with SHH for 30 min decreases PTCH1-βarr interaction levels; however, significant degradation of PTCH1 requires binding of both SHH and βarrs, and is observed at 2-6 h following SHH stimulation. Therefore, given these two results, I suggest that SHH binding promotes recruitment of βarrs to PTCH1, possibly via a conformational change which enhances GRK2/3 phosphorylation (Jiang et al., 2009). This, together with PTCH1 ubiquitination (Chen et al., 2014), promotes the internalisation and degradation of PTCH1, during which βarrs dissociate from PTCH1 to be recycled for other uses in the cell (Figure 7.2). The mechanism by which PTCH1 is internalised is not fully understood but requires ubiquitination at K1426 by HECT-domain containing E3 ligases, and I would suggest exploring this in a continuation of this project. I hypothesise that clathrin-mediated endocytosis plays the biggest role in PTCH1 internalisation, since that is the

process by which GPCRs are internalised following βarr recruitment by interaction of βarrs with AP-2 (Kang et al., 2014).

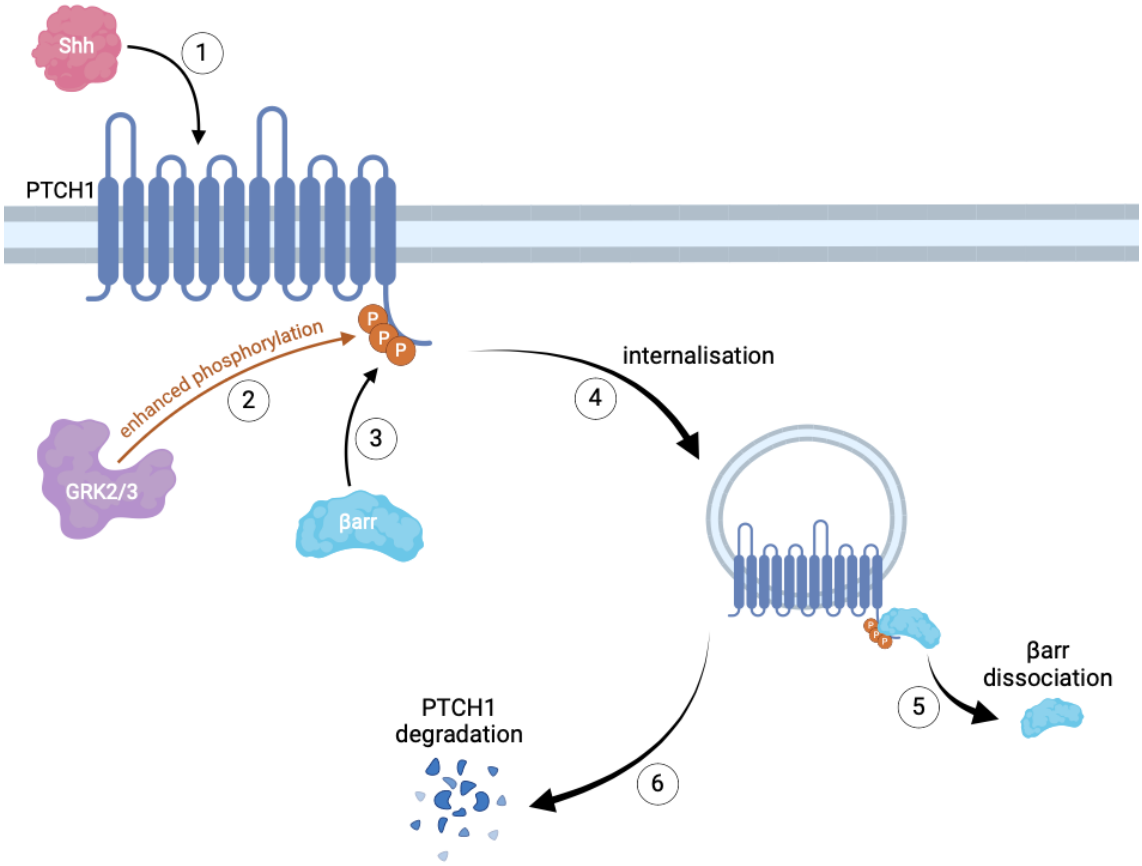

Figure 7.2 Proposed mechanism of SHH- and βarr-mediated PTCH1 degradation
PTCH1, shown initially at the plasma membrane, is bound by extracellular SHH ligand (1), which enhances intracellular GRK2/3 binding and phosphorylation of the SEYSSQT motif with 3 phosphates (2). Subsequent recruitment of βarrs (3) promotes PTCH1 internalisation by an unknown mechanism (4). Following internalisation, βarrs are dissociated from PTCH1 and recycled in the cell (5) before PTCH1 is eventually degraded (6). Created with BioRender.com.

This schematic does not currently include the ubiquitination of PTCH1, since although it is known to be required for PTCH1 internalisation and degradation, it is not fully understood at which point it would occur. However, I have developed a hypothesis linking SHH-mediated enhanced binding of GRK2 to PTCH1 (Jiang et al., 2009), PTCH1-βarr1 binding in the absence of SHH, dissociation of PTCH1-βarr1 after 30 min SHH stimulation, and SHH- and βarr-mediated PTCH1 degradation observed at 4 h. It is possible that under basal conditions, βarr1 binds to PTCH1 only at its CTD, a conformation which does not induce PTCH1 internalisation or degradation. Upon binding of SHH, PTCH1 undergoes a conformational change which enhances GRK2/3 binding, and allows βarr1 to bind PTCH1 via a double

interface, both at the CTD and ICL of PTCH1, perhaps mediated by increased GRK2/3 phosphorylation of PTCH1. This conformation would be much more stable, similar to the additional binding of βarrs to the transmembrane domain and intracellular loops of GPCRs as discussed in Chapter 1. Additionally, this conformation may enable PTCH1 ubiquitination, possibly stabilising the interaction of Itch or scaffolding the interaction between bound Itch and its ubiquitination site K1426. This would then induce internalisation and degradation of PTCH1, during which βarr1 is deubiquitinated and dissociates from PTCH1, which is why we observe reduction in binding after 30 min SHH stimulation, but PTCH1 has already entered endocytic pathway to be degraded, so reduction in protein levels at 4 h can be observed.

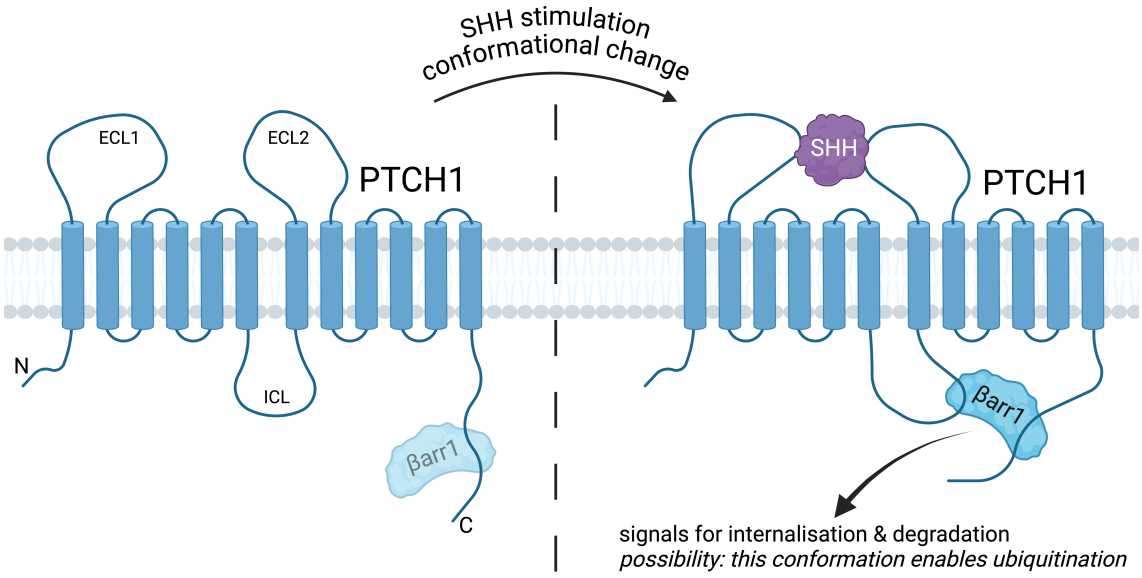

Figure 7.3 Hypothesis of SHH-mediated PTCH1 degradation and βarr1 dissociation
Created in Biorender.com. In addition to Figure 7.2. In the absence of SHH, βarr1 binds to PTCH1. SHH stimulation causes a conformational change and additional βarr1 binding, possibly a conformation that leads to PTCH1 ubiquitination to signal for internalisation and degradation.

An aim of this project was to use mass spectrometry to confirm phosphorylation of S1223, S1226, and T1229. Due to limitations imposed by the uncertainty of phosphate localisation within PTCH1 CTD peptides that contain multiple phosphorylatable residues, this could not be achieved directly. However, using candidate phosphorylation site mutants of PTCH1, it was shown that within the region of interest for βarr binding (residues 1214-1235), only S1223, S1226 and T1229 are phosphorylated, since triple point mutation to 'DDE' removes all detected phosphorylation. It would be beneficial to optimise the experiment to

definitively show phosphorylation of these residues, as well as confirm the kinase responsible via treatment with cmpd101 to block GRK2/3 phosphorylation.

Another interesting result would be to see if phosphorylation levels or patterns are affected by SHH treatment, since GRK2/3 binding has been shown to increase in the presence of SHH (Jiang et al., 2009), and I have hypothesised that SHH binding induces a dynamic increase in βarr recruitment. To achieve this, it is possible that alternative equipment and software would be required, since those available during this project are not the best equipped for phosphoproteomic studies. As well as using alternative or multiple proteases to produce smaller peptides, employing electron transfer dissociation (ETD) instead of higher-energy collisional dissociation (HCD) for fragmentation is likely to be beneficial. ETD is known to better preserve post-translational modifications, such as phosphorylation, whereas HCD can disrupt the phosphoester bond, leading to a loss of the phosphate group and potentially underrepresenting the true level of phosphorylation.

Disruption of the PTCH1-βarr interaction does not affect canonical signalling through GLI when measuring transcriptional activity after 24 h stimulation with co-transfected SHH. It is possible that under different conditions there may be other effects seen, for example using recombinant SHH to achieve shorter incubation times or using lower doses, since it would be expected that βarr-mediated changes in PTCH1 stability would affect the level of SMO activation. However, from the results observed, there is no evidence to support a PTCH1-βarr interaction-mediated effect on canonical signalling, so this was not investigated further at this stage. Future work should explore this however, using various experimental conditions to fully characterise the relationship between the PTCH1-βarr interaction and signalling through SMO. As well as canonical signalling, non-canonical type 2 signalling downstream of SMO could be explored, which was not within the scope of this project but could also be affected by βarr regulation of PTCH1 in different conditions.

Aberrant activation of the MAPK pathway has been implicated in the development and progression of cancer by enhancing cell growth and survival, metastasis, angiogenesis, and resistance, making it a very important target for cancer therapy. PTCH1 has previously been linked to MAPK/ERK and PI3K/AKT signalling (Elia et al., 2007, Seto et al., 2009), and a SHH-mediated increase in ERK activation has been demonstrated (Chang et al., 2010). Early experiments in this project showed that knockdown of βarr1 enhances this SHH-mediated ERK activation, demonstrating a

possible PTCH1-mediated tumour suppressor role of βarr1 as a negative regulator of ERK activity. During this project, the experimental conditions to isolate the specific effect of the PTCH1-βarr interaction on ERK activity (using the SATA mutant) were not fully optimised. Future work could focus on refining these conditions to investigate the effect of this interaction on the MAPK/ERK pathway.

Phenotypically, recruitment of βarrs to PTCH1 negatively regulates apoptotic signalling, and enhances cell viability and clonogenicity. This reflects the negative regulation βarrs have over PTCH1, since they oppose its tumour suppressor functions. As previously discussed, more clarity could be achieved in the experiments that generated these results by producing cell lines expressing the mutated version of PTCH1 (SATA) which does not bind βarrs, and comparing to a wild-type control, since the low transfection efficiency limited the interpretation of cell-based assays. However this is a very complex and time-consuming process, so was not an option in this project, however would be worth exploring in future work.

In addition to the above suggestions for experiments to continue and clarify work on this project, another direction to take would be to solve the structure of the PTCH1-βarr interaction *in vitro*. While this was not within the scope of this project, the *in vitro* and *in silico* studies to characterise the PTCH1-βarr interaction and binding interface provide a good foundation to produce structural data. The cytosolic domains of PTCH1 are intrinsically disordered and therefore have not been solved. A co-crystal with βarr1 may contain more order and therefore could be solved, since βarr1 is a highly ordered soluble protein, however it is more likely that structural studies would need to utilise a small peptide containing the SEYSSQT motif to circumvent the difficulties associated with intrinsically disordered regions.

In summary, the findings described here enhance our knowledge of the HH signalling network, specifically the regulation of PTCH1 and its non-canonical functions. Beyond elucidating molecular mechanisms, the identified PTCH1-βarr interaction emerges as a promising target for therapeutic intervention in HH-driven malignancies, and further characterisation would be valuable in the fight against cancer.

7.2 Final conclusions

The Hedgehog signalling network controls complex developmental processes across metazoan organisms. It is primarily inactive in adult organisms, aside from its requirement in tissue homeostasis and repair. Aberrant HH signalling has been

implicated in onset and progression of several diseases including Gorlin syndrome, holoprosencephaly, and cancers such as basal cell carcinoma, medulloblastoma, and pancreatic cancer.

The limited response to current HH pathway inhibitors in solid tumours other than BCC and the adverse effects observed with many of these drugs demonstrates the limits of existing understanding of the molecular mechanisms controlling HH signalling *in vivo*. Here, a novel avenue of HH research was investigated to characterise regulation of non-canonical signalling through PTCH1.

This project has given valuable insight into the mechanisms governing the stability of the HH receptor PTCH1. Experimental and modelling evidence demonstrates a mechanism of βarr recruitment to the PTCH1 C-terminal domain. The GRK2/3-mediated phosphorylation of PTCH1 at S1223-T1229 to create the βarr binding motif pSEYpSSQpT is promoted by binding of SHH to PTCH1, and in conjunction with ubiquitination of PTCH1, leads to rapid internalisation, dissociation of βarrs for recycling, and PTCH1 degradation. As a consequence of the role of βarrs in PTCH1 turnover, blockade of the PTCH1-βarr interaction was shown to affect phenotypic responses in cells with active HH signalling, increasing PTCH1's proapoptotic activity while reducing cancer cell viability and clonogenic potential.

In vivo competitive inhibition of the PTCH1-βarr interaction could offer a promising alternative therapy for HH-related cancers, as the resulting cellular responses are consistent with decreased tumour growth and cancer progression. The research presented in this thesis suggests that progressing investigation of this interaction and the effects of it manipulation into *in vivo* and clinical studies would be beneficial for the advancement of cancer therapeutics.

Bibliography

Bibliography

Abramson, J., Adler, J., Dunger, J., Evans, R., Green, T., Pritzel, A., Ronneberger, O., Willmore, L., Ballard, A. J. & Bambrick, J. 2024. Accurate structure prediction of biomolecular interactions with AlphaFold 3. *Nature*, 1-3.

Ainsworth, C. 2007. Cilia: tails of the unexpected. *Nature,* 448, 638-642.

Alfaro, A. C., Roberts, B., Kwong, L., Bijlsma, M. F. & Roelink, H. 2014. Ptch2 mediates the Shh response in Ptch1−/− cells. *Development,* 141, 3331-3339.

Arveseth, C. D., Happ, J. T., Hedeen, D. S., Zhu, J.-F., Capener, J. L., Klatt Shaw, D., Deshpande, I., Liang, J., Xu, J. & Stubben, S. L. 2021. Smoothened transduces Hedgehog signals via activity-dependent sequestration of PKA catalytic subunits. *PLoS biology,* 19, e3001191.

Barnes, E. A., Kong, M., Ollendorff, V. & Donoghue, D. J. 2001. Patched1 interacts with cyclin B1 to regulate cell cycle progression. *The EMBO journal,* 20, 2214-2223.

Basler, K. & Struhl, G. 1994. Compartment boundaries and the control of Drosopfiffa limb pattern by hedgehog protein. *Nature,* 368, 208-214.

Belgacem, Y. H. & Borodinsky, L. N. 2011. Sonic hedgehog signaling is decoded by calcium spike activity in the developing spinal cord. *Proceedings of the National Academy of Sciences,* 108, 4482-4487.

Benovic, J., Kühn, H., Weyand, I., Codina, J., Caron, M. & Lefkowitz, R. 1987. Functional desensitization of the isolated beta-adrenergic receptor by the beta-adrenergic receptor kinase: potential role of an analog of the retinal protein arrestin (48-kDa protein). *Proceedings of the National Academy of Sciences,* 84, 8879-8882.

Bhattacharya, R., Kwon, J., Ali, B., Wang, E., Patra, S., Shridhar, V. & Mukherjee, P. 2008. Role of hedgehog signaling in ovarian cancer. *Clinical Cancer Research,* 14, 7659-7666.

Bidet, M., Joubert, O., Lacombe, B., Ciantar, M., Nehmé, R., Mollat, P., Brétillon, L., Faure, H., Bittman, R. & Ruat, M. 2011. The hedgehog receptor patched is involved in cholesterol transport. *PloS one,* 6, e23834.

Bijlsma, M. F., Borensztajn, K. S., Roelink, H., Peppelenbosch, M. P. & Spek, C. A. 2007. Sonic hedgehog induces transcription-independent cytoskeletal rearrangement and migration regulated by arachidonate metabolites. *Cellular signalling,* 19, 2596-2604.

Bissey, P.-A., Mathot, P., Guix, C., Jasmin, M., Goddard, I., Costechareyre, C., Gadot, N., Delcros, J.-G., Mali, S. M. & Fasan, R. 2020. Blocking SHH/Patched interaction triggers tumor growth inhibition through Patched-induced apoptosis. *Cancer research,* 80, 1970-1980.

Blanchette-Mackie, E. J. 2000. Intracellular cholesterol trafficking: role of the NPC1 protein. *Biochimica et Biophysica Acta (BBA)-Molecular and Cell Biology of Lipids,* 1486, 171-183.

Blom, N., Sicheritz-Pontén, T., Gupta, R., Gammeltoft, S. & Brunak, S. 2004. Prediction of post-translational glycosylation and phosphorylation of proteins from the amino acid sequence. *Proteomics,* 4, 1633-1649.

Böttke, T., Ernicke, S., Serfling, R., Ihling, C., Burda, E., Gurevich, V. V., Sinz, A. & Coin, I. 2020. Exploring GPCR-arrestin interfaces with genetically encoded crosslinkers. *EMBO reports,* 21, e50437.

Boutet, N., Bignon, Y.-J., Drouin-Garraud, V., Sarda, P., Longy, M., Lacombe, D. & Gorry, P. 2003. Spectrum of PTCH1 mutations in French patients with Gorlin syndrome. *Journal of investigative dermatology,* 121**,** 478-481.

Brennan-Crispi, D. M., Overmiller, A. M., Tamayo-Orrego, L., Marous, M. R., Sahu, J., Mcguinn, K. P., Cooper, F., Georgiou, I. C., Frankfurter, M. & Salas-Alanis, J. C. 2019. Overexpression of desmoglein 2 in a mouse model of Gorlin syndrome enhances spontaneous basal cell carcinoma formation through STAT3-mediated Gli1 expression. *Journal of Investigative Dermatology,* 139**,** 300-307.

Briscoe, J., Chen, Y., Jessell, T. M. & Struhl, G. 2001. A hedgehog-insensitive form of patched provides evidence for direct long-range morphogen activity of sonic hedgehog in the neural tube. *Molecular cell,* 7**,** 1279-1291.

Brown, A. & Zhang, R. 2020. Primary cilia: A closer look at the antenna of cells. *Current Biology,* 30**,** R1494-R1496.

Buglino, J. A. & Resh, M. D. 2008. Hhat Is a Palmitoylacyltransferase with Specificity for N-Palmitoylation of Sonic Hedgehog*♦. *Journal of Biological Chemistry,* 283**,** 22076-22088.

Burke, R., Nellen, D., Bellotto, M., Hafen, E., Senti, K.-A., Dickson, B. J. & Basler, K. 1999. Dispatched, a novel sterol-sensing domain protein dedicated to the release of cholesterol-modified hedgehog from signaling cells. *Cell,* 99**,** 803-815.

Caballero-Ruiz, B., Gkotsi, D. S., Ollerton, H., Morales-Alcala, C. C., Bordone, R., Jenkins, G. M., Di Magno, L., Canettieri, G. & Riobo-Del Galdo, N. A. 2023. Partial Truncation of the C-Terminal Domain of PTCH1 in Cancer Enhances Autophagy and Metabolic Adaptability. *Cancers,* 15**,** 369.

Cai, E., Zhang, J. & Ge, X. 2022. Control of the Hedgehog pathway by compartmentalized PKA in the primary cilium. *Science China Life Sciences***,** 1-15.

Cai, H., Li, H., Li, J., Li, X., Li, Y., Shi, Y. & Wang, D. 2016. Sonic hedgehog signaling pathway mediates development of hepatocellular carcinoma. *Tumor Biology,* 37**,** 16199-16205.

Chang, H., Li, Q., Moraes, R. C., Lewis, M. T. & Hamel, P. A. 2010. Activation of Erk by sonic hedgehog independent of canonical hedgehog signalling. *The international journal of biochemistry & cell biology,* 42**,** 1462-1471.

Chen, W., Ren, X.-R., Nelson, C. D., Barak, L. S., Chen, J. K., Beachy, P. A., De Sauvage, F. & Lefkowitz, R. J. 2004. Activity-dependent internalization of smoothened mediated by ß-arrestin 2 and GRK2. *Science,* 306**,** 2257-2260.

Chen, X., Morales-Alcala, C. C. & Riobo-Del Galdo, N. A. 2018. Autophagic flux is regulated by interaction between the C-terminal domain of PATCHED1 and ATG101. *Molecular Cancer Research,* 16**,** 909-919.

Chen, X. L., Chinchilla, P., Fombonne, J., Ho, L., Guix, C., Keen, J. H., Mehlen, P. & Riobo, N. A. 2014. Patched-1 proapoptotic activity is downregulated by modification of K1413 by the E3 ubiquitin-protein ligase Itchy homolog. *Molecular and cellular biology,* 34**,** 3855-3866.

Chen, Y., Sasai, N., Ma, G., Yue, T., Jia, J., Briscoe, J. & Jiang, J. 2011. Sonic Hedgehog dependent phosphorylation by CK1α and GRK2 is required for ciliary accumulation and activation of smoothened. *PLoS biology,* 9**,** e1001083.

Cheng, S., Maier, D., Neubueser, D. & Hipfner, D. R. 2010. Regulation of smoothened by Drosophila G-protein-coupled receptor kinases. *Developmental biology,* 337**,** 99-109.

Chinchilla, P., Xiao, L., Kazanietz, M. G. & Riobo, N. A. 2010. Hedgehog proteins activate pro-angiogenic responses in endothelial cells through non-canonical signaling pathways. *Cell cycle,* 9**,** 570-579.

Coffa, S., Breitman, M., Hanson, S. M., Callaway, K., Kook, S., Dalby, K. N. & Gurevich, V. V. 2011. The effect of arrestin conformation on the recruitment of c-Raf1, MEK1, and ERK1/2 activation. *PLoS One,* 6**,** e28723.

Cross, F. 2023. *Phosphorylation of the PTCH1 C-terminal domain: profiling and significance*. University of Leeds.

Denef, N., Neubüser, D., Perez, L. & Cohen, S. M. 2000. Hedgehog induces opposite changes in turnover and subcellular localization of patched and smoothened. *Cell,* 102**,** 521-531.

Dessaud, E., Mcmahon, A. P. & Briscoe, J. 2008. Pattern formation in the vertebrate neural tube: a sonic hedgehog morphogen-regulated transcriptional network.

Dewire, S. M., Ahn, S., Lefkowitz, R. J. & Shenoy, S. K. 2007. β-arrestins and cell signaling. *Annu. Rev. Physiol.,* 69**,** 483-510.

Elia, D., Madhala, D., Ardon, E., Reshef, R. & Halevy, O. 2007. Sonic hedgehog promotes proliferation and differentiation of adult muscle cells: Involvement of MAPK/ERK and PI3K/Akt pathways. *Biochimica et Biophysica Acta (BBA)-Molecular Cell Research,* 1773**,** 1438-1446.

Epstein, E. H. 2008. Basal cell carcinomas: attack of the hedgehog. *Nature Reviews Cancer,* 8**,** 743-754.

Fernández-Arenas, E., Calleja, E., Martínez-Martín, N., Gharbi, S. I., Navajas, R., García-Medel, N., Penela, P., Alcamí, A., Mayor Jr, F. & Albar, J. P. 2014. β-arrestin-1 mediates the TCR-triggered re-routing of distal receptors to the immunological synapse by a PKC-mediated mechanism. *The EMBO journal,* 33**,** 559-577.

Fleet, A., Lee, J. P., Tamachi, A., Javeed, I. & Hamel, P. A. 2016. Activities of the cytoplasmic domains of Patched-1 modulate but are not essential for the regulation of canonical Hedgehog signaling. *Journal of Biological Chemistry,* 291**,** 17557-17568.

Gong, X., Qian, H., Cao, P., Zhao, X., Zhou, Q., Lei, J. & Yan, N. 2018. Structural basis for the recognition of Sonic Hedgehog by human Patched1. *Science,* 361**,** eaas8935.

Guo, Y.-Y., Zhang, J.-Y., Li, X.-F., Luo, H.-Y., Chen, F. & Li, T.-J. 2013. PTCH1 gene mutations in Keratocystic odontogenic tumors: a study of 43 Chinese patients and a systematic review. *PLoS One,* 8**,** e77305.

Gurevich, V. V. & Gurevich, E. V. 2004. The molecular acrobatics of arrestin activation. *Trends in pharmacological sciences,* 25**,** 105-111.

Han, Y., Wang, B., Cho, Y. S., Zhu, J., Wu, J., Chen, Y. & Jiang, J. 2019. Phosphorylation of Ci/Gli by fused family kinases promotes hedgehog signaling. *Developmental cell,* 50**,** 610-626. e4.

Hasanovic, A. & Mus-Veteau, I. 2018. Targeting the multidrug transporter Ptch1 potentiates chemotherapy efficiency. *Cells,* 7**,** 107.

He, M., Subramanian, R., Bangs, F., Omelchenko, T., Liem Jr, K. F., Kapoor, T. M. & Anderson, K. V. 2014. The kinesin-4 protein Kif7 regulates mammalian

Hedgehog signalling by organizing the cilium tip compartment. *Nature cell biology,* 16**,** 663-672.

Hebda, J. K., Leclair, H. M., Azzi, S., Roussel, C., Scott, M. G., Bidère, N. & Gavard, J. 2013. The C-terminus region of β-arrestin1 modulates VE-cadherin expression and endothelial cell permeability. *Cell communication and signaling,* 11**,** 1-7.

Ho, E. K. & Stearns, T. 2021. Hedgehog signaling and the primary cilium: implications for spatial and temporal constraints on signaling. *Development,* 148**,** dev195552.

Ho Wei, L., Arastoo, M., Georgiou, I., Manning, D. R. & Riobo-Del Galdo, N. A. 2018. Activation of the Gi protein-RHOA axis by non-canonical Hedgehog signaling is independent of primary cilia. *PLoS One,* 13**,** e0203170.

Huang, P., Nedelcu, D., Watanabe, M., Jao, C., Kim, Y., Liu, J. & Salic, A. 2016. Cellular cholesterol directly activates smoothened in hedgehog signaling. *Cell,* 166**,** 1176-1187. e14.

Hwang, S.-H., Somatilaka, B. N., White, K. & Mukhopadhyay, S. 2021. Ciliary and extraciliary Gpr161 pools repress hedgehog signaling in a tissue-specific manner. *Elife,* 10**,** e67121.

Ingham, P. W. & Mcmahon, A. P. 2001. Hedgehog signaling in animal development: paradigms and principles. *Genes & development,* 15**,** 3059-3087.

Ingham, P. W., Nakano, Y. & Seger, C. 2011. Mechanisms and functions of Hedgehog signalling across the metazoa. *Nature reviews genetics,* 12**,** 393-406.

Izzi, L., Lévesque, M., Morin, S., Laniel, D., Wilkes, B. C., Mille, F., Krauss, R. S., Mcmahon, A. P., Allen, B. L. & Charron, F. 2011. Boc and Gas1 each form distinct Shh receptor complexes with Ptch1 and are required for Shh-mediated cell proliferation. *Developmental cell,* 20**,** 788-801.

Jaber, M., Koch, W. J., Rockman, H., Smith, B., Bond, R. A., Sulik, K. K., Ross Jr, J., Lefkowitz, R. J., Caron, M. G. & Giros, B. 1996. Essential role of β-adrenergic receptor kinase 1 in cardiac development and function. *Proceedings of the National Academy of Sciences,* 93**,** 12974-12979.

Jean-Charles, P.-Y., Snyder, J. & Shenoy, S. 2016. Chapter one-ubiquitination and deubiquitination of G protein-coupled receptors. *Progress in molecular biology and translational science,* 141**,** 1-55.

Jensen, A. M. & Wallace, V. A. 1997. Expression of Sonic hedgehog and its putative role as a precursor cell mitogen in the developing mouse retina. *Development,* 124**,** 363-371.

Jiang, X., Yang, P. & Ma, L. 2009. Kinase activity-independent regulation of cyclin pathway by GRK2 is essential for zebrafish early development. *Proceedings of the National Academy of Sciences,* 106**,** 10183-10188.

Kang, D. S., Tian, X. & Benovic, J. L. 2014. Role of β-arrestins and arrestin domain-containing proteins in G protein-coupled receptor trafficking. *Current opinion in cell biology,* 27**,** 63-71.

Kang, Y., Zhou, X. E., Gao, X., He, Y., Liu, W., Ishchenko, A., Barty, A., White, T. A., Yefanov, O. & Han, G. W. 2015. Crystal structure of rhodopsin bound to arrestin by femtosecond X-ray laser. *Nature,* 523**,** 561-567.

Karpen, H. E., Bukowski, J. T., Hughes, T., Gratton, J.-P., Sessa, W. C. & Gailani, M. R. 2001. The Sonic Hedgehog Receptor Patched Associates with Caveolin-1

in Cholesterol-rich Microdomains of the Plasma Membrane* 210. *Journal of Biological Chemistry,* 276**,** 19503-19511.

Koide, S. & Sidhu, S. S. 2009. The importance of being tyrosine: lessons in molecular recognition from minimalist synthetic binding proteins. *ACS chemical biology,* 4**,** 325-334.

Komuro, H. & Rakic, P. 1996. Intracellular Ca2+ fluctuations modulate the rate of neuronal migration. *Neuron,* 17**,** 275-285.

Kovacs, J. J., Whalen, E. J., Liu, R., Xiao, K., Kim, J., Chen, M., Wang, J., Chen, W. & Lefkowitz, R. J. 2008. β-Arrestin–mediated localization of smoothened to the primary cilium. *Science,* 320**,** 1777-1781.

Krüger, M., Mennerich, D., Fees, S., Schäfer, R., Mundlos, S. & Braun, T. 2001. Sonic hedgehog is a survival factor for hypaxial muscles during mouse development. *Development,* 128**,** 743-752.

Lally, C. C. M., Bauer, B., Selent, J. & Sommer, M. E. 2017. C-edge loops of arrestin function as a membrane anchor. *Nature communications,* 8**,** 14258.

Lee, Y., Miller, H. L., Russell, H. R., Boyd, K., Curran, T. & Mckinnon, P. J. 2006. Patched2 modulates tumorigenesis in patched1 heterozygous mice. *Cancer research,* 66**,** 6964-6971.

Lefkowitz, R. J., Rajagopal, K. & Whalen, E. J. 2006. New roles for β-arrestins in cell signaling: not just for seven-transmembrane receptors. *Molecular cell,* 24**,** 643-652.

Li, S., Chen, Y., Shi, Q., Yue, T., Wang, B. & Jiang, J. 2012. Hedgehog-regulated ubiquitination controls smoothened trafficking and cell surface expression in Drosophila. *PLoS biology,* 10**,** e1001239.

Li, Z., Zhang, H., Denhard, L. A., Liu, L.-H., Zhou, H. & Lan, Z.-J. 2008. Reduced white fat mass in adult mice bearing a truncated Patched 1. *International journal of biological sciences,* 4**,** 29.

Lin, C. H., Macgurn, J. A., Chu, T., Stefan, C. J. & Emr, S. D. 2008. Arrestin-related ubiquitin-ligase adaptors regulate endocytosis and protein turnover at the cell surface. *Cell,* 135**,** 714-725.

Lin, F.-T., Daaka, Y. & Lefkowitz, R. J. 1998. β-Arrestins regulate mitogenic signaling and clathrin-mediated endocytosis of the insulin-like growth factor I receptor. *Journal of Biological Chemistry,* 273**,** 31640-31643.

Lindström, E., Shimokawa, T., Toftgård, R. & Zaphiropoulos, P. G. 2006. PTCH mutations: distribution and analyses. *Human mutation,* 27**,** 215-219.

Liu, F., Feng, X. X., Zhu, S. L., Huang, H. Y., Chen, Y. D., Pan, Y. F., June, R. R., Zheng, S. G. & Huang, J. L. 2018. Sonic hedgehog signaling pathway mediates proliferation and migration of fibroblast-like synoviocytes in rheumatoid arthritis via MAPK/ERK signaling pathway. *Frontiers in immunology,* 9**,** 2847.

Lo Muzio, L. 2008. Nevoid basal cell carcinoma syndrome (Gorlin syndrome). *Orphanet journal of rare diseases,* 3**,** 1-16.

Lorusso, P. M., Rudin, C. M., Reddy, J. C., Tibes, R., Weiss, G. J., Borad, M. J., Hann, C. L., Brahmer, J. R., Chang, I. & Darbonne, W. C. 2011. Phase I trial of hedgehog pathway inhibitor vismodegib (GDC-0449) in patients with refractory, locally advanced or metastatic solid tumors. *Clinical cancer research,* 17**,** 2502-2511.

Lu, J.-T., Zhao, W.-D., He, W. & Wei, W. 2012. Hedgehog signaling pathway mediates invasion and metastasis of hepatocellular carcinoma via ERK pathway. *Acta Pharmacologica Sinica,* 33**,** 691-700.

Lu, X., Liu, S. & Kornberg, T. B. 2006. The C-terminal tail of the Hedgehog receptor Patched regulates both localization and turnover. *Genes & development,* 20**,** 2539-2551.

Mancuso, M., Pazzaglia, S., Tanori, M., Hahn, H., Merola, P., Rebessi, S., Atkinson, M. J., Di Majo, V., Covelli, V. & Saran, A. 2004. Basal cell carcinoma and its development: insights from radiation-induced tumors in Ptch1-deficient mice. *Cancer research,* 64**,** 934-941.

Marigo, V., Davey, R. A., Zuo, Y., Cunningham, J. M. & Tabin, C. J. 1996. Biochemical evidence that patched is the Hedgehog receptor. *Nature,* 384**,** 176-179.

Martinez-Arias, A. & Lawrence, P. A. 1985. Parasegments and compartments in the Drosophila embryo. *Nature,* 313**,** 639-642.

Mateos, B., Conrad-Billroth, C., Schiavina, M., Beier, A., Kontaxis, G., Konrat, R., Felli, I. C. & Pierattelli, R. 2020. The ambivalent role of proline residues in an intrinsically disordered protein: from disorder promoters to compaction facilitators. *Journal of molecular biology,* 432**,** 3093-3111.

Meloni, A. R., Fralish, G. B., Kelly, P., Salahpour, A., Chen, J. K., Wechsler-Reya, R. J., Lefkowitz, R. J. & Caron, M. G. 2006. Smoothened signal transduction is promoted by G protein-coupled receptor kinase 2. *Molecular and cellular biology,* 26**,** 7550-7560.

Mendez, A., Burns, M. E., Roca, A., Lem, J., Wu, L.-W., Simon, M. I., Baylor, D. A. & Chen, J. 2000. Rapid and reproducible deactivation of rhodopsin requires multiple phosphorylation sites. *Neuron,* 28**,** 153-164.

Mille, F., Thibert, C., Fombonne, J., Rama, N., Guix, C., Hayashi, H., Corset, V., Reed, J. C. & Mehlen, P. 2009. The Patched dependence receptor triggers apoptosis through a DRAL–caspase-9 complex. *Nature cell biology,* 11**,** 739-746.

Mizushima, N. & Levine, B. 2010. Autophagy in mammalian development and differentiation. *Nature cell biology,* 12**,** 823-830.

Morgan, A. A. & Rubenstein, E. 2013. Proline: the distribution, frequency, positioning, and common functional roles of proline and polyproline sequences in the human proteome. *PloS one,* 8**,** e53785.

Nagao, K., Toyoda, M., Takeuchi-Inoue, K., Fujii, K., Yamada, M. & Miyashita, T. 2005. Identification and characterization of multiple isoforms of a murine and human tumor suppressor, patched, having distinct first exons. *Genomics,* 85**,** 462-471.

Nakamura, M., Tanaka, H., Nagayoshi, Y., Nakashima, H., Tsutsumi, K., Ohtsuka, T., Takahata, S., Tanaka, M. & Okada, H. 2012. Targeting the hedgehog signaling pathway with interacting peptides to Patched-1. *Journal of gastroenterology,* 47**,** 452-460.

Nedelcu, D., Liu, J., Xu, Y., Jao, C. & Salic, A. 2013. Oxysterol binding to the extracellular domain of Smoothened in Hedgehog signaling. *Nature chemical biology,* 9**,** 557-564.

Nieuwenhuis, E., Barnfield, P. C., Makino, S. & Hui, C.-C. 2007. Epidermal hyperplasia and expansion of the interfollicular stem cell compartment in mutant mice with a C-terminal truncation of Patched1. *Developmental Biology,* 308**,** 547-560.

Niewiadomski, P., Kong, J. H., Ahrends, R., Ma, Y., Humke, E. W., Khan, S., Teruel, M. N., Novitch, B. G. & Rohatgi, R. 2014. Gli protein activity is controlled by

multisite phosphorylation in vertebrate Hedgehog signaling. *Cell reports,* 6**,** 168-181.

Nüsslein-Volhard, C. & Wieschaus, E. 1980. Mutations affecting segment number and polarity in Drosophila. *Nature,* 287**,** 795-801.

Oakley, R. H., Laporte, S. A., Holt, J. A., Caron, M. G. & Barak, L. S. 2000. Differential affinities of visual arrestin, βarrestin1, and βarrestin2 for G protein-coupled receptors delineate two major classes of receptors. *Journal of Biological Chemistry,* 275**,** 17201-17210.

Odent, S., Attié-Bitach, T., Blayau, M., Mathieu, M., Augé, J., Delezoïde, A., Le Gall, J., Le Marec, B., Munnich, A. & David, V. 1999. Expression of the Sonic hedgehog (SHH) gene during early human development and phenotypic expression of new mutations causing holoprosencephaly. *Human Molecular Genetics,* 8**,** 1683-1689.

Ogden, S. K., Fei, D. L., Schilling, N. S., Ahmed, Y. F., Hwa, J. & Robbins, D. J. 2008. G protein Gαi functions immediately downstream of Smoothened in Hedgehog signalling. *Nature,* 456**,** 967-970.

Okolowsky, N., Furth, P. A. & Hamel, P. A. 2014. Oestrogen receptor-alpha regulates non-canonical Hedgehog-signalling in the mammary gland. *Developmental biology,* 391**,** 219-229.

Pal, K., Hwang, S.-H., Somatilaka, B., Badgandi, H., Jackson, P. K., Defea, K. & Mukhopadhyay, S. 2016. Smoothened determines β-arrestin–mediated removal of the G protein–coupled receptor Gpr161 from the primary cilium. *Journal of Cell Biology,* 212**,** 861-875.

Pathi, S., Pagan-Westphal, S., Baker, D. P., Garber, E. A., Rayhorn, P., Bumcrot, D., Tabin, C. J., Pepinsky, R. B. & Williams, K. P. 2001. Comparative biological responses to human Sonic, Indian, and Desert hedgehog. *Mechanisms of development,* 106**,** 107-117.

Peter, M., Nakagawa, J., Doree, M., Labbe, J. & Nigg, E. 1990. In vitro disassembly of the nuclear lamina and M phase-specific phosphorylation of lamins by cdc2 kinase. *Cell,* 61**,** 591-602.

Petrov, K., De Almeida Magalhaes, T. & Salic, A. 2021. Mechanism and ultrasensitivity in Hedgehog signaling revealed by Patched1 disease mutations. *Proceedings of the National Academy of Sciences,* 118**,** e2006800118.

Plotnikova, O. V., Pugacheva, E. N. & Golemis, E. A. 2009. Primary cilia and the cell cycle. *Methods in cell biology*. Elsevier.

Polizio, A. H., Chinchilla, P., Chen, X., Kim, S., Manning, D. R. & Riobo, N. A. 2011. Heterotrimeric Gi proteins link Hedgehog signaling to activation of Rho small GTPases to promote fibroblast migration. *Journal of Biological Chemistry,* 286**,** 19589-19596.

Porter, J. A., Young, K. E. & Beachy, P. A. 1996. Cholesterol modification of hedgehog signaling proteins in animal development. *Science,* 274**,** 255-259.

Porter, L. A. & Donoghue, D. J. 2003. Cyclin B1 and CDK1: nuclear localization and upstream regulators. *PROGRESS IN CELL CYCLE RESEARCH.,* 5**,** 335-348.

Puca, L. & Brou, C. 2014. α-Arrestins–new players in Notch and GPCR signaling pathways in mammals. *Journal of Cell Science,* 127**,** 1359-1367.

Purzner, T., Purzner, J., Buckstaff, T., Cozza, G., Gholamin, S., Rusert, J. M., Hartl, T. A., Sanders, J., Conley, N. & Ge, X. 2018. Developmental phosphoproteomics identifies the kinase CK2 as a driver of Hedgehog

signaling and a therapeutic target in medulloblastoma. *Science signaling,* 11**,** eaau5147.

Qi, X., Liu, H., Thompson, B., Mcdonald, J., Zhang, C. & Li, X. 2019. Cryo-EM structure of oxysterol-bound human Smoothened coupled to a heterotrimeric Gi. *Nature,* 571**,** 279-283.

Qi, X., Schmiege, P., Coutavas, E., Wang, J. & Li, X. 2018. Structures of human Patched and its complex with native palmitoylated sonic hedgehog. *Nature,* 560**,** 128-132.

Qian, H., Cao, P., Hu, M., Gao, S., Yan, N. & Gong, X. 2019. Inhibition of tetrameric Patched1 by Sonic Hedgehog through an asymmetric paradigm. *Nature communications,* 10**,** 2320.

Raffel, C., Jenkins, R. B., Frederick, L., Hebrink, D., Alderete, B., Fults, D. W. & James, C. D. 1997. Sporadic medulloblastomas contain PTCH mutations. *Cancer research,* 57**,** 842-845.

Riobo, N. A., Saucy, B., Dilizio, C. & Manning, D. R. 2006. Activation of heterotrimeric G proteins by Smoothened. *Proceedings of the National Academy of Sciences,* 103**,** 12607-12612.

Rohatgi, R., Milenkovic, L. & Scott, M. P. 2007. Patched1 regulates hedgehog signaling at the primary cilium. *Science,* 317**,** 372-376.

Routh, M. D., Zalucki, Y., Su, C.-C., Long, F., Zhang, Q., Shafer, W. M. & Edward, W. Y. 2011. Efflux pumps of the resistance-nodulation-division family: A perspective of their structure, function and regulation in gram-negative bacteria. *Advances in enzymology and related areas of molecular biology,* 77**,** 109.

Rudin, C. M., Hann, C. L., Laterra, J., Yauch, R. L., Callahan, C. A., Fu, L., Holcomb, T., Stinson, J., Gould, S. E. & Coleman, B. 2009. Treatment of medulloblastoma with hedgehog pathway inhibitor GDC-0449. *New England Journal of Medicine,* 361**,** 1173-1178.

Seto, M., Ohta, M., Asaoka, Y., Ikenoue, T., Tada, M., Miyabayashi, K., Mohri, D., Tanaka, Y., Ijichi, H. & Tateishi, K. 2009. Regulation of the hedgehog signaling by the mitogen-activated protein kinase cascade in gastric cancer. *Molecular Carcinogenesis: Published in cooperation with the University of Texas MD Anderson Cancer Center,* 48**,** 703-712.

Shenoy, S. K., Barak, L. S., Xiao, K., Ahn, S., Berthouze, M., Shukla, A. K., Luttrell, L. M. & Lefkowitz, R. J. 2007. Ubiquitination of β-arrestin links seven-transmembrane receptor endocytosis and ERK activation. *Journal of Biological Chemistry,* 282**,** 29549-29562.

Shenoy, S. K. & Lefkowitz, R. J. 2003. Trafficking patterns of β-arrestin and G protein-coupled receptors determined by the kinetics of β-arrestin deubiquitination. *Journal of Biological Chemistry,* 278**,** 14498-14506.

Shenoy, S. K., Mcdonald, P. H., Kohout, T. A. & Lefkowitz, R. J. 2001. Regulation of receptor fate by ubiquitination of activated β2-adrenergic receptor and β-arrestin. *Science,* 294**,** 1307-1313.

Shiromizu, T., Adachi, J., Watanabe, S., Murakami, T., Kuga, T., Muraoka, S. & Tomonaga, T. 2013. Identification of missing proteins in the neXtProt database and unregistered phosphopeptides in the PhosphoSitePlus database as part of the Chromosome-centric Human Proteome Project. *Journal of proteome research,* 12**,** 2414-2421.

Shu, Y., Wang, Y., Lv, W.-Q., Peng, D.-Y., Li, J., Zhang, H., Jiang, G.-J., Yang, B.-J., Liu, S. & Zhang, J. 2020. ARRB1-promoted NOTCH1 degradation is suppressed by OncomiR miR-223 in T-cell acute lymphoblastic leukemia. *Cancer research,* 80**,** 988-998.

Shukla, A. K., Manglik, A., Kruse, A. C., Xiao, K., Reis, R. I., Tseng, W.-C., Staus, D. P., Hilger, D., Uysal, S. & Huang, L.-Y. 2013. Structure of active β-arrestin-1 bound to a G-protein-coupled receptor phosphopeptide. *Nature,* 497**,** 137-141.

Shukla, A. K., Westfield, G. H., Xiao, K., Reis, R. I., Huang, L.-Y., Tripathi-Shukla, P., Qian, J., Li, S., Blanc, A. & Oleskie, A. N. 2014. Visualization of arrestin recruitment by a G-protein-coupled receptor. *Nature,* 512**,** 218-222.

Shukla, A. K., Xiao, K. & Lefkowitz, R. J. 2011. Emerging paradigms of β-arrestin-dependent seven transmembrane receptor signaling. *Trends in biochemical sciences,* 36**,** 457-469.

Siebold, C. & Rohatgi, R. 2023. The inseparable relationship between cholesterol and hedgehog signaling. *Annual Review of Biochemistry,* 92**,** 273-298.

Song, X., Raman, D., Gurevich, E. V., Vishnivetskiy, S. A. & Gurevich, V. V. 2006. Visual and both non-visual arrestins in their "inactive" conformation bind JNK3 and Mdm2 and relocalize them from the nucleus to the cytoplasm. *Journal of Biological Chemistry,* 281**,** 21491-21499.

Staus, D. P., Hu, H., Robertson, M. J., Kleinhenz, A. L., Wingler, L. M., Capel, W. D., Latorraca, N. R., Lefkowitz, R. J. & Skiniotis, G. 2020. Structure of the M2 muscarinic receptor–β-arrestin complex in a lipid nanodisc. *Nature,* 579**,** 297-302.

Takizawa, C. G. & Morgan, D. O. 2000. Control of mitosis by changes in the subcellular location of cyclin-B1–Cdk1 and Cdc25C. *Current opinion in cell biology,* 12**,** 658-665.

Tang, J. Y., Aszterbaum, M., Athar, M., Barsanti, F., Cappola, C., Estevez, N., Hebert, J., Hwang, J., Khaimskiy, Y. & Kim, A. 2010. Basal cell carcinoma chemoprevention with nonsteroidal anti-inflammatory drugs in genetically predisposed PTCH1+/− humans and mice. *Cancer prevention research,* 3**,** 25-34.

Tanida, I. 2011. Autophagosome formation and molecular mechanism of autophagy. *Antioxidants & redox signaling,* 14**,** 2201-2214.

Tate, G., Satoh, H., Endo, Y. & Mitsuya, T. 2000. Assignment [sup 1] of Desert Hedgehog (DHH) to human chromosome bands 12q12→ q13. 1 by in situ hybridization. *Cytogenetics & Cell Genetics,* 88.

Technology, C. S. 2014. *Hedgehog Signaling* [Online]. Available: https://www.cellsignal.com/pathways/hedgehog-signaling-pathway#:~:text=Hh%20proteins%20initiate%20signaling%20through,phosphorylation%20of%20its%20cytoplasmic%20tail. [Accessed].

Tenzen, T., Allen, B. L., Cole, F., Kang, J.-S., Krauss, R. S. & Mcmahon, A. P. 2006. The cell surface membrane proteins Cdo and Boc are components and targets of the Hedgehog signaling pathway and feedback network in mice. *Developmental cell,* 10**,** 647-656.

Theillet, F.-X., Kalmar, L., Tompa, P., Han, K.-H., Selenko, P., Dunker, A. K., Daughdrill, G. W. & Uversky, V. N. 2013. The alphabet of intrinsic disorder: I. Act like a Pro: On the abundance and roles of proline residues in intrinsically disordered proteins. *Intrinsically Disordered Proteins,* 1**,** e24360.

Thibert, C., Teillet, M.-A., Lapointe, F., Mazelin, L., Le Douarin, N. M. & Mehlen, P. 2003. Inhibition of neuroepithelial patched-induced apoptosis by sonic hedgehog. *Science,* 301**,** 843-846.

Thomsen, A. R., Plouffe, B., Cahill, T. J., Shukla, A. K., Tarrasch, J. T., Dosey, A. M., Kahsai, A. W., Strachan, R. T., Pani, B. & Mahoney, J. P. 2016. GPCR-G protein-β-arrestin super-complex mediates sustained G protein signaling. *Cell,* 166**,** 907-919.

Timmis, A. J. 2021. *Structure-function relationship of the Patched family of proteins*. University of Leeds.

Tohgo, A., Pierce, K. L., Choy, E. W., Lefkowitz, R. J. & Luttrell, L. M. 2002. β-Arrestin scaffolding of the ERK cascade enhances cytosolic ERK activity but inhibits ERK-mediated transcription following angiotensin AT1a receptor stimulation. *Journal of Biological Chemistry,* 277**,** 9429-9436.

Tukachinsky, H., Kuzmickas, R. P., Jao, C. Y., Liu, J. & Salic, A. 2012. Dispatched and scube mediate the efficient secretion of the cholesterol-modified hedgehog ligand. *Cell reports,* 2**,** 308-320.

Vishnivetskiy, S. A., Raman, D., Wei, J., Kennedy, M. J., Hurley, J. B. & Gurevich, V. V. 2007. Regulation of arrestin binding by rhodopsin phosphorylation level. *Journal of Biological Chemistry,* 282**,** 32075-32083.

Von Hoff, D. D., Lorusso, P. M., Rudin, C. M., Reddy, J. C., Yauch, R. L., Tibes, R., Weiss, G. J., Borad, M. J., Hann, C. L. & Brahmer, J. R. 2009. Inhibition of the hedgehog pathway in advanced basal-cell carcinoma. *New England Journal of Medicine,* 361**,** 1164-1172.

Vortkamp, A., Lee, K., Lanske, B., Segre, G. V., Kronenberg, H. M. & Tabin, C. J. 1996. Regulation of rate of cartilage differentiation by Indian hedgehog and PTH-related protein. *Science,* 273**,** 613-622.

Wang, W., Jack, B. M., Wang, H. H., Kavanaugh, M. A., Maser, R. L. & Tran, P. V. 2021. Intraflagellar transport proteins as regulators of primary cilia length. *Frontiers in cell and developmental biology,* 9**,** 661350.

Wang, Y., Zhou, Z., Walsh, C. T. & Mcmahon, A. P. 2009. Selective translocation of intracellular Smoothened to the primary cilium in response to Hedgehog pathway modulation. *Proceedings of the National Academy of Sciences,* 106**,** 2623-2628.

Wess, J., Oteng, A.-B., Rivera-Gonzalez, O., Gurevich, E. V. & Gurevich, V. V. 2023. β− Arrestins: structure, function, physiology, and pharmacological perspectives. *Pharmacological Reviews,* 75**,** 854-884.

Wierbowski, B. M., Petrov, K., Aravena, L., Gu, G., Xu, Y. & Salic, A. 2020. Hedgehog pathway activation requires coreceptor-catalyzed, lipid-dependent relay of the Sonic Hedgehog ligand. *Developmental cell,* 55**,** 450-467. e8.

Wisler, J. W., Dewire, S. M., Whalen, E. J., Violin, J. D., Drake, M. T., Ahn, S., Shenoy, S. K. & Lefkowitz, R. J. 2007. A unique mechanism of β-blocker action: carvedilol stimulates β-arrestin signaling. *Proceedings of the National Academy of Sciences,* 104**,** 16657-16662.

Wu, N., Hanson, S. M., Francis, D. J., Vishnivetskiy, S. A., Thibonnier, M., Klug, C. S., Shoham, M. & Gurevich, V. V. 2006. Arrestin binding to calmodulin: a direct interaction between two ubiquitous signaling proteins. *Journal of molecular biology,* 364**,** 955-963.

Xia, R., Jia, H., Fan, J., Liu, Y. & Jia, J. 2012. USP8 promotes smoothened signaling by preventing its ubiquitination and changing its subcellular localization. *PLoS biology,* 10**,** e1001238.

Xiao, K., Mcclatchy, D. B., Shukla, A. K., Zhao, Y., Chen, M., Shenoy, S. K., Yates Iii, J. R. & Lefkowitz, R. J. 2007. Functional specialization of β-arrestin interactions revealed by proteomic analysis. *Proceedings of the National Academy of Sciences,* 104**,** 12011-12016.

Yam, P. T., Kent, C. B., Morin, S., Farmer, W. T., Alchini, R., Lepelletier, L., Colman, D. R., Tessier-Lavigne, M., Fournier, A. E. & Charron, F. 2012. 14-3-3 proteins regulate a cell-intrinsic switch from sonic hedgehog-mediated commissural axon attraction to repulsion after midline crossing. *Neuron,* 76**,** 735-749.

Yang, X., Jin, N., Wang, Y., Yao, Y., Wang, Y., Li, T., Liu, C., Yu, T., Yin, H. & Zhang, Z. 2021. Macroautophagy supports sonic Hedgehog signaling by promoting Patched1 degradation. *Biochimica et Biophysica Acta (BBA)-Molecular Cell Research,* 1868**,** 119124.

Yao, S., Lum, L. & Beachy, P. 2006. The ihog cell-surface proteins bind Hedgehog and mediate pathway activation. *Cell,* 125**,** 343-357.

Yu, F.-Y., Hong, Y.-Y., Qu, J.-F., Chen, F. & Li, T.-J. 2014. The large intracellular loop of ptch1 mediates the non-canonical Hedgehog pathway through cyclin B1 in nevoid basal cell carcinoma syndrome. *International Journal of Molecular Medicine,* 34**,** 507-512.

Yu, P., Yang, J. & Zhang, Y. 2017. Identification and characterization of two novel PTCH1 splice variants. *Biochemical and Biophysical Research Communications,* 487**,** 68-75.

Yue, S., Tang, L.-Y., Tang, Y., Tang, Y., Shen, Q.-H., Ding, J., Chen, Y., Zhang, Z., Yu, T.-T. & Zhang, Y. E. 2014. Requirement of Smurf-mediated endocytosis of Patched1 in sonic hedgehog signal reception. *Elife,* 3**,** e02555.

Yuksel-Apak, M., Bögershausen, N., Pawlik, B., Li, Y., Apak, S., Uyguner, O., Milz, E., Nürnberg, G., Karaman, B. & Gülgören, A. 2012. A large duplication involving the IHH locus mimics acrocallosal syndrome. *European journal of human genetics,* 20**,** 639-644.

Zhang, Q. & Jiang, J. 2021. Regulation of Hedgehog signal transduction by ubiquitination and deubiquitination. *International journal of molecular sciences,* 22**,** 13338.

Zhang, Y., Bulkley, D. P., Xin, Y., Roberts, K. J., Asarnow, D. E., Sharma, A., Myers, B. R., Cho, W., Cheng, Y. & Beachy, P. A. 2018. Structural basis for cholesterol transport-like activity of the hedgehog receptor patched. *Cell,* 175**,** 1352-1364. e14.

Zhao, Y., Tong, C. & Jiang, J. 2007. Hedgehog regulates smoothened activity by inducing a conformational switch. *Nature,* 450**,** 252-258.

Zhou, X. E., He, Y., De Waal, P. W., Gao, X., Kang, Y., Van Eps, N., Yin, Y., Pal, K., Goswami, D. & White, T. A. 2017. Identification of phosphorylation codes for arrestin recruitment by G protein-coupled receptors. *Cell,* 170**,** 457-469. e13.

Zhuo, Y., Vishnivetskiy, S. A., Zhan, X., Gurevich, V. V. & Klug, C. S. 2014. Identification of receptor binding-induced conformational changes in non-visual arrestins. *Journal of Biological Chemistry,* 289**,** 20991-21002.